ABIOTIC AND BIOTIC DEGRADATION OF BISPHENOLS

A Dissertation Presented for the

Doctor of Philosophy

Degree

The University of Tennessee, Knoxville

Yanchen Sun

August 2022

Copyright © 2022 by Yanchen Sun.

All rights reserved

ACKNOWLEDGEMENTS

Pursuing science is a long journey without end. Completing the Ph.D. study is one of the most important stages. I have truly enjoyed it for the past five years. All the accomplishments cannot be achieved without the people I have the opportunity to work and collaborate with. I would like to express my sincere gratitude to all of you.

First and foremost, I appreciate my advisor, Dr. Frank E. Löffler, for offering me the opportunity to join his lab and work on challenging projects. His wealth of knowledge and infinite enthusiasm for science inspires me to move forward. What I value most is that he always encourages me to solve challenging research questions and helps me to be an independent scientist.

I would also like to say thanks to Dr. Jie Zhuang. He has made great contributions to the global engagement between UT and many institutions across the world. I was pretty fortunate to come to UT through an international program he established. As one of my committee members, he offered valuable suggestions for my research.

Next, I would like to thank Dr. Qiang He and Dr. Shawn R. Campagna. Thanks for serving on my Ph.D. committee. Your help, guidance, and suggestions not only kept me moving forward throughout my doctoral studies but also far beyond that.

Many thanks go to my collaborators Dr. Jeongdae Im and his student Nusrat Shobnam at Kansas State University. Our biweekly meetings have been very enriching and benefited my research. Thanks Dr. Lilin He at the Oak Ridge National Laboratory. Our collaborative work explored sorption and degradation processes at the nanoscale using advanced small-angle neutron scattering, a technique with broad utility in the environmental engineering field.

Thanks to the members of Dr. Löffler's lab. Thanks to Cynthia Swift for managing the lab, ordering supplies, and beyond. Thank you, Dr. Gao Chen, Dr. Yongchao Yin, Dr. Yongchao Xie, Dr. Amanda L. May, Dr. Fadime Kara-Murdoch, Dr. Robert W. Murdoch, Dr. Briana McDowell, Guang He, Qiao Chen, and Diana Ramirez, for supporting me and my research over the past five years.

Lastly, I would like to express my gratitude to my parents. Their unconditional love and endless support make me confident, brave, and strong. Thanks to my sister and her family for making my life full of happiness. Special thanks to my beloved wife Huihui Sun. We have been accompanying each other for over a decade. Her continued support and encouragement made tackling challenging tasks, overcoming difficulties, and successfully completing doctoral studies possible.

ABSTRACT

Bisphenol A (BPA), as well as its substitutes bisphenol S (BPS) and bisphenol AF (BPAF), are high production volume chemicals and potential endocrine disruptors. The oxidized manganese (Mn) species, soluble Mn(III) and solid Mn(IV) (i.e., MnO_2), are typically generated in Mn-cycling driven by Mn-oxidizing bacteria and Mn-reducing bacteria. MnO_2 is a strong oxidant capable of oxidizing a variety of organic contaminants including bisphenols. Soluble Mn(III) commonly occurs near oxic-anoxic interfaces and is an important environmental oxidant. Mn(III) is also associated with both biogenic and synthesized MnO_2. However, the effect of Mn(III) on the degradation of bisphenols is lacking. Mn-oxidizing bacteria effectively remove BPA through enzymatic reactions, which may also be capable of transforming BPA substitutes. Therefore, the present study conducted a series of experiments to demonstrate how Mn-cycling affects the fate of bisphenols. In addition, soluble Mn(III) was demonstrated to mediate BPA degradation. Mn(III) affected the reactivity of MnO_2 thereby affecting BPA degradation. Comparative studies of MnO_2- versus Mn(III)-mediated BPA degradation revealed the formation of distinct transformation products and mechanistic differences. Notably, soluble Mn(III), but not solid MnO_2, degraded adsorbed BPA, and small-angle neutron scattering experiments revealed that both adsorption and degradation of adsorbed BPA occurred in solid matrix pores. *Erythrobacter* sp. strain SD21, an Mn-oxidizing bacterium, effectively transformed BPA, and the BPA substitutes BPS and BPAF, in the absence of Mn. Hydroxylated bisphenol transformation products were detected, suggesting that hydroxylation is the initial step for bisphenol transformation. Genomic analysis of strain SD21 identified genes encoding monooxygenases and the inhibition experiment suggested that a monooxygenase was involved in the transformation of

BPA, BPS, and BPAF. The findings demonstrate that the fate of bisphenols is closely related to Mn-cycling, with crucial roles of Mn(II)-oxidizing microorganisms implicated in the formation of oxidized Mn species. Active Mn-cycling occurs near oxic-anoxic transition zones and the observation that bisphenols are susceptible to degradation/transformation by oxidized Mn species and Mn(II)-oxidizing bacteria has implications for predicting, and possibly managing, the fate and longevity of bisphenols in environmental systems.

Keywords: bisphenols, Mn-cycling, MnO_2, Mn(III), *Erythrobacter* sp. strain SD21, degradation, transformation.

TABLE OF CONTENTS

Chapter 1. Introduction **1**

1.1 Bisphenol A (BPA) **2**

1.1.1 Background on BPA 2

1.1.2 Toxicity of BPA 3

1.1.3 The environmental fate of BPA 3

1.2 BPA substitutes: bisphenol AF (BPAF) and bisphenol S (BPS) **4**

1.2.1 Background on BPAF and BPS 4

1.2.2 Toxicity of BPAF and BPS 5

1.2.3 The environmental fate of BPAF and BPS 6

1.3 Oxidized manganese (Mn) species **7**

1.3.1 Mn(IV) cycling and involved reactions 7

1.3.2 Mn(III) cycling and involved reactions 9

1.4 Degradation mechanisms of BPA, BPAF, and BPS **10**

1.4.1 Biotic degradation mechanisms 10

1.4.2 Abiotic degradation mechanisms 12

1.5 Rationale, hypotheses and research objectives **13**

References **16**

Appendix **29**

Chapter 2. The Role of Mn(III) in MnO_2-mediated Bisphenol A (BPA) Degradation **35**

2.1 Abstract **36**

2.2 Introduction **38**

2.3 Materials and Methods **40**

2.3.1 Chemicals 40

2.3.2 Preparation and characterization of soluble Mn(III), MnO_2, and surface-Mn(III)-free MnO_2 41

2.3.3 Oxidative degradation of BPA by soluble Mn(III), MnO_2, and surface-Mn(III)-free MnO_2 42
2.3.4 Detection of transformation intermediates 42
2.3.5 Incubation conditions 43
2.3.6 Analytical procedures 43
2.3.7 Quantum chemical calculations 44
2.3.8 Toxicity prediction 45
2.4 Results 45
2.4.1 Effect of Mn(III) on BPA degradation 45
2.4.2 Pyrophosphate extractable Mn(III) from MnO_2 46
2.4.3 Effect of surface-associated Mn(III) on BPA degradation 46
2.4.4 Identification of BPA transformation intermediates generated by soluble Mn(III) 47
2.4.5 Reaction schemes 49
2.5 Discussion 51
2.5.1 Contribution of Mn(III) in MnO_2-mediated BPA degradation 52
2.5.2 Theoretical considerations of MnO_2-mediated BPA degradation 53
2.5.3 BPA degradation products generated by Mn(III) 54
2.5.4 Environmental implications 56
References 58
Appendix 66
Chapter 3. Degradation of Adsorbed Bisphenol A (BPA) by Soluble Mn(III) 80
3.1 Abstract 81
3.2 Introduction 82
3.3 Materials and Methods 84
3.3.1 Chemicals 84
3.3.2 Soluble Mn(III) and MnO_2 preparation and quantification 85
3.3.3 Incubation conditions 86
3.3.4 Oxidative transformation of BPA by soluble Mn(III) and MnO_2 86

3.3.5 Adsorption experiments 87
3.3.6 Desorption kinetics 88
3.3.7 Degradation of BPA adsorbed to SPAC 88
3.3.8 Extraction procedures 89
3.3.9 SANS experiment and data analysis 89
3.3.10 Analytical procedures 91
3.4 Results 91
3.4.1 BPA degradation by oxidized Mn species 91
3.4.2 Adsorption isotherms 93
3.4.3 Degradation of BPA adsorbed to SPAC 93
3.4.4 Changes in pore size due to BPA adsorption and degradation 94
3.5 Discussion 97
3.5.1 BPA degradation by oxidized Mn species 98
3.5.2 Adsorption of BPA to activated carbon (SPAC) nanopores 98
3.5.3 SANS analysis of Mn(III)-treated SPAC 99
3.5.4 Environmental implications 101
References 103
Appendix 113
Chapter 4. Biotransformation of Bisphenols by *Erythrobacter* sp. Strain SD21 in the Absence of Manganese 126
4.1 Abstract 127
4.2 Introduction 129
4.3 Materials and Methods 131
4.3.1 Chemicals 131
4.3.2 Bacterial strain and growth condition 131
4.3.3 Biotransformation experiments 132
4.3.4 Intracellular or extracellular transformation 132
4.3.5 Transformation products identification 133

4.3.6 Functional analysis of the genome of the strain SD21 134
4.3.7 Phylogenetic analysis of the phenylalanine 4-monooxygenase 134
4.3.8 Monooxygenase inhibition experiments 134
4.3.9 Analytical procedures 135
4.3.10 Toxicity prediction 136
4.4 Results 136
4.4.1 Bisphenols biotransformation by the strain SD21 136
4.4.2 Inhibitory effects of BPS and BPAF on strain SD21 137
4.4.3 Intracellular biotransformation of bisphenols 138
4.4.4 Biotransformation products of bisphenols 138
4.4.5 Functional analysis of strain SD21 140
4.4.6 Azide inhibit bisphenols biotransformation 140
4.5 Discussion 141
4.5.1 Biotransformation of BPA, BPS, and BPAF by strain SD21 142
4.5.2 Mechanisms of bisphenols biotransformation by strain SD21 143
4.5.3 Toxicity evaluation of bisphenols transformation products 144
4.5.4 Environmental implications 145
References 147
Appendix 156
Chapter 5. Summary and Conclusion 166
Vita 170

LIST OF TABLES

Table 1.1. Physical and chemical properties of BPA, BPAF, and BPS summarized from previous studies. 29

Table 2.1. Removal of BPA (1.76 μmol) after 10- and 60-min incubation periods in the presence of 0.05, 0.25, and 1 mM of Mn(III), MnO_2, and surface-Mn(III)-free MnO_2. 66

Table 2.2. Accurate mass measurements of BPA transformation intermediates by UHPLC-HRMS/MS. 67

Table 2.3. Spin densities and charge densities on carbon and oxygen atoms of BPA and HCA radicals calculated by using Gaussian 09 program at the B3LYP/6-311** level. 68

Table 2.4. Predicted acute and chronic toxicity of BPA and its transformation products using the ECOSAR program. 69

Table 3.1. Radii of pore structure levels of SPAC, SPAC with adsorbed deuterated BPA, and SPAC after Mn(III)-mediated degradation of adsorbed deuterated BPA. 113

Table 3.2. Particle size distribution of SPAC and MnO_2. 113

Table 3.3. Modeling parameters of SANS profiles. 114

Table 4.1. The putative hydroxylase/monooxygenase encoded by *Erythrobacter* sp. strain SD21. 156

Table 4.2. Predicted acute and chronic toxicity of BPA, BPS, and BPAF, and their transformation products using the ECOSAR program. 157

LIST OF FIGURES

Figure 1.1. Chemical structures of BPA, BPAF, and BPS. 29

Figure 1.2. Summary of known pathways and intermediates in the processes of BPA degradation/transformation. 30

Figure 1.3. Summary of Mn cycling in environmental systems. 30

Figure 1.4. Electron flow in the BPA hydroxylation system and predicted enzymatic reaction of the P450bisd monooxygenase system. 31

Figure 1.5. Initiation of BPA degradation by *Sphingobium* sp. strain BiD32 (Simplified pathway). 31

Figure 1.6. Intermediates generated in BPAF biodegradation (data was collected from a prior study) 32

Figure 1.7. Proposed biodegradation pathway of BPS (Data were collected from several published studies). 33

Figure 1.8. The proposed reaction pathway for BPA treated by MnO_2 (Pathways were modified). 33

Figure 1.9. The proposed reaction pathways for BPAF (left) and BPS (right) treated by MnO_2 (Pathways were modified). 34

Figure 2.1. BPA degradation and HCA formation in the presence of various concentrations of soluble Mn(III). 70

Figure 2.2. Extraction of Mn(III) from MnO_2 with pyrophosphate. 71

Figure 2.3. BPA removal in the presence of various nominal concentrations of MnO_2 and surface-Mn(III)-free MnO_2. 72

Figure 2.4. Effect of MnO_2 and surface-Mn(III)-free MnO_2 loadings on BPA degradation rate constants. 73

Figure 2.5. Proposed reaction pathways for BPA degradation by Mn(III) in phosphate buffer (pH 7.2). 74

Figure 2.6. Frontier electron densities on carbon and oxygen atoms of BPA (A) and HCA (B) calculated by using Gaussian 09 program at the B3LYP/6-311** level. 75

Figure 3.1. BPA concentration profiles in the presence of different concentrations of oxidized Mn species. 115

Figure 3.2. Degradation of BPA adsorbed to SPAC by oxidized Mn species. 116

Figure 3.3. SANS profiles and data modelling. 117

Figure 4.1. BPA, BPS, and BPAF concentration profiles in strain SD21. 158

Figure 4.2. BPA, BPS, and BPAF concentration profiles in resting cell suspension and cell-free filtrate. 159

Figure 4.3. Biotransformation pathways of BPA, BPS, and BPAF by strain SD21. 160

Figure 4.4. Azide inhibits transformation of BPA, BPS, and BPAF. 161

Figure S2.1. HPLC-FLD chromatograms documenting the degradation of BPA to HCA. 76

Figure S2.2. Evidence for the formation of HCA as transformation intermediate. 76

Figure S2.3. BPA conversion efficiency to HCA in the presence of different concentrations of oxidized Mn species. 77

Figure S2.4. UHPLC-HRMS/MS detection of transformation intermediates (TI1-TI8) of BPA following Mn(III) treatment. 78

Figure S2.5. Charge densities on carbon and oxygen atoms of BPA (A) and HCA (B) calculated by using Gaussian 09 program at the B3LYP/6-311** level. 79

Figure S3.1. UV spectra of soluble Mn(III) (A) and BPA (B) analyzed with a PerkinElmer Lambda 35 UV-vis spectrophotometer. 118

Figure S3.2. Representative standard curve used to determine nominal MnO_2 concentrations in the incubation vessels. 119

Figure S3.3. XRD pattern of α-MnO_2 synthesized in the present study (red) and the standard XRD spectrum of α-MnO_2 (JCPDS 42-1169) (blue). 119

Figure S3.4. Representative standard curve for determining BPA concentrations. 120

Figure S3.5. Effect of dissolved Mn(III) (A) and MnO_2 (B) loadings on initial BPA degradation rate constants. 120

Figure S3.6. Mn(III)-mediated BPA degradation in incubation vessels with phosphate buffer (pH 7.2) with a starting concentration of 44 μM BPA monitored over a 15-day incubation period. 121

Figure S3.7. Adsorption characteristics of BPA to SPAC in systems without Mn. 121

Figure S3.8. Recovery of BPA from SPAC following organic solvent extraction as a function of time. 122

Figure S3.9. Desorption kinetics of BPA from SPAC at pH 6.0, 7.2 and 8.2. 123

Figure S3.10. Schematics of a SPAC particle featuring three micropores (level 1) and one macropore (level 2). 124

Figure S3.11. Decomposition of total scattering intensity into micropore and macropore levels. 125

Figure S4.1. Transformation rates of BPA, BPS, and BPAF by strain SD21..... 162

Figure S4.2. SD21 growth profiles in the presence of BPA, BPS, and BPAF. 163

Figure S4.3. Metabolic potential of strain SD21 to pyruvate and acetate based on the KEGG annotation..... 164

Figure S4.4. Amino acid sequence-based phylogenetic tree of selected phenylalanine 4-monooxygenase..... 165

Chapter 1. Introduction

1.1 Bisphenol A (BPA)

1.1.1 Background on BPA

Bisphenol A (4,4'-(propane-2,2-diyl) diphenol, BPA), firstly synthesized by the chemist Aleksandr Dianin in 1891, is an organic compound with two connected phenolic ring systems connected by a bridge carrying two methyl groups (Figure 1.1). BPA is a precursor in the manufacturing of polycarbonate plastics, epoxy resins, flame retardants, as well as other products (Staples et al., 1998; Im and Löffler, 2016). The global BPA market was about 8 million metric tons in 2016 and a further increase is projected (Experts, 2016). Approximately 65% of total BPA is used in the production of polycarbonate plastics, and 28% is used in the production of epoxy resins. The final products are mainly used as packaging material for food and drinks, coating on food cans, additives in thermal paper, adhesives, and antioxidants in plastics (Staples et al., 1998; Fromme et al., 2002; Zhang et al., 2013).

The release of BPA into the environment occurs mainly through two processes. BPA is either directly discharged from the manufacturing process or indirectly released from various end products that contain the BPA monomer or that are converted to BPA (Staples et al., 1998; Zhang et al., 2013). Due to widespread use and high volume production, BPA has been detected in various environmental matrices, ranging from 0.5−776 ng L^{-1} in surface water bodies (Fromme et al., 2002), 0.5−325 ng g^{-1} (dry weight) in soil (Huang et al., 2014), 0.20−39.1 μg g^{-1} (dry weight) in the dust (Liao et al., 2012b), and 1.49−13,370 ng g^{-1} (dry weight) in sediments (Liao et al., 2012a). BPA was also detected in human urine (0.88−5.08 ng mL^{-1}) (Yang et al., 2014; Xue et al., 2015) and serum (~2.91 ng mL^{-1}) (Cobellis et al., 2009). Given the globally increasing demand for BPA, the BPA concentration in environmental systems will continue to increase in the coming years.

1.1.2 Toxicity of BPA

The presence of BPA in environmental systems, as well as human bodies, has raised concerns to eco-toxicologists since the 1930s (Dodds and Lawson, 1936). Human epidemiological studies showed that BPA is an endocrine disruptor and BPA exposure has been linked to reproductive health (Fujimoto et al., 2011; Li et al., 2011), neurological disorder (Kajta and Wójtowicz, 2013), obesity (Shankar et al., 2012), and cardiovascular disease (Melzer et al., 2012a; Melzer et al., 2012b). For example, low μg per liter concentrations of BPA in the urine of women increased the risk of retarded fetal growth (Lee et al., 2008), showed a positive correlation to obesity (Shankar et al., 2012), and contributes to coronary artery stenoses (Melzer et al., 2012a). Therefore, the wide distribution and estrogenic properties of BPA have triggered considerable interest in its environmental fate (Staples et al., 1998; Zhang et al., 2013; Im and Löffler, 2016; Balgooyen et al., 2017; Sun et al., 2021).

1.1.3 The environmental fate of BPA

Several biotic and abiotic processes are known to degrade and transform BPA that has entered the environmental systems (Figure 1.2). BPA can be degraded and transformed under oxic conditions by bacteria (Zhang et al., 2013), fungi (Chen et al., 2016b), and algae (Eio et al., 2015); however, microbial degradation under anoxic conditions has not been observed (Im and Löffler, 2016). BPA is susceptible to abiotic degradation mediated by Mn(IV) oxide mineral phases (Lin et al., 2009; Im et al., 2015; Balgooyen et al., 2017), photodegradation (Ju et al., 2018), and advanced oxidation using hydroxyl radicals (Zhang et al., 2019). A number of studies have documented abiotic BPA degradation and 4-hydroxycumyl alcohol (HCA) was identified as a major intermediate (Lin et al., 2009; Nakamura et al., 2011; Im et al., 2015; Balgooyen et al.,

2017). Of note, complete mineralization of BPA to CO_2 has been reported in the reaction with solid MnO_2 (Im et al., 2015).

With a log K_{ow} of 3.32−3.4, an aqueous solubility of 300 mg L^{-1} at 25°C, and Henry's constant of 1.0×10^{-10} atm m^3 mol^{-1} (Table 1.1), BPA is not volatile at ambient temperature and has a high tendency for sorption to soil and sediment, in which oxygen is often deficient. Therefore, knowledge about the processes that affect the fate and longevity of BPA under anoxic conditions is relevant for predicting potential BPA exposure to humans. In addition, a number of microbes degrade BPA in the presence of oxygen; however, the anaerobic microbial metabolism of BPA has not been demonstrated. Abiotic degradation of BPA has been observed with MnO_2 as an oxidant, a reaction that does not require oxygen and can occur under oxic and anoxic conditions (Im et al., 2015).

1.2 BPA substitutes: bisphenol AF (BPAF) and bisphenol S (BPS)

1.2.1 Background on BPAF and BPS

Widespread use of BPA has led to ubiquitous environmental contamination and human exposure. BPA exhibits endocrine-disrupting activity in mammals and is of human health concern (Fujimoto et al., 2011; Li et al., 2011; Shankar et al., 2012; Kajta and Wójtowicz, 2013; Kinch et al., 2015). Since the 2000s, many developed countries gradually replaced BPA by its analogues, bisphenol AF (BPAF) and bisphenol S (BPS), especially in the manufacture of thermal receipts, food and drink packaging, and the coatings of food cans (NITE, 2003; Stout, 2008; Simoneau et al., 2011; Grignard et al., 2012).

BPAF and BPS are structurally similar to BPA (Figure 1.1), but the two substitutes have higher thermal stability than BPA due to the trifluoromethyl group in BPAF and the sulfonyl

group in BPS. Due to the restriction on the use of BPA, the production and consumption of BPAF and BPS have increased. The annual production of BPAF was approximately 10,000−50,000 pounds in the U.S. (Stout, 2008); the production of BPS reached 10,000 tons in Europe (ECHA, 2015). Recent studies have reported the occurrence of BPAF and BPS in various environmental systems as well as in human urine samples. BPAF was detected in freshwater with a concentration of up to 15.3 μg L^{-1} (Song et al., 2012), in sediments with a concentration of up to 4.23 ng g^{-1} (dry weight) (Liao et al., 2012b), in sludge with the concentration of 0.42−45.1 ng g^{-1} (dry weight) (Song et al., 2014), and in dust with the concentration of up to 739 ng g^{-1} (Liao et al., 2012a; Song et al., 2012). BPS has been detected in thermal receipts (mean: 0.181 mg g^{-1}) (Liao et al., 2012c), sediments (mean: 12.37 ng g^{-1}) (Liao et al., 2012b), dust (mean: 0.36 μg g^{-1}) (Liao et al., 2012a), as well as sludge (4.34 μg g^{-1}) (Song et al., 2014). Also, BPS has been detected in 81% of human urine samples in the United States as well as in some Asian countries with an average level of 0.168 μg L^{-1} (Liao et al., 2012d). BPAF was detected at a lower frequency and present in less than 3% of the total urinary samples collected from adults in the United States (Ye et al., 2015).

1.2.2 Toxicity of BPAF and BPS

Although BPAF and BPS are widely used in the production of "BPA-free" products, public concern was raised about using structural analogues of BPA that are now environmental contaminants. Recently, a number of studies reported that BPAF and BPS exhibit estrogenic effects comparable to BPA. Exposure to BPAF could cause genotoxicity (Fic et al., 2015), inhibit the androgenic activity of 5*α*-dihydrotestosterone (Kitamura et al., 2005), and BPAF exhibits a strong binding affinity to the estrogen receptor ER*α* (Matsushima et al., 2010). The adverse effects of BPS have been linked to reproductive issues (Gingrich et al., 2019),

neurodevelopment (Kinch et al., 2015), gene expression (Rezg et al., 2019), and obesity (Chen et al., 2016a). Given that BPAF and BPS have been widely used as substitutes for BPA and the production will continue to increase, the fate and longevity of BPAF and BPS in environmental systems require urgent attention.

1.2.3 The environmental fate of BPAF and BPS

The increasing production of BPA substitutes with potential estrogenic properties have triggered interest in the environmental fate of BPAF and BPS. Although the application of BPAF as a monomer in the production of polycarbonate plastic can increase chemical and thermal stability, BPAF exhibited resistance to chemical and biological degradation, presumably due to the high stability of the trifluoromethyl groups (Choi and Lee, 2017; Li et al., 2018). Previous studies documented that BPAF was recalcitrant to photo-degradation, whereas its degradation required additional conditions, such as cooccurrence of natural organic matters or exogenous energy (e.g., ultrasound) (Wang et al., 2020). Similar to the reaction between BPA and MnO_2, BPAF can also react with MnO_2, but its half-life is approximately 20 times longer than that of BPA (Li et al., 2018). Biodegradation is an important process controlling the fate of organic contaminants in the environmental systems. However, few studies documented the biodegradation of BPAF and degradation by axenic cultures have not been reported. BPAF has higher persistence than BPA and other analogues in wastewater treatment plants, lake water, and soils, and BPAF has a longer half-life than other bisphenols (Choi and Lee, 2017; Sun et al., 2017; Zhou et al., 2020). Moreover, the trifluoromethyl groups are stable and existed in all detected transformation products, and these fluorinated compounds may also threaten environmental and human health (Solomon et al., 2016).

BPS is one of the most frequently detected BPA analogues in the environment, and advanced oxidation processes (AOPs) and biodegradation are the two major approaches responsible for its removal (Fang et al., 2020). Previous experimental efforts demonstrated that BPS can be effectively removed through UV-based oxidation (Cao et al., 2012; Park and Kim, 2012), sulfate radical-based oxidation (Shao et al., 2017a), photocatalysis (Shao et al., 2017b), ferrate oxidation (Yang et al., 2019), as well as other processes (Li et al., 2018). Such chemical methods cannot fully mineralize BPS to CO_2, and some intermediates have the potential to adversely impact the ecosystem and human health. In addition, biological degradation of BPS has been documented in soil, river water, and wastewater treatment plant (Choi and Lee, 2017; Sun et al., 2017; Frankowski et al., 2020). The degradation of BPS is through phenolic ring hydroxylation and meta-cleavage, which is independent of the central sulfonyl group that connects the two phenolic rings (Choi and Lee, 2017). To date, only one axenic culture, *Sphingobium fuliginis* strain OMI, has been reported to remove BPS, but the degradation products, as well as the mechanisms, have not been elucidated (Ogata et al., 2013).

1.3 Oxidized manganese (Mn) species

1.3.1 Mn(IV) cycling and involved reactions

Following iron and titanium, manganese (Mn) is the third most abundant transition metal and commonly occurs in three oxidation states, Mn(II), Mn(III), and Mn(IV) (Sigel, 2000). Mn cycles among these three oxidation states through oxidation, reduction, disproportionation, and conproportionation reactions (Figure 1.3). Microbial oxidation via one-step electron transfer of Mn(II) is a primary process leading to the formation of Mn(IV), typically in the form of MnO_2. Under oxic conditions, diverse microorganisms, including members of the *Actinobacteria*, *Firmicutes*, and *Alpha-*, *Beta-* and *Gammaproteobacteria* contribute to the formation of MnO_2

(Hansel, 2017). Mn(II) oxidation is not limited to oxic environments and can occur without oxygen in the presence of light (Daye et al., 2019; Yu and Leadbetter, 2020). Biologically Mn oxidation through direct and indirect enzymatic reactions (Francis and Tebo, 2001; Learman et al., 2011; Geszvain et al., 2016). Two extensively studied Mn-oxidizing bacteria, *Erythrobacter* sp. strain SD-21 and *Pseudomonas putida* strain GB-1, expressed peroxidase cyclooxygenases and multicopper oxidase that can directly oxidize Mn(II) to MnO_2; however, *Roseobacter* sp. strain Azwk-3b indirectly oxidizes Mn(II) through the enzymatic generation of extracellular superoxide radicals (Learman et al., 2011).

MnO_2 is a reactive mineral with high oxidation potential ($E_H^o{}_{(Mn(IV)/Mn(II))}$ = 1.23 V) and is capable of oxidizing various types of organic compounds (Beal et al., 2009; Im et al., 2015; Huang et al., 2018). Systematic studies investigating the mechanisms of the MnO_2-involved reactions have improved our understanding of MnO_2 reactivity (Remucal and Ginder-Vogel, 2014). The key process is the interactions between the surface sites of MnO_2 and the reductant. Experimental evidence in the oxidation of phenols by MnO_2 suggests that the formation of surface complexes is the most important step in controlling the reaction rate (Stone and Morgan, 1984). The phase structure of MnO_2 is another factor that could affect the rate of the reactions (Huang et al., 2018). δ-MnO_2 showed the highest oxidation rate of BPA while the reaction rate by β-MnO_2 was the lowest. Interestingly, the spectroscopic analysis demonstrated that δ-MnO_2 has a higher Mn(III) (~36%) content than β-MnO_2 (~20%) (Huang et al., 2018).

MnO_2 commonly occurs in soils and sediments (Burdige, 1993; Post, 1999). Average natural levels of soil Mn range from 300 to 600 mg kg^{-1} (dry weight) (Saric, 1986). Considering the typical percentage of the oxidizable fraction of Mn is approximately 20% (Habibah et al., 2014), the concentration of soil manganese oxides ranges from 60 to 120 mg kg^{-1}. In addition, MnO_2 is

abundant in natural sediments, and 26−348 mg L^{-1} of MnO_2 have been reported in freshwater sediments (Kepkay, 1985; Sigg et al., 1987), and 2−16 mg L^{-1} in the surface layer of marine sediments (Vandieken et al., 2012). Most studies used a nominal MnO_2 concentration of less than 2 mM (~174 mg L^{-1}) (Lin et al., 2009; Im et al., 2015; Balgooyen et al., 2017; Li et al., 2018), which is in the range of MnO_2 levels reported in natural soils and sediments.

1.3.2 Mn(III) cycling and involved reactions

Mn(III) can be formed via the oxidation of Mn(II) (Webb et al., 2005), the one-electron reduction of Mn(IV) (Lin et al., 2012), and a conproportionation reaction between Mn(II) and Mn(IV) (Figure 1.3) (Webb et al., 2005; Liu et al., 2019). Mn(III) is prone to disproportionation to yield dissolved Mn(II) and solid Mn(IV) and is assumed to be short-lived, which has led to a general underappreciation of Mn(III) in the traditional paradigm of Mn redox cycling (Johnson, 2006). Several studies have now demonstrated that soluble Mn(III) commonly occurs near oxic-anoxic interfaces (Trouwborst et al., 2006; Madison et al., 2013; Oldham et al., 2017). Enzymatic processes involved in Mn(II) oxidation and MnO_2 reduction also generate stable Mn(III) in the presence of ligands (e.g., pyrophosphate, citrate, oxalate) (Learman et al., 2011; Wright et al., 2018).

Similar to MnO_2, Mn(III) is also an important environmental oxidant ($E_H^o{}_{(Mn(III)/Mn(II))}$ = 1.56 V) (Skoog and West, 1982). Mn(III) has been shown to oxidize a variety of organic compounds including lignin (Jones et al., 2018), atrazine (Hu et al., 2017), chlorophenol (Hu et al., 2017), and ciprofloxacin (Sun et al., 2015), as well as inorganics such as the radionuclide uranium(IV) (Wang et al., 2014). The reactions between Mn(III) and organic compounds are quite complicated, but there are two main mechanisms (Hu et al., 2017). First, the non-oxidative

reactions between free Mn(III) and organic contaminants, such as the *β*-elimination of atrazine. Second, the Mn(III) ligand complexes mediate oxidative transformation reactions.

In hemipelagic sediments, soluble Mn(III) concentrations of 12−82 μM were measured, which constituted up to 90% of the total dissolved Mn pool (i.e., Mn[II] + Mn[III]) (Madison et al., 2013). In addition, Mn(III) commonly occurs in biogenic MnO_2 with relative abundances ranging from 7.1 to 30% (Villalobos et al., 2003; Yu et al., 2012; Zhang et al., 2019) and in synthetic MnO_2 with reported Mn(III) contents of 21.4−36.6% (Huang et al., 2018). Therefore, Mn(III) may play a role in the reactions observed when MnO_2 was used as a catalyst. Indeed, a few studies have demonstrated that Mn(III) contained in MnO_2 plays a role as an oxidant in reactions mediated by MnO_2 (Nico and Zasoski, 2000; 2001; Chen et al., 2013; Huang et al., 2018).

1.4 Degradation mechanisms of BPA, BPAF, and BPS

1.4.1 Biotic degradation mechanisms

BPA in environmental systems can be degraded by a variety of microorganisms under oxic conditions (Dorn et al., 1987; Staples et al., 1998). The first bacterial isolate documented to degrade BPA was *Sphingomonas* sp. strain MV1 which was isolated from activated sludge (Lobos et al., 1992). As of 2021, 25 genera have been reported to harbor species able to degrade BPA under aerobic conditions (Im and Löffler, 2016; Santana De et al., 2019; Shobnam et al., 2021). Microbial BPA degradation pathways have been exhaustively investigated, and previous efforts documented four types of enzymes responsible for initiating BPA degradation, including cytochrome P450, laccase, *p*-hydroxybenzoate hydroxylase, and ammonia monooxygenase (Sasaki et al., 2005; Kolvenbach et al., 2007; Roh et al., 2009; Telke et al., 2009; Zhou et al., 2015).

The first three enzymes were identified in pure cultures capable of BPA degradation. *Sphingomonas* sp. strain AO1 cultures expressing the cytochrome P450 system were able to degrade BPA. Bioinformatic analysis identified the *bisdA* and *bisdB* genes encoding cytochrome P450 and ferredoxin (Sasaki et al., 2005). In the presence of purified P450 monooxygenase, BPA was predicted that either a carbon atom of a methyl group or the quaternary carbon is attacked by water and then hydroxylated (Figure 1.4) (Sasaki et al., 2005). *Pseudomonas* sp. strain LBC1 produces extracellular laccase capable of BPA degradation (Telke et al., 2009). The laccase purified from strain LBC1 readily mediated BPA transformation with higher efficiency than laccases secreted from eukaryotic organisms. Fourteen intermediates were identified in laccase-mediated BPA degradation (Telke et al., 2009). The third enzyme implicated in BPA transformation is *p*-hydroxybenzoate hydroxylase encoded by *Sphingobium* sp. BiD32 (Zhou et al., 2015). The first step of BPA degradation catalyzed by *p*-hydroxybenzoate hydroxylase is the hydroxylation of BPA to 1,2-bis(4-hydroxyphenyl)-2-propanol (Figure 1.5), which is identical to the first step of cytochrome P450 mediated BPA degradation. Then, the carbon-carbon bond of 1,2-bis(4-hydroxyphenyl)-2-propanol was broken leading to the formation of intermediates with a single aromatic ring. Subsequent enzymatic conversions include hydroxylation and ring cleavage (Zhou et al., 2015).

Biological degradation of BPAF and BPS has been documented in soil, river water, and wastewater treatment plant samples (Choi and Lee, 2017; Sun et al., 2017; Frankowski et al., 2020; Zhou et al., 2020). To date, no axenic cultures with the ability to degrade BPAF have been obtained, and only a single axenic culture, *Sphingobium fuliginis* strain OMI, has been described to degrade BPS (Ogata et al., 2013).

The first study documenting aerobic BPAF degradation in soil was published in 2017 (Choi and Lee, 2017). The half-life of BPAF was substantially (about 24 times) longer than the half-life of BPA under the same incubation conditions. LC-MS analysis identified eight intermediates during BPAF degradation (Figure 1.6). Firstly, the central carbon carrying the two trifluoromethyl groups remained intact in all intermediates indicating that oxidation of polyfluorinated alkyl metabolites did not occur. Secondly, the degradation pathway proposed based on the detected intermediates inferred that BPAF degradation followed a meta-cleavage pathway. However, several studies reported that BPAF resisted degradation in some water systems and sediments (Sun et al., 2017; Zhou et al., 2020). BPAF is more recalcitrant than BPA, and the formation of stable polyfluorinated intermediates as a result of BPAF transformation is an environmental concern.

Similar to BPAF, the study on the biodegradation of BPS is mainly concentrated in environmental-related systems (Choi and Lee, 2017; Sun et al., 2017; Zhou et al., 2020). The degradation occurred through phenolic ring hydroxylation and meta-cleavage, which is independent of the central sulfonyl group that connects the two phenolic rings (Figure 1.7) (Choi and Lee, 2017).

1.4.2 Abiotic degradation mechanisms

The first systematic study investigating BPA degradation by MnO_2 was published in 2009 (Lin et al., 2009). Typically, each abiotic redox reaction is composed of three indispensable steps including pre-reaction complex formation, electron transfer, and postreaction complex break up (Nico and Zasoski, 2000). Therefore, the oxidation of BPA by MnO_2 involves complex formation, electron transfer, and complex dissociation (Lin et al., 2009). During this process, BPA loses one electron leading to the formation of several radical species due to resonance

(Figure 1.8). Some of the radicals react to form dimers through C-C or C-O coupling reactions. Also, some radicals can be further oxidized to form intermediates with lower molecular weights. Among 11 identified intermediates (Lin et al., 2009), 4-hydroxycumyl alcohol (HCA) was a major intermediate and up to 60% of BPA was recovered as HCA (Im et al., 2015). Mineralization of BPA to CO_2 by MnO_2 was also observed, indicating that MnO_2 could alleviate environmental concerns associated with BPA (Im et al., 2015).

Due to the trifluoromethyl group in BPAF and sulfonyl group in BPS, abiotic degradation of these two bisphenols generally required higher energy or extreme conditions (Fang et al., 2020; Wang et al., 2020). Previous studies documented that BPAF was recalcitrant to photo-degradation, but degradation was observed in the presence of natural organic matter or exogenous energy (e.g., ultrasound) (Wang et al., 2020). BPS can be effectively removed through UV-based oxidation (Cao et al., 2012; Park and Kim, 2012), sulfate radical-based oxidation (Shao et al., 2017a), photocatalysis (Shao et al., 2017b), ferrate oxidation (Yang et al., 2019), as well as other processes (Li et al., 2018). However, only one study reported BPAF and BPS degradation by MnO_2 without the need of exogenous energy input (Li et al., 2018). Similar to BPA, BPAF or BPS oxidation by MnO_2 resulted in the formation of radicals through the loss of a single electron. These radicals can form coupling products or undergo further oxidation by MnO_2 (Figure 1.9) (Li et al., 2018).

1.5 Rationale, hypotheses and research objectives

MnO_2, an environmentally relevant oxidant, is involved in many biogeochemical processes. MnO_2 can be generated by aerobic Mn(II)-oxidizing bacteria or it can be directly generated by anaerobes (Learman et al., 2011; Daye et al., 2019; Yu and Leadbetter, 2020). An intermediate,

Mn(III) is generated during both aerobic and anoxic Mn(II) oxidation and anoxic Mn(IV) reduction involving two consecutive one-electron transfer reactions (Webb et al., 2005; Lin et al., 2012). In natural environmental systems, the oxic-anoxic interface is a hotspot for Mn cycling, where soluble Mn(III) is abundant and stable (Trouwborst et al., 2006; Madison et al., 2013). Recent studies demonstrated that Mn(III) easily accepts one electron and oxidizes a variety of organic compounds (Sun et al., 2015; Hu et al., 2017; Jones et al., 2018). BPA resists microbial degradation under anoxic conditions and anoxic sediments represent a reservoir of BPA (Im and Löffler, 2016). Therefore, knowledge about the effect of Mn(III) on the fate of BPA will expand our understanding of BPA's natural attenuation potential. Aerobic microbial Mn oxidation is a key process for Mn cycling and can be studied in axenic cultures. For example, *Erythrobacter* sp. strain SD21 (Francis and Tebo, 2001), *Roseobacter* sp. Strain Azwk-3b (Learman et al., 2011), and *Pseudomonas putida* strain GB-1 (Geszvain et al., 2016) serve as model organisms to study Mn(II) oxidation. The availability of aerobic Mn(II) oxidizing bacterial cultures offers the opportunity to explore direct and coupled biotic-abiotic degradation of BPA and its substitutes in more detail.

The current research is based on the following hypotheses:

Hypothesis 1: Mn(III), an environmentally relevant oxidant, can participate in BPA degradation. Mn(III)-rich MnO_2 mediated BPA degradation is a combination effect of Mn(III) and Mn(IV).

Hypothesis 2: Sorbed BPA can be degraded by soluble Mn(III) but not by solid MnO_2.

Hypothesis 3: *Erythrobacter* sp. strain SD21 transformed BPA biologically, which may also transform BPA substitutes, BPS and BPAF, due to the similar molecular structure.

The research objectives, based on the hypotheses, are as follows:

Objective 1: To demonstrate if soluble Mn(III) degrades BPA and if it affects Mn(III)-rich MnO_2 mediated BPA degradation.

Objective 2: To explore if oxidized Mn species, solid MnO_2 and soluble Mn(III), degrade adsorbed BPA or if the reactivity is limited to dissolved phase BPA.

Objective 3: To investigate if the Mn-oxidizing bacterium that is capable of transforming BPA can also transform BPS and BPAF.

References

Balgooyen, S., Alaimo, P.J., Remucal, C.K. and Ginder-Vogel, M. 2017. Structural transformation of MnO_2 during the oxidation of bisphenol A. Environ. Sci. Technol. 51(11), 6053-6062.

Beal, E.J., House, C.H. and Orphan, V.J. 2009. Manganese- and iron-dependent marine methane oxidation. Science 325(5937), 184-187.

Burdige, D.J. 1993. The biogeochemistry of manganese and iron reduction in marine sediments. Earth-Sci. Rev. 35(3), 249-284.

Cao, G., Lu, J. and Wang, G. 2012. Photolysis kinetics and influencing factors of bisphenol S in aqueous solutions. J. Environ. Sci. 24(5), 846-851.

Chen, D., Kannan, K., Tan, H., Zheng, Z., Feng, Y.-L., Wu, Y. and Widelka, M. 2016a. Bisphenol analogues other than BPA: environmental occurrence, human exposure, and toxicity: a review. Environ. Sci. Technol. 50(11), 5438-5453.

Chen, W., Liu, C., Boyd, S.A., Teppen, B.J. and Li, H. 2013. Reduction of carbadox mediated by reaction of Mn(III) with oxalic acid. Environ. Sci. Technol. 47(3), 1357-1364.

Chen, Y., Stemple, B., Kumar, M. and Wei, N. 2016b. Cell surface display fungal laccase as a renewable biocatalyst for degradation of persistent micropollutants bisphenol A and sulfamethoxazole. Environ. Sci. Technol. 50(16), 8799-8808.

Choi, Y.J. and Lee, L.S. 2017. Aerobic soil biodegradation of bisphenol (BPA) alternatives bisphenol S and bisphenol AF compared to BPA. Environ. Sci. Technol. 51(23), 13698-13704.

Cobellis, L., Colacurci, N., Trabucco, E., Carpentiero, C. and Grumetto, L. 2009. Measurement of bisphenol A and bisphenol B levels in human blood sera from healthy and endometriotic women. Biomed. Chromatogr. 23(11), 1186-1190.

Daye, M., Klepac-Ceraj, V., Pajusalu, M., Rowland, S., Farrell-Sherman, A., Beukes, N., Tamura, N., Fournier, G. and Bosak, T. 2019. Light-driven anaerobic microbial oxidation of manganese. Nature 576(7786), 311-314.

Dodds, E. and Lawson, W. 1936. Synthetic estrogenic agents without the phenanthrene nucleus. Nature 137, 996.

Dorn, P.B., Chou, C.-S. and Gentempo, J.J. 1987. Degradation of bisphenol A in natural waters. Chemosphere 16(7), 1501-1507.

ECHA 2015. Bisphenol S registration data, European Chemicals Agency, Finland.

Eio, E.J., Kawai, M., Niwa, C., Ito, M., Yamamoto, S. and Toda, T. 2015. Biodegradation of bisphenol A by an algal-bacterial system. Environ. Sci. Pollut. Res. 22(19), 15145-15153.

Experts, I. 2016. Bisphenol-A - A Global Market Overview.

Fang, Z., Gao, Y., Wu, X., Xu, X., Sarmah, A.K., Bolan, N., Gao, B., Shaheen, S.M., Rinklebe, J. and Ok, Y.S. 2020. A critical review on remediation of bisphenol S (BPS) contaminated water: Efficacy and mechanisms. Crit. Rev. Environ. Sci. Technol. 50(5), 476-522.

Fic, A., Mlakar, S.J., Juvan, P., Mlakar, V., Marc, J., Dolenc, M.S., Broberg, K. and Mašič, L.P. 2015. Genome-wide gene expression profiling of low-dose, long-term exposure of human osteosarcoma cells to bisphenol A and its analogs bisphenols AF and S. Toxicol. In Vitro 29(5), 1060-1069.

Francis, C.A. and Tebo, B.M. 2001. Enzymatic manganese (II) oxidation by a marine α-proteobacterium. Appl. Environ. Microbiol. 67(9), 4024-4029.

Frankowski, R., Zgoła-Grześkowiak, A., Smułek, W. and Grześkowiak, T. 2020. Removal of bisphenol A and its potential substitutes by biodegradation. Appl. Biochem. Biotechnol., 1-11.

Fromme, H., Küchler, T., Otto, T., Pilz, K., Müller, J. and Wenzel, A. 2002. Occurrence of phthalates and bisphenol A and F in the environment. Water Res. 36(6), 1429-1438.

Fujimoto, V.Y., Kim, D., vom Saal, F.S., Lamb, J.D., Taylor, J.A. and Bloom, M.S. 2011. Serum unconjugated bisphenol A concentrations in women may adversely influence oocyte quality during in vitro fertilization. Fertil. Steril. 95(5), 1816-1819.

Geszvain, K., Smesrud, L. and Tebo, B.M. 2016. Identification of a third Mn (II) oxidase enzyme in *Pseudomonas putida* GB-1. Appl. Environ. Microbiol. 82(13), 3774-3782.

Gingrich, J., Pu, Y., Ehrhardt, R., Karthikraj, R., Kannan, K. and Veiga-Lopez, A. 2019. Toxicokinetics of bisphenol A, bisphenol S, and bisphenol F in a pregnancy sheep model. Chemosphere 220, 185-194.

Grignard, E., Lapenna, S. and Bremer, S. 2012. Weak estrogenic transcriptional activities of bisphenol A and bisphenol S. Toxicol. In Vitro 26(5), 727-731.

Habibah, J., Khairiah, J., Ismail, B. and Kadderi, M. 2014. Manganese speciation in selected agricultural soils of peninsular Malaysia. Am. J. Environ. Sci. 10(2), 148.

Hansel, C.M. (2017) Adv. Microb. Physiol., pp. 37-83, Elsevier.

Hu, E., Zhang, Y., Wu, S., Wu, J., Liang, L. and He, F. 2017. Role of dissolved Mn(III) in transformation of organic contaminants: non-oxidative versus oxidative mechanisms. Water Res. 111, 234-243.

Huang, D., Zhao, H., Liu, C. and Sun, C. 2014. Characteristics, sources, and transport of tetrabromobisphenol A and bisphenol A in soils from a typical e-waste recycling area in South China. Environ. Sci. Pollut. Res. 21(9), 5818-5826.

Huang, J., Zhong, S., Dai, Y., Liu, C.-C. and Zhang, H. 2018. Effect of MnO_2 phase structure on the oxidative reactivity toward bisphenol A degradation. Environ. Sci. Technol. 52(19), 11309-11318.

Im, J. and Löffler, F.E. 2016. Fate of bisphenol A in terrestrial and aquatic environments. Environ. Sci. Technol. 50(16), 8403-8416.

Im, J., Prevatte, C.W., Campagna, S.R. and Löffler, F.E. 2015. Identification of 4-hydroxycumyl alcohol as the major MnO_2-mediated bisphenol A transformation product and evaluation of its environmental fate. Environ. Sci. Technol. 49(10), 6214-6221.

Johnson, K.S. 2006. Manganese redox chemistry revisited. Science 313(5795), 1896-1897.

Jones, M.E., Nico, P.S., Ying, S., Regier, T., Thieme, J.r. and Keiluweit, M. 2018. Manganese-driven carbon oxidation at oxic–anoxic interfaces. Environ. Sci. Technol. 52(21), 12349-12357.

Ju, L., Wu, P., Yang, Q., Ahmed, Z. and Zhu, N. 2018. Synthesis of ZnAlTi-LDO supported C60@ AgCl nanoparticles and their photocatalytic activity for photo-degradation of bisphenol A. Appl. Catal. B. 224, 159-174.

Kajta, M. and Wójtowicz, A.K. 2013. Impact of endocrine-disrupting chemicals on neural development and the onset of neurological disorders. Pharmacol. Rep. 65(6), 1632-1639.

Kepkay, P.E. 1985. Kinetics of microbial manganese oxidation and trace metal binding in sediments: Results from an in situ dialysis technique. Limnol. Oceanogr. 30(4), 713-726.

Kinch, C.D., Ibhazehiebo, K., Jeong, J.-H., Habibi, H.R. and Kurrasch, D.M. 2015. Low-dose exposure to bisphenol A and replacement bisphenol S induces precocious hypothalamic neurogenesis in embryonic zebrafish. Proc. Natl. Acad. Sci. U. S. A. 112(5), 1475-1480.

Kitamura, S., Suzuki, T., Sanoh, S., Kohta, R., Jinno, N., Sugihara, K., Yoshihara, S.i., Fujimoto, N., Watanabe, H. and Ohta, S. 2005. Comparative study of the endocrine-disrupting activity of bisphenol A and 19 related compounds. Toxicol. Sci. 84(2), 249-259.

Kolvenbach, B., Schlaich, N., Raoui, Z., Prell, J., Zühlke, S., Schäffer, A., Guengerich, F. and Corvini, P. 2007. Degradation pathway of bisphenol A: does *ipso* substitution apply to phenols containing a quaternary α-carbon structure in the *para* position? Appl. Environ. Microbiol. 73(15), 4776-4784.

Learman, D., Voelker, B., Vazquez-Rodriguez, A. and Hansel, C. 2011. Formation of manganese oxides by bacterially generated superoxide. Nature Geoscience 4(2), 95-98.

Lee, B., Ha, E., Park, H., Kim, B., Seo, J., Chang, M., Ha, M., Kim, Y., Roh, Y. and Hong, Y. 2008. Exposure to bisphenol A in pregnant women and early fetal growth. Epidemiology 19(6), S365.

Li, D.-K., Zhou, Z., Miao, M., He, Y., Wang, J., Ferber, J., Herrinton, L.J., Gao, E. and Yuan, W. 2011. Urine bisphenol-A (BPA) level in relation to semen quality. Fertil. Steril. 95(2), 625-630. e624.

Li, J., Pang, S., Zhou, Y., Sun, S., Wang, L., Wang, Z., Gao, Y., Yang, Y. and Jiang, J. 2018. Transformation of bisphenol AF and bisphenol S by manganese dioxide and effect of iodide. Water Res. 143, 47-55.

Liao, C., Liu, F., Alomirah, H., Loi, V.D., Mohd, M.A., Moon, H.-B., Nakata, H. and Kannan, K. 2012d. Bisphenol S in urine from the United States and seven Asian countries: occurrence and human exposures. Environ. Sci. Technol. 46(12), 6860-6866.

Liao, C., Liu, F., Guo, Y., Moon, H.-B., Nakata, H., Wu, Q. and Kannan, K. 2012a. Occurrence of eight bisphenol analogues in indoor dust from the United States and several Asian countries: implications for human exposure. Environ. Sci. Technol. 46(16), 9138-9145.

Liao, C., Liu, F. and Kannan, K. 2012c. Bisphenol S, a new bisphenol analogue, in paper products and currency bills and its association with bisphenol A residues. Environ. Sci. Technol. 46(12), 6515-6522.

Liao, C., Liu, F., Moon, H.-B., Yamashita, N., Yun, S. and Kannan, K. 2012b. Bisphenol analogues in sediments from industrialized areas in the United States, Japan, and Korea: spatial and temporal distributions. Environ. Sci. Technol. 46(21), 11558-11565.

Lin, H., Szeinbaum, N.H., DiChristina, T.J. and Taillefert, M. 2012. Microbial Mn(IV) reduction requires an initial one-electron reductive solubilization step. Geochim. Cosmochim. Acta. 99, 179-192.

Lin, K., Liu, W. and Gan, J. 2009. Oxidative removal of bisphenol A by manganese dioxide: efficacy, products, and pathways. Environ. Sci. Technol. 43(10), 3860-3864.

Liu, W., Sun, B., Qiao, J. and Guan, X. 2019. Influence of pyrophosphate on the generation of soluble Mn(III) from reactions involving Mn oxides and Mn(VII). Environ. Sci. Technol. 53(17), 10227-10235.

Lobos, J.H., Leib, T. and Su, T.-M. 1992. Biodegradation of bisphenol A and other bisphenols by a gram-negative aerobic bacterium. Appl. Environ. Microbiol. 58(6), 1823-1831.

Madison, A.S., Tebo, B.M., Mucci, A., Sundby, B. and Luther, G.W. 2013. Abundant porewater Mn(III) is a major component of the sedimentary redox system. Science 341(6148), 875-878.

Matsushima, A., Liu, X., Okada, H., Shimohigashi, M. and Shimohigashi, Y. 2010. Bisphenol AF is a full agonist for the estrogen receptor ERα but a highly specific antagonist for ERβ. Environ. Health Perspect. 118(9), 1267-1272.

Melzer, D., Gates, P., Osborn, N.J., Henley, W.E., Cipelli, R., Young, A., Money, C., McCormack, P., Schofield, P. and Mosedale, D. 2012a. Urinary bisphenol A concentration and angiography-defined coronary artery stenosis. PLoS One 7(8), e43378.

Melzer, D., Osborne, N.J., Henley, W.E., Cipelli, R., Young, A., Money, C., McCormack, P., Luben, R., Khaw, K.-T. and Wareham, N.J. 2012b. Urinary bisphenol A concentration and risk of future coronary artery disease in apparently healthy men and women. Circulation 125(12), 1482-1490.

Nakamura, S., Tezuka, Y., Ushiyama, A., Kawashima, C., Kitagawara, Y., Takahashi, K., Ohta, S. and Mashino, T. 2011. *Ipso* substitution of bisphenol A catalyzed by microsomal cytochrome P450 and enhancement of estrogenic activity. Toxicol. Lett. 203(1), 92-95.

Nico, P.S. and Zasoski, R.J. 2000. Importance of Mn(III) availability on the rate of Cr(III) oxidation on δ-MnO_2. Environ. Sci. Technol. 34(16), 3363-3367.

Nico, P.S. and Zasoski, R.J. 2001. Mn(III) center availability as a rate controlling factor in the oxidation of phenol and sulfide on δ-MnO_2. Environ. Sci. Technol. 35(16), 3338-3343.

NITE 2003. Summary of the Interim Report - Bisphenol A, National Institute of Technology and Evaluation, Japan.

Ogata, Y., Goda, S., Toyama, T., Sei, K. and Ike, M. 2013. The 4-*tert*-butylphenol-utilizing bacterium *Sphingobium fuliginis* OMI can degrade bisphenols via phenolic ring hydroxylation and *meta*-cleavage pathway. Environ. Sci. Technol. 47(2), 1017-1023.

Oldham, V.E., Mucci, A., Tebo, B.M. and Luther III, G.W. 2017. Soluble Mn(III)–L complexes are abundant in oxygenated waters and stabilized by humic ligands. Geochimica et Cosmochimica Acta 199, 238-246.

Park, C. and Kim, J. 2012. Effects of nitrate on the advanced UV photolysis of di (2-ethylhexyl) phthalate degradation in aqueous solution. Desalination Water Treat. 47(1-3), 163-170.

Post, J.E. 1999. Manganese oxide minerals: Crystal structures and economic and environmental significance. Proc. Natl. Acad. Sci. U. S. A. 96(7), 3447-3454.

Remucal, C.K. and Ginder-Vogel, M. 2014. A critical review of the reactivity of manganese oxides with organic contaminants. Environmental Science: Processes & Impacts 16(6), 1247-1266.

Rezg, R., Abot, A., Mornagui, B. and Knauf, C. 2019. Bisphenol S exposure affects gene expression related to intestinal glucose absorption and glucose metabolism in mice. Environ. Sci. Pollut. Res. 26(4), 3636-3642.

Roh, H., Subramanya, N., Zhao, F., Yu, C.-P., Sandt, J. and Chu, K.-H. 2009. Biodegradation potential of wastewater micropollutants by ammonia-oxidizing bacteria. Chemosphere 77(8), 1084-1089.

Santana De, F.S., Gracioso, L.H., Karolski, B., Baltazar, M.d.P.G., Mendes, M.A., do Nascimento, C.A.O. and Perpetuo, E.A. 2019. Isolation of Bisphenol A-tolerating/degrading *Shewanella haliotis* strain MH137742 from an estuarine environment. Biotechnol. Appl. Biochem. 189(1), 103-115.

Saric, M. 1986. Manganese. Handbook on the toxicology of metals, vol. II: Specific metals, New York: Elsevier Science Publishing Co.

Sasaki, M., Akahira, A., Oshiman, K.-i., Tsuchido, T. and Matsumura, Y. 2005. Purification of cytochrome P450 and ferredoxin, involved in bisphenol A degradation, from *Sphingomonas* sp. strain AO1. Appl. Environ. Microbiol. 71(12), 8024-8030.

Shankar, A., Teppala, S. and Sabanayagam, C. 2012. Urinary bisphenol a levels and measures of obesity: results from the national health and nutrition examination survey 2003–2008. ISRN Endocrinol. 2012.

Shao, P., Duan, X., Xu, J., Tian, J., Shi, W., Gao, S., Xu, M., Cui, F. and Wang, S. 2017a. Heterogeneous activation of peroxymonosulfate by amorphous boron for degradation of bisphenol S. J. Hazard. Mater. 322, 532-539.

Shao, P., Ren, Z., Tian, J., Gao, S., Luo, X., Shi, W., Yan, B., Li, J. and Cui, F. 2017b. Silica hydrogel-mediated dissolution-recrystallization strategy for synthesis of ultrathin α-Fe_2O_3 nanosheets with highly exposed (1 1 0) facets: a superior photocatalyst for degradation of bisphenol S. Chem. Eng. J. 323, 64-73.

Shobnam, N., Sun, Y., Mahmood, M., Löffler, F.E. and Im, J. 2021. Biologically mediated abiotic degradation (BMAD) of bisphenol A by manganese-oxidizing bacteria. J. Hazard. Mater., 125987.

Sigel, H. (2000) Met. Ions Biol. Syst., pp. 49-82, CRC Press.

Sigg, L., Sturm, M. and Kistler, D. 1987. Vertical transport of heavy metals by settling particles in Lake Zurich. Limnol. Oceanogr. 32(1), 112-130.

Simoneau, C., Valzacchi, S., Morkunas, V. and Van den Eede, L. 2011. Comparison of migration from polyethersulphone and polycarbonate baby bottles. Food Addit. Contam.: Part A 28(12), 1763-1768.

Skoog, D. and West, D. 1982. Fundamentals of analytical chemistry, Saunders College Publishing.

Solomon, K.R., Velders, G.J., Wilson, S.R., Madronich, S., Longstreth, J., Aucamp, P.J. and Bornman, J.F. 2016. Sources, fates, toxicity, and risks of trifluoroacetic acid and its salts: Relevance to substances regulated under the Montreal and Kyoto Protocols. Journal of Toxicology and Environmental Health, Part B 19(7), 289-304.

Song, S., Ruan, T., Wang, T., Liu, R. and Jiang, G. 2012. Distribution and preliminary exposure assessment of bisphenol AF (BPAF) in various environmental matrices around a manufacturing plant in China. Environ. Sci. Technol. 46(24), 13136-13143.

Song, S., Song, M., Zeng, L., Wang, T., Liu, R., Ruan, T. and Jiang, G. 2014. Occurrence and profiles of bisphenol analogues in municipal sewage sludge in China. Environ. Pollut. 186, 14-19.

Staples, C.A., Dome, P.B., Klecka, G.M., Oblock, S.T. and Harris, L.R. 1998. A review of the environmental fate, effects, and exposures of bisphenol A. Chemosphere 36(10), 2149-2173.

Stone, A.T. and Morgan, J.J. 1984. Reduction and dissolution of manganese(III) and manganese(IV) oxides by organics: 2. Survey of the reactivity of organics. Environ. Sci. Technol. 18(8), 617-624.

Stout, M. 2008. Chemical Information Profile for Bisphenol AF.

Sun, B., Guan, X., Fang, J. and Tratnyek, P.G. 2015. Activation of manganese oxidants with bisulfite for enhanced oxidation of organic contaminants: the involvement of Mn(III). Environ. Sci. Technol. 49(20), 12414-12421.

Sun, Q., Wang, Y., Li, Y., Ashfaq, M., Dai, L., Xie, X. and Yu, C.-P. 2017. Fate and mass balance of bisphenol analogues in wastewater treatment plants in Xiamen City, China. Environ. Pollut. 225, 542-549.

Sun, Y., Im, J., Shobnam, N., Fanourakis, S.K., He, L., Anovitz, L.M., Erickson, P.R., Sun, H., Zhuang, J. and Löffler, F.E. 2021. Degradation of adsorbed bisphenol A by soluble Mn(III). Environ. Sci. Technol. 55(19), 13014-13023.

Telke, A.A., Kalyani, D.C., Jadhav, U.U., Parshetti, G.K. and Govindwar, S.P. 2009. Purification and characterization of an extracellular laccase from a *Pseudomonas* sp. LBC1 and its application for the removal of bisphenol A. J. Mol. Catal. B: Enzym. 61(3-4), 252-260.

Trouwborst, R.E., Clement, B.G., Tebo, B.M., Glazer, B.T. and Luther, G.W. 2006. Soluble Mn(III) in suboxic zones. Science 313(5795), 1955-1957.

USEPA 2012. Exposure assessment tools and models, estimation program Interface (EPI) suite, V 4.11, US Environmental Protection Agency, Exposure Assessment Branch Washington, DC.

Vandieken, V., Pester, M., Finke, N., Hyun, J.-H., Friedrich, M.W., Loy, A. and Thamdrup, B. 2012. Three manganese oxide-rich marine sediments harbor similar communities of acetate-oxidizing manganese-reducing bacteria. ISME J. 6(11), 2078-2090.

Villalobos, M., Toner, B., Bargar, J. and Sposito, G. 2003. Characterization of the manganese oxide produced by *Pseudomonas putida* strain MnB1. Geochim. Cosmochim. Acta. 67(14), 2649-2662.

Wang, J., Wang, C., Guo, H., Ye, T., Liu, Y., Cheng, X., Li, W., Yang, B. and Du, E. 2020. Crucial roles of oxygen and superoxide radical in bisulfite-activated persulfate oxidation of bisphenol AF: Mechanisms, kinetics and DFT studies. J. Hazard. Mater. 391, 122228.

Wang, Z., Xiong, W., Tebo, B.M. and Giammar, D.E. 2014. Oxidative UO_2 dissolution induced by soluble Mn(III). Environ. Sci. Technol. 48(1), 289-298.

Webb, S.M., Dick, G.J., Bargar, J.R. and Tebo, B.M. 2005. Evidence for the presence of Mn(III) intermediates in the bacterial oxidation of Mn (II). Proc. Natl. Acad. Sci. U. S. A. 102(15), 5558-5563.

Wright, M.H., Geszvain, K., Oldham, V.E., Luther III, G.W. and Tebo, B.M. 2018. Oxidative formation and removal of complexed Mn(III) by Pseudomonas species. Front. Microbiol. 9, 560.

Xue, J., Wu, Q., Sakthivel, S., Pavithran, P.V., Vasukutty, J.R. and Kannan, K. 2015. Urinary levels of endocrine-disrupting chemicals, including bisphenols, bisphenol A diglycidyl ethers, benzophenones, parabens, and triclosan in obese and non-obese Indian children. Environ. Res. 137, 120-128.

Yang, T., Wang, L., Liu, Y., Huang, Z., He, H., Wang, X., Jiang, J., Gao, D. and Ma, J. 2019. Comparative study on ferrate oxidation of BPS and BPAF: Kinetics, reaction mechanism, and the improvement on their biodegradability. Water Res. 148, 115-125.

Yang, Y., Guan, J., Yin, J., Shao, B. and Li, H. 2014. Urinary levels of bisphenol analogues in residents living near a manufacturing plant in south China. Chemosphere 112, 481-486.

Ye, X., Wong, L.-Y., Kramer, J., Zhou, X., Jia, T. and Calafat, A.M. 2015. Urinary concentrations of bisphenol A and three other bisphenols in convenience samples of US adults during 2000–2014. Environ. Sci. Technol. 49(19), 11834-11839.

Yu, H. and Leadbetter, J.R. 2020. Bacterial chemolithoautotrophy via manganese oxidation. Nature 583(7816), 453-458.

Yu, Q., Sasaki, K., Tanaka, K., Ohnuki, T. and Hirajima, T. 2012. Structural factors of biogenic birnessite produced by fungus *Paraconiothyrium* sp. WL-2 strain affecting sorption of Co^{2+}. Chem. Geol. 310, 106-113.

Zhang, W., Yin, K. and Chen, L. 2013. Bacteria-mediated bisphenol A degradation. Biotechnol. Appl. Biochem. 97(13), 5681-5689.

Zhang, Y., Tang, Y., Qin, Z., Luo, P., Ma, Z., Tan, M., Kang, H. and Huang, Z. 2019. A novel manganese oxidizing bacterium-*Aeromonas hydrophila* strain DS02: Mn (II) oxidization and biogenic Mn oxides generation. J. Hazard. Mater. 367, 539-545.

Zhou, N., Liu, Y., Cao, S., Guo, R., Ma, Y. and Chen, J. 2020. Biodegradation of bisphenol compounds in the surface water of Taihu Lake and the effect of humic acids. Sci. Total Environ. 723, 138164.

Zhou, N.A., Kjeldal, H., Gough, H.L. and Nielsen, J.L. 2015. Identification of putative genes involved in bisphenol A degradation using differential protein abundance analysis of *Sphingobium* sp. BiD32. Environ. Sci. Technol. 49(20), 12232-12241.

Appendix

Table 1.1. Physical and chemical properties of BPA, BPAF, and BPS summarized from previous studies (Staples et al., 1998; USEPA, 2012; Choi and Lee, 2017).

Compound	Log K_{ow}	Log K_{oc}	Solubility[a]	pK_{a1}, pK_{a2}	Henry's Constant[b]
BPA	3.32−3.4	2.4−3.71	300	9.78, 10.39	1.0×10^{-10}
BPAF	2.82−4.77	3.23−5.88	0.84	9.13, 9.74	5.7×10^{-10}
BPS	1.65−2.14	2.20−3.88	1,774	7.42, 8.03	2.7×10^{-15}

[a]Unit: mg L^{-1}. [b]Unit: atm m^3.

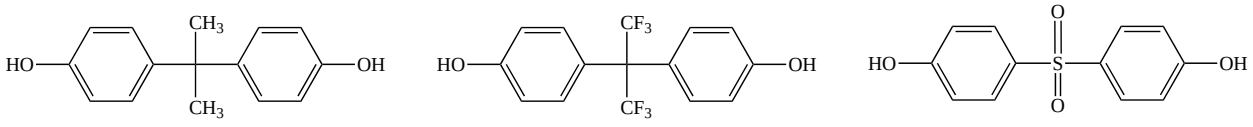

BPA BPAF BPS

Figure 1.1. Chemical structures of BPA, BPAF, and BPS.

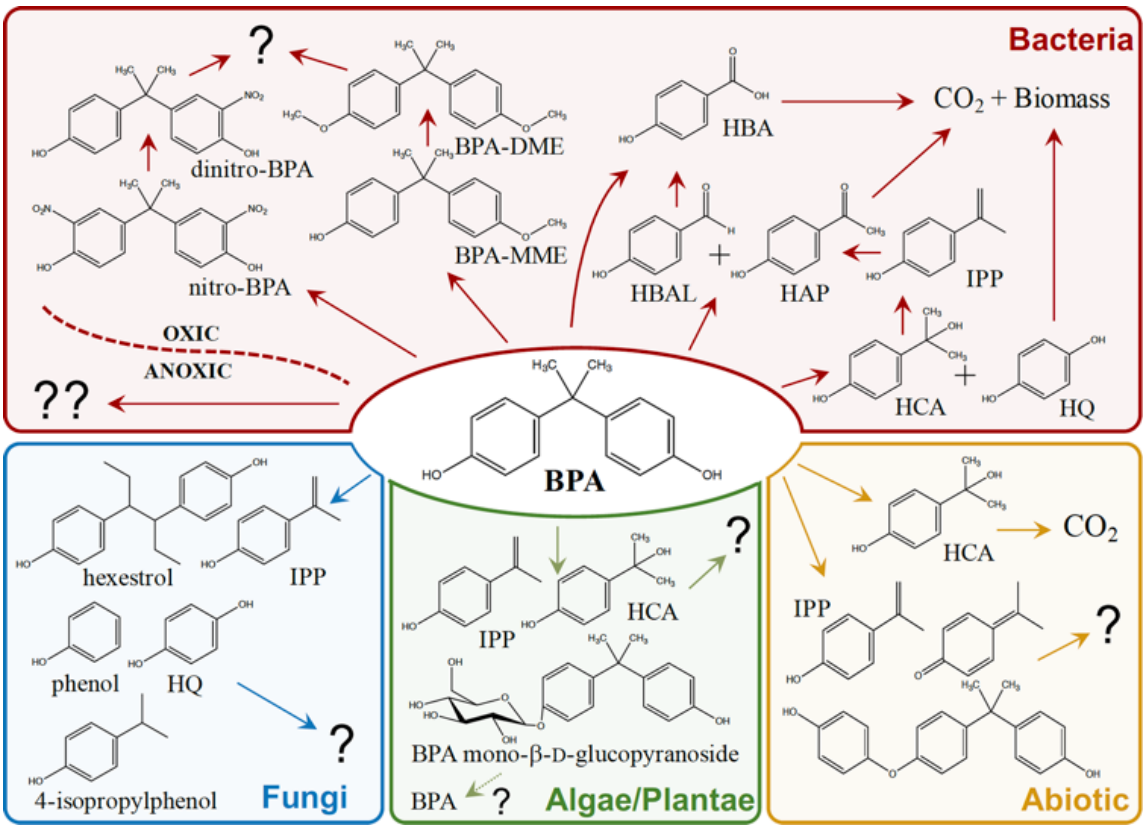

Figure 1.2. Summary of known pathways and intermediates in the processes of BPA degradation/transformation (Im and Löffler, 2016).

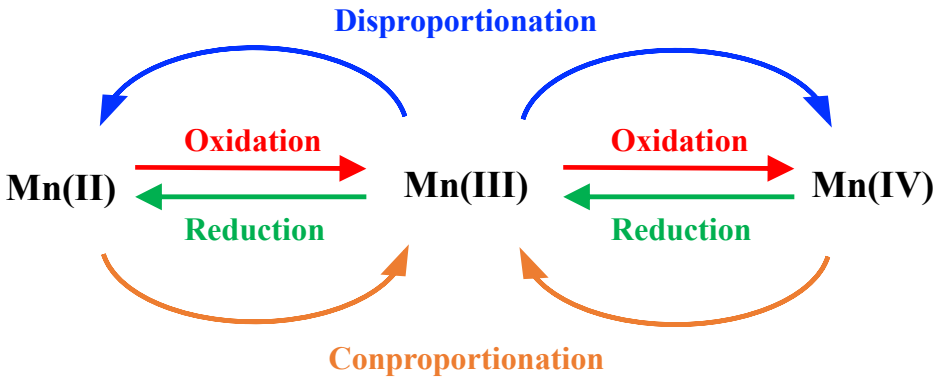

Figure 1.3. Summary of Mn cycling in environmental systems (Webb et al., 2005; Lin et al., 2012; Hansel, 2017; Liu et al., 2019).

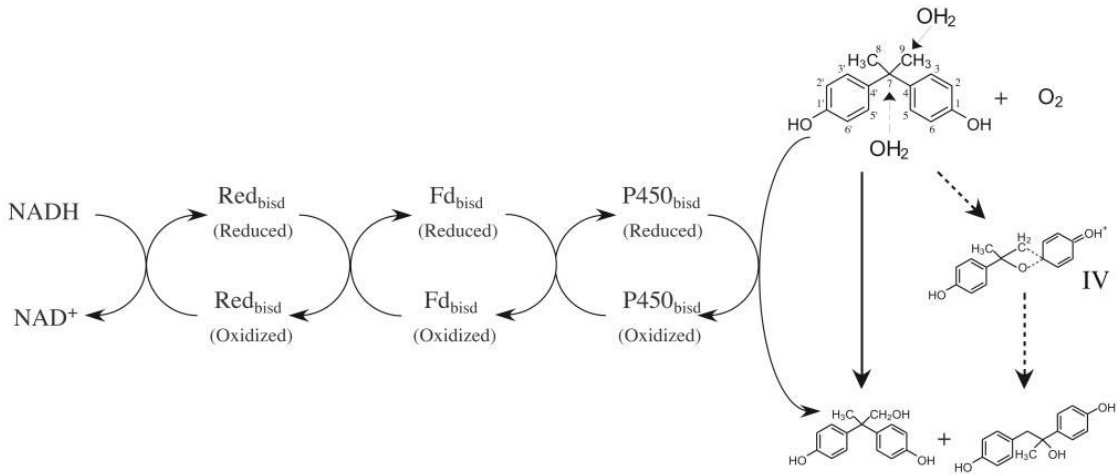

Figure 1.4. Electron flow in the BPA hydroxylation system and predicted enzymatic reaction of the P450bisd monooxygenase system (Sasaki et al., 2005).

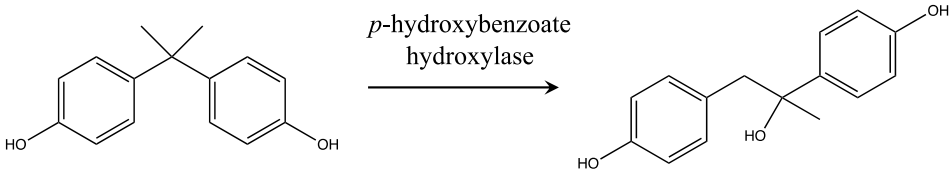

Figure 1.5. Initiation of BPA degradation by *Sphingobium* sp. strain BiD32 (Simplified pathway) (Zhou et al., 2015).

BPAF Metabolites	
Formula Mass	**Structure**
$C_{15}H_{10}F_6O_5$ 384.0432 (L)	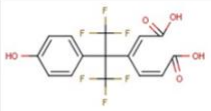
$C_{14}H_{12}F_6O_5$ 374.0589 (M)	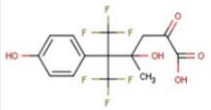
$C_{14}H_{10}F_6O_4$ 356.0483 (N)	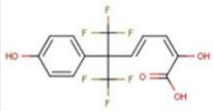
$C_{11}H_8F_6O_3$ 302.0378 (O)	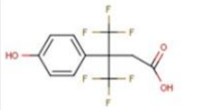
$C_9H_6F_6O$ 44.0323 (P)	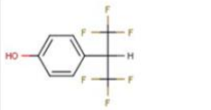
$C_{11}H_8F_6O_2$ 286.0429 (S)	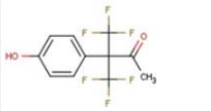
$C_{14}H_{10}F_6O_5$ 372. 0432 (T)	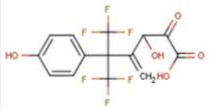
$C_{13}H_{10}F_6O_5$ 360.0432 (V)	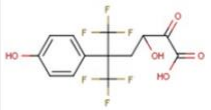

Figure 1.6. Intermediates generated in BPAF biodegradation (data was collected from a prior study) (Choi and Lee, 2017).

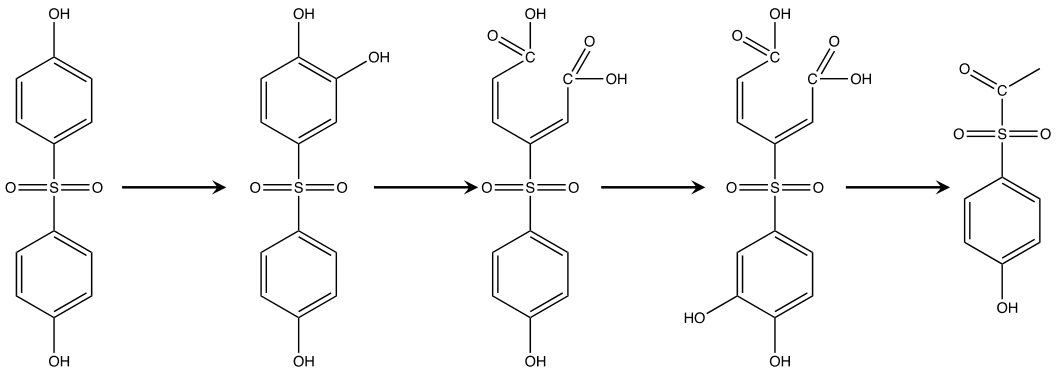

Figure 1.7. Proposed biodegradation pathway of BPS (Data were collected from several published studies) (Choi and Lee, 2017; Fang et al., 2020).

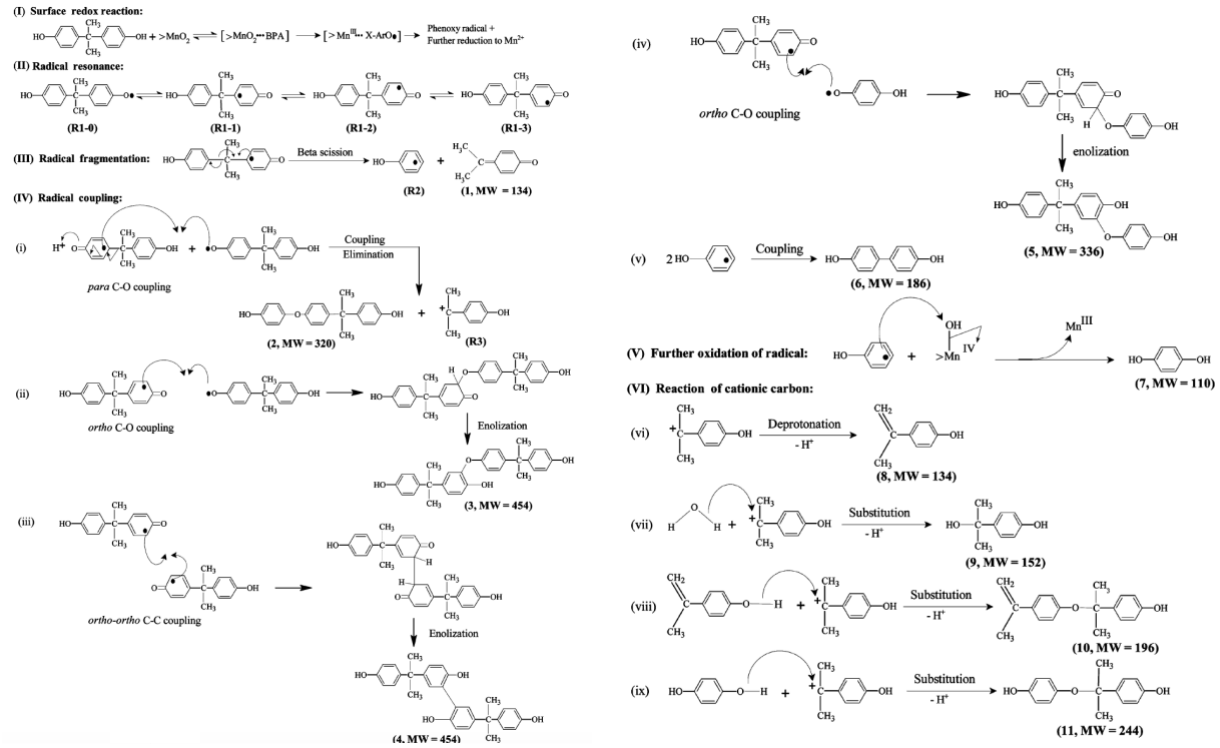

Figure 1.8. The proposed reaction pathway for BPA treated by MnO_2 (Pathways were modified) (Lin et al., 2009).

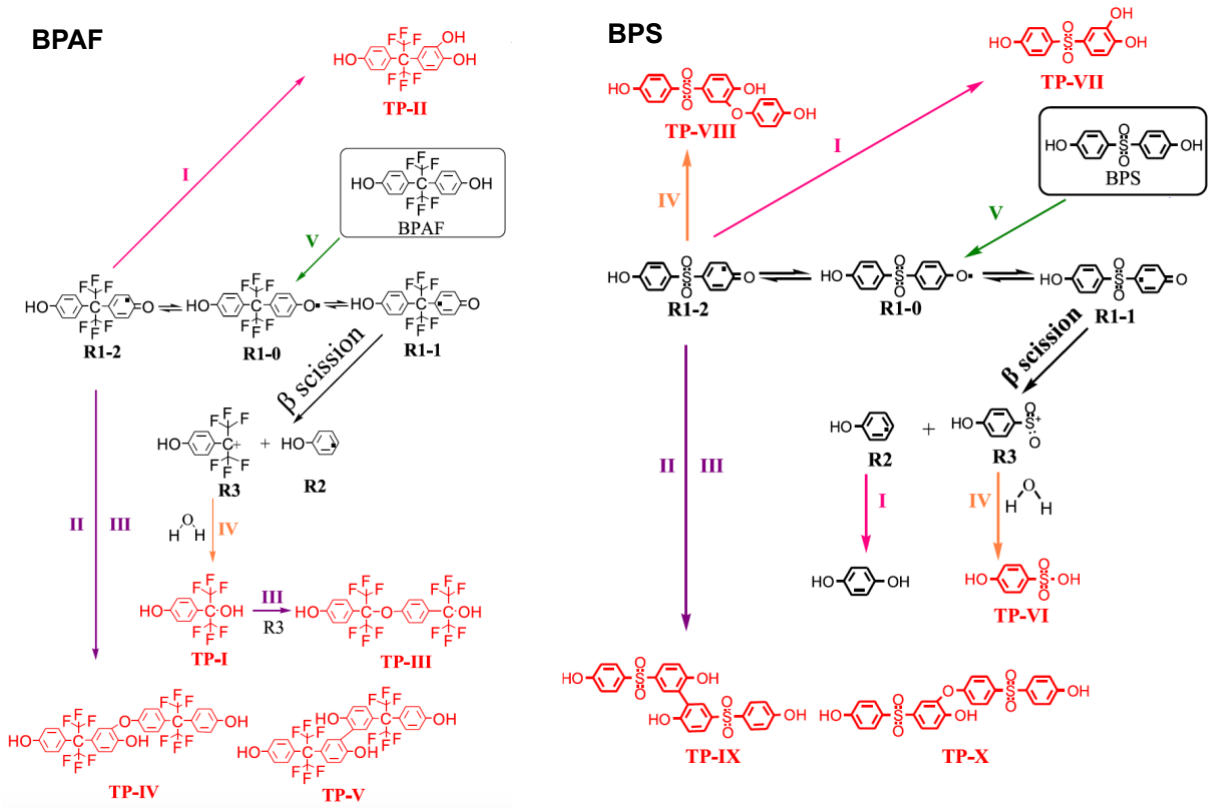

Figure 1.9. The proposed reaction pathways for BPAF (left) and BPS (right) treated by MnO_2 (Pathways were modified) (Li et al., 2018).

Chapter 2. The Role of Mn(III) in MnO_2-mediated Bisphenol A (BPA) Degradation

The following chapter is in the review for potential publication in the journal Environmental Science & Technology.

2.1 Abstract

Bisphenol A (BPA), a high production volume chemical with potential estrogenic effects, is susceptible to abiotic degradation by solid phase MnO_2. MnO_2 commonly comprises Mn(III), but the role of Mn(III) in BPA degradation is unclear and has not been quantified. Batch experiments with soluble Mn(III), synthetic MnO_2, and surface-Mn(III)-free MnO_2 as oxidants demonstrated that about 10-35% of BPA degradation could be attributed to Mn(III) in synthetic MnO_2 during the early stage of reaction. Rapid degradation of BPA occurred in batch vessels with 1 mM Mn(III) and 63.9 ± 0.7% of 1.76 ± 0.02 μM BPA was degraded in 1 hour. Synthetic MnO_2 comprised approximately 13% (mol/mol) surface-associated Mn(III) and exhibited 1.86 ± 0.09-fold higher BPA degradation rates than surface-Mn(III)-free synthetic MnO_2. Ultra-high-performance liquid chromatography high-resolution tandem mass spectrometry (UHPLC-HRMS/MS) analysis identified eight transformation intermediates. Density functional theory calculations proposed 14 BPA degradation products in reactions with Mn(III) based on these eight transformation intermediates, nine of which had not been observed during MnO_2-mediated BPA degradation, suggesting mechanistic differences. The findings demonstrate that both Mn(III) and Mn(IV) can effectively degrade BPA and indicate that surface-associated Mn(III) increases the reactivity of MnO_2, offering opportunities for engineering more reactive MnO_2 (nano)particles for BPA removal.

Keywords: bisphenol A, MnO_2, Mn(III), quantum chemical calculation, degradation pathway.

2.2 Introduction

Bisphenol A (BPA) is a widely used industrial chemical for the production of polycarbonates and epoxy resins (Staples et al., 1998). The global BPA market reached a value of 10.92 billion dollars in 2020 and will reach 30.62 billion dollars by 2026 with increasing demand projected (Research, 2021). High production volume and widespread use introduced BPA to various environmental systems (Fromme et al., 2002; Im and Löffler, 2016). Laboratory studies suggested estrogenic effects of BPA (Staples et al., 1998), what has triggered research exploring the fate of BPA (Staples et al., 1998; Im and Löffler, 2016; Shobnam et al., 2021; Sun et al., 2021). With a K_{ow} of 3.42, BPA has a tendency for sorption, and considerable mass exists in soils, sediments, and landfills (Liao et al., 2012b; Kalmykova et al., 2013; Huang et al., 2014). BPA resists anaerobic microbial degradation but is susceptible to abiotic degradation mediated by MnO_2 in oxic and anoxic environments (Im et al., 2014; Im et al., 2015; Balgooyen et al., 2017; Huang et al., 2018). Abiotic BPA degradation by MnO_2 involves a radical mechanism and several degradation products, foremost 4-hydroxycumyl alcohol (HCA), but also products with higher molecular weight than BPA, have been identified (Lin et al., 2009; Im et al., 2015).

Manganese dioxide (MnO_2) is a strong and environmentally relevant oxidant that has been shown to transform a variety of organic compounds, including priority pollutants (Stone, 1987; Zhang and Huang, 2003; Im et al., 2015; Li et al., 2018). The oxidation state of Mn in fully oxidized MnO_2 is 4; however, actual measurements indicate an average oxidation state of synthetic MnO_2 between 3.3 and 3.9 (Feng et al., 2010; Learman et al., 2011b; Balgooyen et al., 2017). This discrepancy has been explained by the presence of Mn(III) in synthetic and biogenic MnO_2 with reported Mn(III) contents ranging from 7% to 36% (Nico and Zasoski, 2001; Villalobos et al., 2003; Feng et al., 2010; Learman et al., 2011b; Huang et al., 2018). A few

studies have demonstrated that Mn(III) contained in MnO_2 preparations plays a role as an oxidant in reactions mediated by MnO_2 (Nico and Zasoski, 2000; 2001; Huang et al., 2018). For example, the absence of Mn(III) in the surface of MnO_2 has been shown to decrease chromium (III) and phenol oxidation (Nico and Zasoski, 2000; 2001). In addition, Mn(III) has been detected in various environments including oxic-anoxic interfaces in soils (Jones et al., 2018) and hemipelagic sediments (Trouwborst et al., 2006; Madison et al., 2013) at micromolar concentrations (Madison et al., 2013). Recent studies documented that Mn(III) effectively oxidizes a variety of organic compounds including lignin (Jones et al., 2018), chlorophene (Wang et al., 2018), and ciprofloxacin (Sun et al., 2015), as well as inorganics such as the radionuclide uranium(IV) (Wang et al., 2014). These findings changed the traditional paradigm of Mn biogeochemistry and Mn(III) is now considered an environmentally relevant oxidant; however, its role in BPA degradation by MnO_2 remains uncertain.

The reactivity of phenolic compounds (e.g., BPA) is mainly dependent on the frontier electron density (FED), specifically electron densities in the highest occupied molecular orbital (HOMO) and the lowest unoccupied molecular orbital (LUMO) (Fukui et al., 1952; Fukui et al., 1954). According to the frontier orbital theory, the atom with a higher $2FED^2_{HOMO}$ is more likely lose an electron, and the atom with a higher $FED^2_{HOMO}+FED^2_{LUMO}$ is more susceptible to attack by a hydroxyl radical (Ohko et al., 2002; An et al., 2010). Also, oxidation of organic compounds is generally more prone to occur at atoms with greater negative charges (Wang et al., 2018). The oxidant generates radicals in reaction solutions (e.g., H_2O), which will trigger secondary reactions leading to transformation and degradation of organic compounds. Potential coupling sites for the formation of polymeric intermediates can be predicted using the spin density, which represents the nonbonding molecular orbital with the unpaired electron (Lowe and Peterson,

2011; Chen et al., 2018; Fleck et al., 2019). Density functional theory (DFT), a computational quantum mechanical modeling approach, can predict chemical reactivity and has been widely applied to study reaction mechanisms (Chempath et al., 2010; Chen et al., 2013b; Xu et al., 2018).

The objectives of this study were to investigate the role of Mn(III) in MnO_2-mediated BPA degradation and to explore the mechanisms of BPA degradation by Mn(III). To demonstrate the role of Mn(III), a series of BPA degradation experiments with Mn(III), MnO_2, and surface-Mn(III)-free MnO_2 were conducted. Intermediates and their fragmentation patterns were detected using high-resolution tandem mass spectrometry (HRMS/MS). These data, paired with quantum chemical calculations, generated mechanistic and pathway information for Mn(III)-mediated BPA degradation, which involves intermediates distinct from those reported for MnO_2-mediated BPA degradation.

2.3 Materials and Methods

2.3.1 Chemicals

BPA (>99% purity) was purchased from Sigma-Aldrich (St. Louis, MO, USA). Leucoberbelin blue (LBB), sulfuric acid (H_2SO_4), methanol, acetonitrile, acetic acid (CH_3COOH), ammonium acetate (CH_3COONH_4), L-ascorbic acid, potassium permanganate ($KMnO_4$), manganese(III) oxide (Mn_2O_3) (>98% purity), manganese(II) chloride tetrahydrate ($MnCl_2 \times 4\ H_2O$), and sodium pyrophosphate decahydrate ($Na_4P_2O_7 \times 10\ H_2O$) were obtained from Fisher Scientific (Waltham, MA, USA). All chemicals used were of reagent grade purity or higher. HCA (> 95% purity confirmed by nuclear magnetic resonance spectroscopy) was

synthesized using a modified procedure (see the Supporting Information for details) (Im et al., 2015).

2.3.2 Preparation and characterization of soluble Mn(III), MnO_2, and surface-Mn(III)-free MnO_2

Soluble Mn(III) and MnO_2 were prepared following established procedures (see the Supporting Information for details) (Sun et al., 2021).

Pyrophosphate was used to extract surface Mn(III) from MnO_2 to produce surface-Mn(III)-free MnO_2 (Nico and Zasoski, 2001; Liu et al., 2019). Because pyrophosphate can promote the conproportionation of Mn(II) and Mn(IV) to generate Mn(III) (Liu et al., 2019), the synthesized MnO_2 was sequentially washed with 30 mM H_2SO_4 and Milli-Q water (at least 18.2 MΩ × cm) to remove Mn(II) (Wright et al., 2016). Surface-Mn(III)-free MnO_2 suspensions were prepared in 160-mL glass serum bottles with a total volume of 100 mL of 0.05, 0.1, 0.25, 0.5, and 1 mM (nominal concentrations) MnO_2 at pH 7.2. To extract surface-associated Mn(III), pyrophosphate was added to the MnO_2 suspensions at a pyrophosphate:Mn ratio of 50 (Klewicki and Morgan, 1998). The mixtures were continuously agitated at 120 rpm in an upright position at room temperature. Aliquots (1 mL) were periodically collected and filtered through 0.22 μm polyethersulfone (PES) membrane (Nalgene, Rochester, NY, USA) into 1-cm light path quartz cuvettes (Corning Inc., Corning, NY, USA) for measuring absorbance by UV-vis spectrophotometer.

To collect surface-Mn(III)-free MnO_2, the pyrophosphate/MnO_2 suspensions were centrifuged at 15,000 × *g* (Sorvall RC6 Plus centrifuge, Langenselbold, Germany) for 15 min after pyrophosphate extraction was complete. The surface-Mn(III)-free MnO_2 preparations were washed five times with Milli-Q water to remove pyrophosphate. Finally, the surface-Mn(III)-free

MnO_2 was suspended in 5 mM phosphate buffer (pH 7.2) to achieve nominal concentrations of 0.05, 0.1, 0.25, 0.5, and 1 mM.

2.3.3 Oxidative degradation of BPA by soluble Mn(III), MnO_2, and surface-Mn(III)-free MnO_2

Experiments were performed in 60-mL glass serum bottles with a total volume of 40 mL of 5 mM phosphate buffer, pH 7.2, containing 44 μM BPA. Sodium chloride was added to reach a constant ionic strength of 10 mM. To measure BPA degradation rates and extents, Mn(III) was added to serum bottles to achieve concentrations of 0.01, 0.02, 0.05, 0.25, and 1 mM; MnO_2 and surface-Mn(III)-free MnO_2 suspensions were added to the serum bottles to achieve nominal concentrations of 0.05, 0.1, 0.25, 0.5, and 1 mM using plastic syringes. The vessels were manually shaken before 0.5 mL aliquots were periodically collected and transferred to 1.5 mL plastic centrifuge tubes containing 20 μL of L-ascorbic acid solution (5 g L^{-1}) and immediately vortexed. The samples were centrifuged at 10,000 × *g* (Eppendorf centrifuge 5415D, Hamburg, Germany) for 10 min, and the supernatant was transferred to 2 mL glass HPLC autosampler vials. The conversion efficiency of BPA to HCA was calculated by dividing the amount (μmol) HCA generated by the amount BPA oxidized (Im et al., 2015), and shown in percentage. The pseudo-first-order rate constants were obtained by plotting the natural log of BPA concentrations as a function of time using six early time points where linear relationships were observed (Im et al., 2015).

2.3.4 Detection of transformation intermediates

Degradation experiments were performed in 160-mL glass serum bottles with a total volume of 100 mL of 5 mM phosphate buffer, pH 7.2, containing 44 μM BPA and 0.5 mM soluble

Mn(III). Following a 2-hour incubation period, the entire vessels were extracted (Yan et al., 2018). Briefly, Sep-Pak C18 cartridges (Waters Corp, Milford, MA, USA) were rinsed with 3 mL of methanol followed by a wash with 60 mL of Milli-Q water. Residual water was removed by pushing air through the cartridges using a 20-mL plastic syringe. Following these preparation steps, 100 mL of BPA reaction mixture was slowly passed (approximately one drop per second) through the column. Then, the column was rinsed with 5 mL of Milli-Q water, which was removed by pushing air through the cartridge using a 10-mL plastic syringe. Bound compounds were eluted from the column in 2 mL of methanol. The extracts were stored at 4 °C for no longer than 24 h before analysis. Extracts were analyzed using the ultra-high-performance liquid chromatography high-resolution tandem mass spectrometry (UHPLC-HRMS/MS) with a modified method (see the Supporting Information for details) (Choi and Lee, 2017).

2.3.5 Incubation conditions

The experiments were performed under ambient air conditions and at room temperature (~21°C), and all vessels were incubated in the dark on a rotary shaker (200 rpm, unless indicated otherwise) with the stoppers facing up.

2.3.6 Analytical procedures

BPA and HCA were quantified using an Agilent 1100 Series HPLC system equipped with a diode array detector and a fluorescence detector (FLD) (Sun et al., 2021). Separation was performed on an Agilent Eclipse XDB C18 column (4.6 mm × 150 mm, 5 μm) using isocratic elution at a flow rate of 1 mL min^{-1} of acetonitrile and Milli-Q water (50:50, *v/v*) at pH 7.2. The FLD was set at excitation and emission wavelengths of 226 nm and 310 nm, respectively. For standard curve construction, vials containing 0.4, 1.1, 2.2, 11, 44, and 88 μM BPA and 50 mg

mL^{-1} L-ascorbic acid were prepared in triplicates. HCA standard curves were created using solutions of 0.7, 1.4, 2.8, 11.1, and 44.4 μM. The limit of detection and limit of quantification were 0.4 μM and 1.1 μM for BPA and 0.2 μM and 0.7 μM for HCA with signal-to-noise ratios of 3:1 and 10:1, respectively.

Mn(III) was quantified by measuring the absorbance at a wavelength of 258 nm (PerkinElmer Lambda 35 UV-vis spectrophotometer) immediately after collecting (Sun et al., 2015). A molar extinction coefficient of 6,750 M^{-1} cm^{-1} was used to calculate soluble Mn(III) concentrations (Liu et al., 2019). The percentage of extractable Mn(III), on a molar basis, was calculated by dividing the amount (μmol) of Mn(III)-pyrophosphate formed by the initial amount (μmol) of MnO_2. The kinetics of Mn(III)-pyrophosphate extracted from MnO_2 were simulated with the first-order rate law (Eq.[1]) (Klewicki and Morgan, 1999; Liu et al., 2019).

$$[\text{Mn(III)-pyrophosphate}]=[\text{Mn(III)-pyrophosphate}]_{max}(1-e^{-k_L t}) \quad (1)$$

Where $[\text{Mn(III)-pyrophosphate}]_{max}$ is the concentration of Mn(III)-pyrophosphate at equilibrium, k_L ($hour^{-1}$) is the first-order rate constant, and t (hour) is the incubation period.

2.3.7 Quantum chemical calculations

The Gaussian 09 software package was applied for all quantum chemical calculations (Frisch et al., 2009). The structure of BPA with minimum energy was optimized using the DFT method at the B3LYP/6-311G** level (Wang et al., 2018). The FED values of the HOMO and LUMO, charge density, and spin density were obtained from the Gaussian output files. Values of $2FED^2_{HOMO}$ and $FED^2_{HOMO} + FED^2_{LUMO}$ were obtained to predict the reaction sites of electron extraction and hydroxyl attack (Fukui et al., 1952; Fukui et al., 1954). The charge density and spin density of radicals were used to predict the coupling reactions between radicals. Finally, the

molecular structure of transformation intermediates and degradation pathways were proposed based on the results of the UHPLC-HRMS/MS analysis and the quantum calculations.

2.3.8 Toxicity prediction

Acute and chronic toxicity of BPA and its degradation products were predicted using the US EPA Ecological Structure Activity Relationships (ECOSAR) software (Version 2.0) (USEPA, 2017). The ECOSAR software evaluates the exposure risks of organic compounds to fish, *Daphnia*, and green algae, by using quantitative structure activity relationships model. The prediction results include the half-maximum effective concentrations (EC_{50}), half-maximum lethal concentrations (LC_{50}), and chronic toxicity (ChV) of each compound.

2.4 Results

2.4.1 Effect of Mn(III) on BPA degradation

In vessels with 0.01 to 1 mM Mn(III), a rapid decline of BPA was observed and 20-26% of the initial 1.76 ± 0.02 μmol of BPA was consumed within the first 2 min of incubation, suggesting Mn(III)-mediated BPA degradation is a fast process (Figure 2.1). Additional BPA was removed over time albeit at lower rates, and 20-64% of the initial amount of BPA was consumed following a 1-hour incubation period (Figure 2.1).

In incubations with soluble Mn(III), HPLC analysis detected a degradation product with a retention time that matched a synthetic HCA standard (Figure S2.1), and was further confirmed via UHPLC-HRMS/MS (Figure S2.2). When 0.05 mM Mn(III) was incubated with 44 μM BPA, the conversion efficiency of BPA to HCA reached 7.42 ± 0.54% following a 10-min incubation period (Figure 2.1 and Figure S2.3). Similar conversion efficiencies were observed with Mn(III)

loadings > 0.05 mM (Figure S2.3), suggesting that Mn(III) reacts preferentially with BPA rather than with HCA.

2.4.2 Pyrophosphate extractable Mn(III) from MnO_2

To determine the amount of Mn(III) associated with synthetic MnO_2, Mn(III) extractions with pyrophosphate were performed. Figure 2.2A shows UV-vis spectra of the extract obtained following pyrophosphate treatment for 150 h. The spectrum shows the characteristic absorption peak of the Mn(III)-pyrophosphate complex at 258 nm. No absorbance increases at 258 nm were observed in incubations lacking MnO_2 indicating pyrophosphate did not contribute to the signal. Mn(III)-pyrophosphate formation only occurred in the presence of MnO_2 and a linear relationship (R^2 = 0.994) between 258 nm readings and the nominal concentrations of MnO_2 was observed (Figure 2.2A), demonstrating that the amount of pyrophosphate extractable Mn(III) correlated with the initial MnO_2 loadings. Extraction of Mn(III) with pyrophosphate was fast during the first 24 h of incubation and plateaued after about 170 h. Mn(III) extracted from vessels with 0.05-2 mM nominal concentration of MnO_2 accounted for 8.3 ± 0.1% to 13.1 ± 1.0% of the total MnO_2 loadings (Figure 2.2B).

2.4.3 Effect of surface-associated Mn(III) on BPA degradation

The amounts of BPA removed increased with higher loadings of MnO_2 or surface-Mn(III)-free MnO_2 (Figure 2.3). When 0.05 mM (nominal) MnO_2 was added to a solution with 1.76 μmol BPA, 0.26 ± 0.03 μmol BPA was removed during a 10-min incubation period and increased to 1.57 ± 0.02 μmol with 1 mM MnO_2 (Table 2.1). Surface-Mn(III)-free MnO_2 also removed BPA (Figure 2.3B), but the amounts were relatively lower compared to incubations vessels with the

same amount of MnO_2. Over a 10-min reaction period, approximately 0.09 ± 0.02 and 0.92 ± 0.06 μmol BPA were removed with 0.05 and 1 mM surface-Mn(III)-free MnO_2, respectively.

The initial BPA concentration decreases followed pseudo-first-order reaction kinetics, but the rates declined after 10 min in both systems that received MnO_2 or surface-Mn(III)-free MnO_2. Therefore, the initial rate constants (k_{init}, min^{-1}) were calculated from six early time points where linear relationships between the BPA removal and the loadings of MnO_2 and surface-Mn(III)-free MnO_2 were observed (Figure 2.4). The reaction rates of BPA removed by MnO_2 were 1.86 ± 0.09-fold higher than those measured for surface-Mn(III)-free MnO_2 (Figure 2.4), indicating that Mn(III) contributes significantly to MnO_2-mediated BPA degradation.

BPA degradation with MnO_2 yielded HCA, a finding consistent with prior reports (Im et al., 2015; Balgooyen et al., 2017). Over a 1-hour reaction period, the maximum conversion efficiencies of BPA to HCA were 8.32 ± 1.15% and 13.66 ± 0.51% with 0.05 to 1 mM MnO_2, respectively. With higher MnO_2 loadings (i.e., > 1 mM), HCA concentrations decreased after reaching a maximum after about 20 min, indicating that HCA is also susceptible to MnO_2-mediated degradation. Higher BPA to HCA conversion efficiencies of 12.40 ± 0.8% to 17.9 ± 0.1% were observed with surface-Mn(III)-free MnO_2 (Figure S2.3), suggesting that MnO_2 with associated Mn(III) has a higher reactivity towards HCA (i.e., HCA is more susceptible to degradation by MnO_2 than by surface-Mn(III)-free MnO_2).

2.4.4 Identification of BPA transformation intermediates generated by soluble Mn(III)

BPA transformation intermediates via soluble Mn(III) were identified using UHPLC-HRMS/MS based analysis (Table 2.2). Two transformation intermediates (TIs) were identified with a mass-to-charge (*m*/*z*) lower than BPA while several TI were identified with a *m*/*z* higher than BPA. Combined chromatograms as determined using parallel reaction monitoring

chromatograms with the associated fragmentation spectrum of eight TIs are shown in Figure S2.4. The first transformation intermediate of interest (TI-1, Figure S2.4A & B) eluted at 4.7 min with a *m*/*z* of 151.0671 ($[M-H]^-$) and matches the mass spectrum of the HCA standard (Figure S2.2). The HCA standard and TI-1 (P3 in Figure 2.5) had the same fragmentation spectrum with the most intense *m*/*z* matching the dehydration product (*m*/*z* 133.0652, loss of H_2O). The second TI of interest (TI-2, Figure S2.4A & C) eluted at 4.6 min with a *m*/*z* of 133.0656 ($[M-H]^-$) and correlates to the dehydration product of HCA, P4 seen in Figure 2.5. Fragmentation of TI-2 yielded ions with a relative intensity of 0.5-1% of the TI-2 ion.

The remaining TIs all had a *m*/*z* higher than the parent molecule, BPA. These reaction intermediates are likely formed via further reactions between BPA, HCA (TI-1) and hydroxyl radicals. Intermediate 3 (TI-3, Figure S2.4A & D) had a *m/z* of 243.1019 with a predictive molecular formula of $C_{15}H_{15}O_3^-$ likely represents an oxidized BPA analogue with an O atom addition. All fragments were detected with a relative intensity <10%. Since the fragmentation data does not show evidence of a dehydrated product like HCA, it is unlikely that TI-3 contains the similar isopropanol functional group suggesting the structures similar to P1 over P9 or P13 (Figure 2.5). The HCA dimer (P10 and P14, Figure 2.5) can be seen in TI-4 as the *m*/*z* of 301.1436 is twice the molecular mass of HCA (TI-1). Fragmentation of this intermediate yields both a single and double loss of water with the fragment *m*/*z*'s of 283.1340 and 265.1234, respectively (Figure S2.4E). Intermediate 5, *m/z* of 319.13277, could be formed from the coupling reaction between BPA and a phenol. Fragmentation of the TI-5 (Figure S2.4F) yielded only a single *m*/*z* of 108.0207 at a relative intensity >55% corresponding a radical anion fragment with the potential formula of $[C_6H_4O_2]^{\bullet-}$. This fragment may correspond to a bisphenol moiety seen in P2 and P5 in Figure 2.5. Fragmentation of the TI-6 (*m/z* 377.17725) yielded the

fragment *m*/*z* of 359.16641 (loss of water) as the most abundant fragment in the spectrum (Figure S2.4G). Further fragmentation gave several low intensity species including a loss of a second water ($[C_{24}H_{21}O_2]^-$), phenolate loss ($[C_{18}H_{17}O_2]^-$), and a methyl radical loss ($[C_{23}H_{20}O_3]^{\bullet-}$). The low relative intensity of the second water loss indicates it is not likely from an isopropanol group, but instead from a cyclization forming a dibenzofuran product. Fragmentation pattern of TI-6 best supports connectivity resembling P12 over P8 and P11 from Figure 2.5 as it contains a 2,2'-dihydroxydiphenyl moiety capable of forming a dibenzofuran from a loss of water. Intermediates 7 and 8 had a *m*/*z* of 453.209 but differed in retention time by 1.4 min (Figure S2.4A, H & I). Fragmentation of both intermediates yielded a single common *m*/*z* of 359.166 at an intensity of 15% (TI-7) and 25% (TI-8) which likely corresponds to a phenolate loss ($[C_{24}H_{23}O_3]^-$) in both cases. Intermediate 7 yielded a single other fragment (*m*/*z* 423.16227) with a relative intensity greater that 10% while intermediate 8 yielded no other fragments greater than 10%. These data along with the retention time shift indicated TI-7 and TI-8 are structural isomers, same chemical formula but different connectivity. These two intermediates correspond to the dimer of bisphenol A shown in P6 and P7 (Figure 2.5).

2.4.5 Reaction schemes

Based on the identified transformation intermediates, a reaction scheme for BPA degradation by soluble Mn(III) can be proposed (Figure 2.5). The quantum calculations supported the proposed pathways and two major reaction types including hydroxylation and single electron coupling contributed to the formation of the identified BPA degradation products (Figure 2.5). Hydroxylation of BPA most likely occurred at position 7C/13C due to the highest FED^2_{HOMO} + FED^2_{LUMO} value (Figure 2.6). Thus, the hydroxyl substitution reaction could generate a mono-

hydroxylated intermediate product 1 (P1) (Figure 2.5). TI-3 with *m*/*z* 243.1033 identified by UHPLC-HRMS/MS is consistent with the FED prediction of a hydroxylated product.

The degradation of BPA is likely initiated by a single electron transfer to Mn(III) resulting in the formation of a BPA radical. Positions with higher values of $2FED^2_{HOMO}$ and more negative charges are more prone to losing one electron and generating radicals. The electron-rich position 1O/11O is a preferred target for Mn(III) attack and the formation of radical R1 (Figure 2.5) by considering both $2FED^2_{HOMO}$ and charge density (Figure 2.6 and Figure S2.5). Resonance stabilization of BPA radical R1 explains the formation of radicals R2 and R3, which is supported by the calculated spin densities of R1 (Table 2.3). The calculation results show that the unpaired electron in R1 is likely to delocalize to 3C/7C and 5C and form R2 and R3, respectively (Figure 2.5 and Table 2.3).

Following radical formation, coupling reactions via carbon-carbon (C-C) and carbon-oxygen (C-O) can occur and generate BPA dimers. A coupling reaction is likely to occur between R1 and R2 by taking both spin densities and charge into account (Table 2.3). The *para* C-O coupling reaction between R1 and R2 would yield a sterically unstable intermediate, which re-aromatizes into P2 and either P3 (hydration), or P4 (elimination) (Figure 2.5). R2 could also undergo *β*-scission to produce R2-1. The newly formed radical R2-1 may engage in coupling reactions with R1 and R3 and yield products P2 and P5 with the same chemical formula, respectively. Other coupling reactions can theoretically occur between R1 and R3 through *ortho* C-O coupling, and between R3 and R3 through *ortho-ortho* C-C coupling yielding products P6 and P7 (Figure 2.5). Consistent with the formation of BPA dimers, the UHPLC-HRMS/MS analysis determined the formation of a compound with an *m*/*z* value of 453.2095 representing a degradation product with the molecular mass of two BPA molecules minus the mass of two hydrogen atoms.

HCA (P3 in Figure 2.5) was identified as a major BPA degradation intermediate (Figure 2.1), which was susceptible to further degradation by Mn(III). The quantum calculations suggest that position 1O is most likely to lose an electron due to a higher $2FED^2_{HOMO}$ value and the lowest charge density (Figure 2.6 and Figure S2.5), suggesting that R4 (Figure 2.5) could be formed via a one-electron extraction, and subsequently yield R5 and R6 due to electron resonance (Table 2.3 and Figure 2.5). These three radicals, together with the radicals directly derived from BPA, could trigger a series of reactions that give rise to several additional degradation products. For example, the coupling reactions between R4 and either R3, R2-1, or R6 would yield products P8, P9 and P10 (Figure 2.5), respectively. In addition, the *para* C-O coupling reactions between R5 and R1 and between R5 and R4 could yield final products P2 and P9, respectively, through sterically unstable intermediates (Figure 2.5). Lastly, R6 could be coupling with R1, R3, R2-1, as well as R6 resulting in the formation of P11, P12, P13, and P14 (Figure 2.5), respectively. UHPLC-HRMS/MS fragmentation of the transformation intermediates indicate that P10, P12, and P14 are the most likely products from reactions with HCA.

2.5 Discussion

MnO_2 is a naturally occurring oxidant and plays an important role in biogeochemical cycling. A number of studies have documented MnO_2-mediated BPA degradation (Lin et al., 2009; Im et al., 2015; Shobnam et al., 2021; Sun et al., 2021). More recently, Mn(III) has been recognized as a strong oxidant and relevant contributor to redox processes in environmental systems (Wang et al., 2014; Johnson et al., 2018; Sun et al., 2021). BPA degradation by soluble Mn(III) has been investigated (Sun et al., 2021), which raises the question about the role of Mn(III) in MnO_2-mediated BPA degradation. The experimental efforts demonstrated that synthetic MnO_2 contains

up to 13% (mol/mol) Mn(III) (Figure 2.2), similar to what other studies have reported (Nico and Zasoski, 2001; Liu et al., 2019). Solid MnO_2 is a mixed valence mineral phase consisting of Mn(IV) and Mn(III) oxides, and previous work documented that surface-associated Mn(III) in MnO_2 affects the rates of MnO_2-mediated reactions (Nico and Zasoski, 2000; 2001; Huang et al., 2018). These observations emphasize a role of Mn(III) when studying MnO_2-mediated degradation reactions.

2.5.1 Contribution of Mn(III) in MnO_2-mediated BPA degradation

The experimental efforts demonstrate that BPA is efficiently degraded by environmentally relevant concentrations of soluble Mn(III) (<80 μM), suggesting that Mn(III) plays a role in attenuating BPA in environmental systems. Similar to prior work studying MnO_2-mediated BPA degradation, HCA was a major degradation intermediate in reaction vessels with soluble Mn(III), although a lower BPA to HCA conversion efficiency of 7.4% was measured compared to >30% during MnO_2-mediated BPA degradation previously (Im et al., 2015; Balgooyen et al., 2017). The differences in conversion efficiencies suggest that MnO_2 has a higher reactivity towards BPA than Mn(III) (i.e., BPA is more susceptible to degradation by MnO_2 than by Mn(III)).

In addition to differences in HCA conversion efficiency, the experimental efforts demonstrate that surface-Mn(III)-free MnO_2 mediates BPA degradation at lower rates than MnO_2 prior to Mn(III) removal. The pseudo-first-order reaction kinetics in the early stage are consistent with previous efforts that investigated MnO_2-mediated degradation of organic contaminants (Zhang and Huang, 2003; Im et al., 2015). A likely explanation for the lower reaction rates observed with surface-Mn(III)-free MnO_2 is the absence of Mn(III). Mn(III)-mediated oxidation activity was most apparent during the early stages of incubation (Figure 2.1A), which overlaps with the time period generally used for determining degradation rates in

systems with MnO_2. Mn(III) associated with MnO_2 contributes to BPA degradation and impacts the reaction rates. Therefore, the oxidation rates reported in systems with MnO_2 and attributed to Mn(IV) likely represent the combined reactivity of MnO_2 and surface-associated Mn(III).

The measurements in systems with MnO_2 as oxidant represent the combined reactivity of Mn(III) and Mn(IV) in MnO_2. The participation of two distinct reactants is consistent with the observation of two different reaction mechanisms (i.e., Mn(III) involved and Mn(IV) involved) in aqueous systems with MnO_2 (Nico and Zasoski, 2001). The data (Figures 2.1 and 2.2) demonstrate that the Mn(III) associated with the surface of MnO_2 is insufficient to completely degrade the initial 1.76 μmol of BPA over the same incubation period.

2.5.2 Theoretical considerations of MnO_2-mediated BPA degradation

Abiotic redox reaction proceed in three indispensable steps including pre-reaction complex formation, electron transfer, and post-reaction complex dissociation (Nico and Zasoski, 2000). Electron transfer is generally considered the rate-limiting step (Metzler-Nolte and Kraatz, 2006). The overall Gibbs free energy change ($\Delta G = -nEF$) of the reaction is related to the reduction potential (E) and controls the rate of electron transfer between two reactants (Marcus, 1993). The standard reduction potential (E^o) values for the reduction of Mn(IV) to Mn(II) and Mn(III) to Mn(II) are 1.29 V (Wang and Stone, 2006) and 1.51 V (Kostka et al., 1995), respectively. Thus, the reduction of Mn(III) to Mn(II) should be a faster reaction assuming that the E^o of BPA oxidation in both reactions is the same. Also, Mn(III) can directly coordinate with BPA through the empty σ orbital ($t_{2g}^3e_g^1 \rightarrow t_g^3e_g^2$) to accept electrons, whereas Mn(IV) would have to undergo outer sphere electron transfer ($t_{2g}^3 \rightarrow t_{2g}^3e_g^2$) during the oxidation process (Ukrainczyk and McBride, 1992). The latter process is more challenging because an outer electron transfer into a π orbital requires a change in the Mn spin state (Ukrainczyk and McBride, 1992). Our results are

consistent with these theories, and lower BPA degradation rates were observed in systems with surface-Mn(III)-free MnO_2 as oxidant (Figure 2.4).

2.5.3 BPA degradation products generated by Mn(III)

The UHPLC-HRMS/MS analysis identified intermediates with eight different mass-to-charge ratios (*m/z*) and quantum calculations predicted 14 different degradation products based on these eight intermediates (Figure 2.5). Prior work documented the utility of this combined approach to identify degradation products and propose degradation pathways (Ohko et al., 2002; Huang and Weber, 2005; Blotevogel et al., 2010; Wang et al., 2018). In laboratory systems with MnO_2, 11 BPA degradation products were experimentally identified (Lin et al., 2009). Compared the present study with this prior work, five degradation products are shared between these two studies, but the remaining nine of the 14 degradation products proposed in the present study are different. The main differences in the BPA degradation pathways mediated by Mn(III) versus Mn(IV) occur following the formation of HCA, the major degradation intermediate in both pathways. HCA is susceptible to oxidization by Mn(III), and the transformation of HCA gave rise to seven (i.e., P8-P14) of the nine distinct degradation products identified. Prior studies demonstrated that HCA is susceptible to further degradation by MnO_2; however, no transformation intermediates of HCA had been identified (Im et al., 2015; Shobnam et al., 2021).

BPA is a potential hormonally active agent and transformation/degradation should result in reduced endocrine disrupting activity; however, the human health concerns associated with the degradation products are not clear. Some BPA degradation products have been documented to impact human cancer cells more than the parent compound (Suzuki et al., 2004; McCormick et al., 2011; Nakamura et al., 2011), and the major product observed in biotic and abiotic degradation, HCA, has been shown to have a higher estrogen receptor binding affinity than BPA

(Nakamura et al., 2011). The ECOSAR program has predictive capabilities and can estimate toxicity to aquatic organisms such as fish, *Daphnia*, and green algae. ECOSAR categorizes BPA as toxic to very toxic (LC50/EC50/ChV<10 mg L^{-1}) to aquatic organisms (Table 2.4). BPA degradation yielded products with lower ECOSAR-predicted toxicity (i.e., P1, P3, P13, and P14); however, several (e.g., P2, P5, P6, P7, P8, P11, and P12) are predicted to have higher toxicity than BPA, and ECOSAR categorizes these compounds as very toxic (LC50/EC50/ChV<1 mg L^{-1}). Therefore, the fate of BPA degradation products should be understood for a meaningful and comprehensive risk assessment. The major degradation products (e.g., HCA, mono-hydroxylated BPA) are susceptible to biotic (Suzuki et al., 2004) and abiotic (Im et al., 2015) degradation making it unlikely that toxicity to aquatic organisms increase as a result of BPA transformation. Of note, BPA concentrations detected in sediments range from 1.49 to 13,370 ng BPA g^{-1} (dry weight) (Liao et al., 2012b). Even the highest reported BPA concentration of about 0.1 mg L^{-1} in landfill leachate (Kalmykova et al., 2013) is substantially lower than the concentrations used in many toxicological studies (Suzuki et al., 2004). Assuming a maximum conversion efficiency of BPA to HCA of 10%, as was observed in the present study, a maximum amount of approximately 7 μg L^{-1} of HCA would be expected. This concentration is at least 230-fold lower than the predicted value for acute and chronic toxicity based on the ECOSAR categorization (Table 2.4). Considering that BPA concentrations in impacted sediments are generally well below 0.1 mg L^{-1}, it is not likely that Mn(III)- /Mn(IV)-mediated degradation will generate BPA degradation intermediates at concentrations that would result in acute or chronic toxicity (Table 2.4).

2.5.4 Environmental implications

The study demonstrated that Mn(III) efficiently removes BPA and illustrates its role in MnO_2-mediated BPA degradation. Active Mn cycling occurs at oxic-anoxic transition zones and concentrations of Mn(III) and MnO_2 of up to 80 μM and 348 mg L^{-1}, respectively, have been observed in natural environments (Sigg et al., 1987; Trouwborst et al., 2006; Vandieken et al., 2012; Madison et al., 2013). The formation of soluble Mn(III) via Mn(II) oxidation (Webb et al., 2005), Mn(IV) reduction (Lin et al., 2012), and conproportionation between Mn(II) and Mn(IV) (Qian et al., 2019) have been demonstrated, and a recent study illustrated that soluble Mn(III) degrades adsorbed BPA (Sun et al., 2021). MnO_2, including both synthetic and biogenic types, typically contain Mn(III) of up to 36% (Nico and Zasoski, 2001; Villalobos et al., 2003; Feng et al., 2010; Learman et al., 2011b; Huang et al., 2018). These observations suggest that attenuation of BPA in natural systems can occur in environments with active Mn-cycling. In addition, the finding that both Mn(III) and Mn(IV) can effectively degrade BPA and surface-associated Mn(III) increases the reactivity of MnO_2, advances our understanding of natural attenuation processes that affect the fate and longevity of BPA. Engineered approaches aimed at generating more reactive MnO_2 for BPA removal and increasing Mn cycling near oxic-anoxic transition zones could be a productive strategy to enhance BPA transformation and generate products that are susceptible to further abiotic degradation and aerobic microbial metabolism.

Acknowledgments

This work was supported by the Polycarbonate/BPA Global Group of the American Chemistry Council (ACC), Washington, DC. Samples were processed in the Biological and

Small Molecule Mass Spectrometry Core (BSMMSC), University of Tennessee, Knoxville, TN (RRID: SCR_021368).

References

An, T., Yang, H., Li, G., Song, W., Cooper, W.J. and Nie, X. 2010. Kinetics and mechanism of advanced oxidation processes (AOPs) in degradation of ciprofloxacin in water. Applied Catalysis B: Environmental 94(3-4), 288-294.

Balgooyen, S., Alaimo, P.J., Remucal, C.K. and Ginder-Vogel, M. 2017. Structural transformation of MnO_2 during the oxidation of bisphenol A. Environ. Sci. Technol. 51(11), 6053-6062.

Blotevogel, J., Borch, T., Desyaterik, Y., Mayeno, A.N. and Sale, T.C. 2010. Quantum chemical prediction of redox reactivity and degradation pathways for aqueous phase contaminants: An example with HMPA. Environ. Sci. Technol. 44(15), 5868-5874.

Chempath, S., Boncella, J.M., Pratt, L.R., Henson, N. and Pivovar, B.S. 2010. Density functional theory study of degradation of tetraalkylammonium hydroxides. J. Phys. Chem. C 114(27), 11977-11983.

Chen, J., Wu, N., Xu, X., Qu, R., Li, C., Pan, X., Wei, Z. and Wang, Z. 2018. Fe (VI)-mediated single-electron coupling processes for the removal of chlorophene: a combined experimental and computational study. Environ. Sci. Technol. 52(21), 12592-12601.

Chen, W.-R., Liu, C., Boyd, S.A., Teppen, B.J. and Li, H. 2013. Reduction of carbadox mediated by reaction of Mn(III) with oxalic acid. Environ. Sci. Technol. 47(3), 1357-1364.

Choi, Y.J. and Lee, L.S. 2017. Aerobic soil biodegradation of bisphenol (BPA) alternatives bisphenol S and bisphenol AF compared to BPA. Environ. Sci. Technol. 51(23), 13698-13704.

Feng, X.H., Zhu, M., Ginder-Vogel, M., Ni, C., Parikh, S.J. and Sparks, D.L. 2010. Formation of nano-crystalline todorokite from biogenic Mn oxides. Geochim. Cosmochim. Acta. 74(11), 3232-3245.

Fleck, N., Hett, T., Brode, J., Meyer, A., Richert, S. and Schiemann, O. 2019. C–C cross-coupling reactions of trityl radicals: spin density delocalization, exchange coupling, and a spin label. J. Org. Chem. 84(6), 3293-3303.

Frisch, M., Trucks, G., Schlegel, H., Scuseria, G., Robb, M., Cheeseman, J., Scalmani, G., Barone, V., Mennucci, B. and Petersson, G. 2009. Gaussian 09; Gaussian, Inc. J Wallingford, CT 32, 5648-5652.

Fromme, H., Küchler, T., Otto, T., Pilz, K., Müller, J. and Wenzel, A. 2002. Occurrence of phthalates and bisphenol A and F in the environment. Water Res. 36(6), 1429-1438.

Fukui, K., Yonezawa, T., Nagata, C. and Shingu, H. 1954. Molecular orbital theory of orientation in aromatic, heteroaromatic, and other conjugated molecules. J. Chem. Phys 22(8), 1433-1442.

Fukui, K., Yonezawa, T. and Shingu, H. 1952. A molecular orbital theory of reactivity in aromatic hydrocarbons. J. Chem. Phys 20(4), 722-725.

Huang, D., Zhao, H., Liu, C. and Sun, C. 2014. Characteristics, sources, and transport of tetrabromobisphenol A and bisphenol A in soils from a typical e-waste recycling area in South China. Environ. Sci. Pollut. Res. 21(9), 5818-5826.

Huang, J., Zhong, S., Dai, Y., Liu, C.-C. and Zhang, H. 2018. Effect of MnO_2 phase structure on the oxidative reactivity toward bisphenol A degradation. Environ. Sci. Technol. 52(19), 11309-11318.

Huang, Q. and Weber, W.J. 2005. Transformation and removal of bisphenol A from aqueous phase via peroxidase-mediated oxidative coupling reactions: efficacy, products, and pathways. Environ. Sci. Technol. 39(16), 6029-6036.

Im, J. and Löffler, F.E. 2016. Fate of bisphenol A in terrestrial and aquatic environments. Environ. Sci. Technol. 50(16), 8403-8416.

Im, J., Prevatte, C.W., Campagna, S.R. and Löffler, F.E. 2015. Identification of 4-hydroxycumyl alcohol as the major MnO_2-mediated bisphenol A transformation product and evaluation of its environmental fate. Environ. Sci. Technol. 49(10), 6214-6221.

Im, J., Prevatte, C.W., Lee, H.G., Campagna, S.R. and Löffler, F.E. 2014. 4-Methylphenol produced in freshwater sediment microcosms is not a bisphenol A metabolite. Chemosphere 117, 521-526.

Johnson, K.L., McCann, C.M., Wilkinson, J.-L., Jones, M., Tebo, B.M., West, M., Elgy, C., Clarke, C.E., Gowdy, C. and Hudson-Edwards, K.A. 2018. Dissolved Mn(III) in water treatment works: Prevalence and significance. Water Res. 140, 181-190.

Jones, M.E., Nico, P.S., Ying, S., Regier, T., Thieme, J.r. and Keiluweit, M. 2018. Manganese-driven carbon oxidation at oxic–anoxic interfaces. Environ. Sci. Technol. 52(21), 12349-12357.

Kalmykova, Y., Björklund, K., Strömvall, A.-M. and Blom, L. 2013. Partitioning of polycyclic aromatic hydrocarbons, alkylphenols, bisphenol A and phthalates in landfill leachates and stormwater. Water Res. 47(3), 1317-1328.

Klewicki, J. and Morgan, J. 1999. Dissolution of β-MnOOH particles by ligands: pyrophosphate, ethylenediaminetetraacetate, and citrate. Geochim. Cosmochim. Acta. 63(19-20), 3017-3024.

Klewicki, J.K. and Morgan, J.J. 1998. Kinetic behavior of Mn(III) complexes of pyrophosphate, EDTA, and citrate. Environ. Sci. Technol. 32(19), 2916-2922.

Kostka, J.E., Luther III, G.W. and Nealson, K.H. 1995. Chemical and biological reduction of Mn(III)-pyrophosphate complexes: potential importance of dissolved Mn(III) as an environmental oxidant. Geochim. Cosmochim. Acta. 59(5), 885-894.

Learman, D., Wankel, S., Webb, S., Martinez, N., Madden, A. and Hansel, C. 2011. Coupled biotic–abiotic Mn (II) oxidation pathway mediates the formation and structural evolution of biogenic Mn oxides. Geochim. Cosmochim. Acta. 75(20), 6048-6063.

Li, J., Pang, S., Zhou, Y., Sun, S., Wang, L., Wang, Z., Gao, Y., Yang, Y. and Jiang, J. 2018. Transformation of bisphenol AF and bisphenol S by manganese dioxide and effect of iodide. Water Res. 143, 47-55.

Liao, C., Liu, F., Moon, H.-B., Yamashita, N., Yun, S. and Kannan, K. 2012. Bisphenol analogues in sediments from industrialized areas in the United States, Japan, and Korea: spatial and temporal distributions. Environ. Sci. Technol. 46(21), 11558-11565.

Lin, H., Szeinbaum, N.H., DiChristina, T.J. and Taillefert, M. 2012. Microbial Mn(IV) reduction requires an initial one-electron reductive solubilization step. Geochim. Cosmochim. Acta. 99, 179-192.

Lin, K., Liu, W. and Gan, J. 2009. Oxidative removal of bisphenol A by manganese dioxide: efficacy, products, and pathways. Environ. Sci. Technol. 43(10), 3860-3864.

Liu, W., Sun, B., Qiao, J. and Guan, X. 2019. Influence of pyrophosphate on the generation of soluble Mn(III) from reactions involving Mn oxides and Mn(VII). Environ. Sci. Technol. 53(17), 10227-10235.

Lowe, J.P. and Peterson, K. (2011) Quantum chemistry, Elsevier.

Madison, A.S., Tebo, B.M., Mucci, A., Sundby, B. and Luther, G.W. 2013. Abundant porewater Mn(III) is a major component of the sedimentary redox system. Science 341(6148), 875-878.

Marcus, R.A. 1993. Electron transfer reactions in chemistry. Theory and experiment. Rev. Mod. Phys. 65(3), 599.

McCormick, J.M., Es, T.V., Cooper, K.R., White, L.A. and Häggblom, M.M. 2011. Microbially mediated *O*-methylation of bisphenol A results in metabolites with increased toxicity to the developing zebrafish (*Danio rerio*) embryo. Environ. Sci. Technol. 45(15), 6567-6574.

Metzler-Nolte, N. and Kraatz, H. (2006) Concepts and models in bioinorganic chemistry, Wiley-Vch New York.

Nakamura, S., Tezuka, Y., Ushiyama, A., Kawashima, C., Kitagawara, Y., Takahashi, K., Ohta, S. and Mashino, T. 2011. *Ipso* substitution of bisphenol A catalyzed by microsomal cytochrome P450 and enhancement of estrogenic activity. Toxicol. Lett. 203(1), 92-95.

Nico, P.S. and Zasoski, R.J. 2000. Importance of Mn(III) availability on the rate of Cr(III) oxidation on δ-MnO_2. Environ. Sci. Technol. 34(16), 3363-3367.

Nico, P.S. and Zasoski, R.J. 2001. Mn(III) center availability as a rate controlling factor in the oxidation of phenol and sulfide on δ-MnO_2. Environ. Sci. Technol. 35(16), 3338-3343.

Ohko, Y., Iuchi, K.-i., Niwa, C., Tatsuma, T., Nakashima, T., Iguchi, T., Kubota, Y. and Fujishima, A. 2002. 17β-Estradiol degradation by TiO_2 photocatalysis as a means of reducing estrogenic activity. Environ. Sci. Technol. 36(19), 4175-4181.

Qian, A., Zhang, W., Shi, C., Pan, C., Giammar, D.E., Yuan, S., Zhang, H. and Wang, Z. 2019. Geochemical stability of dissolved Mn(III) in the presence of pyrophosphate as a model ligand: Complexation and disproportionation. Environ. Sci. Technol. 53(10), 5768-5777.

Research, E.M. 2021 Global bisphenol A (BPA) market report and forecast 2021-2026.

Shobnam, N., Sun, Y., Mahmood, M., Löffler, F.E. and Im, J. 2021. Biologically mediated abiotic degradation (BMAD) of bisphenol A by manganese-oxidizing bacteria. J. Hazard. Mater., 125987.

Sigg, L., Sturm, M. and Kistler, D. 1987. Vertical transport of heavy metals by settling particles in Lake Zurich. Limnol. Oceanogr. 32(1), 112-130.

Staples, C.A., Dome, P.B., Klecka, G.M., Oblock, S.T. and Harris, L.R. 1998. A review of the environmental fate, effects, and exposures of bisphenol A. Chemosphere 36(10), 2149-2173.

Stone, A.T. 1987. Reductive dissolution of manganese (III/IV) oxides by substituted phenols. Environ. Sci. Technol. 21(10), 979-988.

Sun, B., Guan, X., Fang, J. and Tratnyek, P.G. 2015. Activation of manganese oxidants with bisulfite for enhanced oxidation of organic contaminants: the involvement of Mn(III). Environ. Sci. Technol. 49(20), 12414-12421.

Sun, Y., Im, J., Shobnam, N., Fanourakis, S.K., He, L., Anovitz, L.M., Erickson, P.R., Sun, H., Zhuang, J. and Löffler, F.E. 2021. Degradation of adsorbed bisphenol A by soluble Mn(III). Environ. Sci. Technol. 55(19), 13014-13023.

Suzuki, T., Nakagawa, Y., Takano, I., Yaguchi, K. and Yasuda, K. 2004. Environmental fate of bisphenol A and its biological metabolites in river water and their xeno-estrogenic activity. Environ. Sci. Technol. 38(8), 2389-2396.

Trouwborst, R.E., Clement, B.G., Tebo, B.M., Glazer, B.T. and Luther, G.W. 2006. Soluble Mn(III) in suboxic zones. Science 313(5795), 1955-1957.

Ukrainczyk, L. and McBride, M.B. 1992. Oxidation of phenol in acidic aqueous suspensions of manganese oxides. Clays Clay Miner. 40(2), 157-166.

USEPA 2017. USEPA ECOSAR (Ecological Structure Activity Relationships) v.2.0. https://www.epa.gov/tsca-screening-tools/ecological-structure-activity-relationships-ecosar-predictive-model (accessed Aug 31, 2021).

Vandieken, V., Pester, M., Finke, N., Hyun, J.-H., Friedrich, M.W., Loy, A. and Thamdrup, B. 2012. Three manganese oxide-rich marine sediments harbor similar communities of acetate-oxidizing manganese-reducing bacteria. ISME J. 6(11), 2078-2090.

Villalobos, M., Toner, B., Bargar, J. and Sposito, G. 2003. Characterization of the manganese oxide produced by *Pseudomonas putida* strain MnB1. Geochim. Cosmochim. Acta. 67(14), 2649-2662.

Wang, X., Wang, S., Qu, R., Ge, J., Wang, Z. and Gu, C. 2018. Enhanced removal of chlorophene and 17β-estradiol by Mn(III) in a mixture solution with humic acid: investigation of reaction kinetics and formation of co-oligomerization products. Environ. Sci. Technol. 52(22), 13222-13230.

Wang, Y. and Stone, A.T. 2006. The citric acid–$Mn^{III,IV}O_2$(birnessite) reaction. Electron transfer, complex formation, and autocatalytic feedback. Geochim. Cosmochim. Acta. 70(17), 4463-4476.

Wang, Z., Xiong, W., Tebo, B.M. and Giammar, D.E. 2014. Oxidative UO_2 dissolution induced by soluble Mn(III). Environ. Sci. Technol. 48(1), 289-298.

Webb, S.M., Dick, G.J., Bargar, J.R. and Tebo, B.M. 2005. Evidence for the presence of Mn(III) intermediates in the bacterial oxidation of Mn (II). Proc. Natl. Acad. Sci. U. S. A. 102(15), 5558-5563.

Wright, M.H., Farooqui, S.M., White, A.R. and Greene, A.C. 2016. Production of manganese oxide nanoparticles by Shewanella species. Appl. Environ. Microbiol. 82(17), 5402-5409.

Xu, X., Chen, J., Wang, S., Ge, J., Qu, R., Feng, M., Sharma, V.K. and Wang, Z. 2018. Degradation kinetics and transformation products of chlorophene by aqueous permanganate. Water Res. 138, 293-300.

Yan, J., Bi, M., Bourdon, A.K., Farmer, A.T., Wang, P.-H., Molenda, O., Quaile, A.T., Jiang, N., Yang, Y., Yin, Y., Şimşir, B., Campagna, S.R., Edwards, E.A. and Löffler, F.E. 2018. Purinyl-cobamide is a native prosthetic group of reductive dehalogenases. Nat. Chem. Biol. 14(1), 8.

Zhang, H. and Huang, C. 2003. Oxidative transformation of triclosan and chlorophene by manganese oxides. Environ. Sci. Technol. 37(11), 2421-2430.

Appendix

Table 2.1. Removal of BPA (1.76 µmol) after 10- and 60-min incubation periods in the presence of 0.05, 0.25, and 1 mM of Mn(III), MnO_2, and surface-Mn(III)-free MnO_2. MnO_2 and surface-Mn(III)-free MnO_2 are expressed as nominal concentrations. The data represent the averages and the standard deviations of duplicate incubations.

Oxidant	Concentration (mM)	µmol BPA removed (%)	
		Incubation time	
		10 min	60 min
Mn(III)	0.05	35.55 ± 0.75	43.59 ± 0.19
	0.25	44.62 ± 0.13	61.82 ± 0.32
	1	43.46 ± 3.61	63.89 ± 0.73
MnO_2	0.05	15.16 ± 1.53	24.42 ± 2.35
	0.25	35.47 ± 2.41	81.79 ± 1.19
	1	87.61 ± 0.23	100
Surface-Mn(III)-free-MnO_2	0.05	5.15 ± 1.15	22.16 ± 0.56
	0.25	19.78 ± 0.11	70.56 ± 2.78
	1	52.83 ± 2.67	100

Table 2.2. Accurate mass measurements of BPA transformation intermediates by UHPLC-HRMS/MS.

ID[a]	Retention time (min)	Experimental mass (*m*/*z*)	Calculated mass (*m*/*z*)	Formula $[M-H]^-$	Formula	Mass error (ppm)
TI-1	4.71	151.0757	151.0759	$C_9H_{11}O_2^-$	$C_9H_{12}O_2$	1.32
TI-2	4.6	133.0651	133.0653	$C_9H_9O^-$	$C_9H_{10}O$	1.50
TI-3	6.44	243.1033	243.1027	$C_{15}H_{15}O_3^-$	$C_{15}H_{16}O_3$	2.63
TI-4	5.76	301.1454	301.1445	$C_{18}H_{21}O_4^-$	$C_{18}H_{22}O_4$	3.02
TI-5	10.27	319.1348	319.1340	$C_{21}H_{19}O_3^-$	$C_{21}H_{20}O_3$	2.51
TI-6	8.11	377.1772	377.1758	$C_{24}H_{25}O_4^-$	$C_{24}H_{26}O_4$	3.76
TI-7	10.7	453.2095	453.2071	$C_{30}H_{29}O_4^-$	$C_{30}H_{30}O_4$	5.16
TI-8	12.1	453.2093	453.2071	$C_{30}H_{29}O_4^-$	$C_{30}H_{30}O_4$	4.87

[a]The ID number indicates transformation intermediates identified by UHPLC-HRMS/MS.

Table 2.3. Spin densities and charge densities on carbon and oxygen atoms of BPA and HCA radicals calculated by using Gaussian 09 program at the B3LYP/6-311** level.

BPA structure	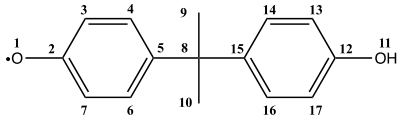		**HCA structure**	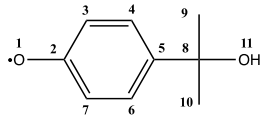	
BPA (atom number)	**Spin density (e/Å^3)**	**Charge density (e/Å^3)**	**HCA (atom number)**	**Spin density (e/Å^3)**	**Charge density (e/Å^3)**
1O	0.376	-0.378	1O	0.399	-0.544
2C	-0.056	0.185	2C	-0.071	0.386
3C	0.310	-0.111	3C	0.304	-0.119
4C	-0.151	-0.054	4C	-0.156	-0.105
5C	0.410	-0.041	5C	0.402	0.095
6C	-0.136	-0.030	6C	-0.150	-0.110
7C	0.250	-0.119	7C	0.280	-0.124
8C	-0.028	-0.217	8C	0.025	0.225
9C	0.002	-0.252	9C	0.013	-0.319
10C	0.014	-0.251	10C	0.013	-0.318
11O	0.002	-0.389	11O	0.000	-0.584
12C	0.005	0.152	-	-	-
13C	-0.003	-0.131	-	-	-
14C	0.005	-0.062	-	-	-
15C	0.012	-0.066	-	-	-
16C	0.002	-0.082	-	-	-
17C	0.002	-0.110	-	-	-

The letters O and C represent the oxygen and carbon atoms, respectively, in BPA and HCA radicals. The hydrogen atoms are not shown. Å, Ångström (10^{-10} m).

Table 2.4. Predicted acute and chronic toxicity of BPA and its transformation products using the ECOSAR program.

Compounds	Acute toxicity (mg L^{-1})			Chronic toxicity (mg L^{-1})		
	Fish (LC_{50})	Daphnid (LC_{50})	Green algae (EC_{50})	Fish	Daphnid	Green algae
BPA	1.28	5.24	1.33	0.550	1.77	0.227
P1	2.65	13.1	2.07	1.22	4.57	0.329
P2	0.107	0.193	0.377	0.034	0.058	0.087
P3 (HCA)	48.3	16.4	4.17	4.53	1.64	7.79
P4	3.99	2.67	0.364	0.435	0.345	0.971
P5	0.310	0.758	0.688	0.109	0.238	0.142
P6	0.026	0.028	0.196	0.0067	0.0077	0.055
P7	0.024	0.025	0.186	0.0060	0.0068	0.052
P8	0.381	0.377	0.486	0.062	0.128	0.520
P9	2.99	2.57	0.279	0.346	0.367	0.850
P10	7.90	5.48	0.724	0.870	0.720	1.97
P11	0.381	0.377	0.486	0.062	0.128	0.520
P12	0.332	0.331	0.438	0.055	0.114	0.477
P13	16.2	13.6	7.93	1.68	2.74	4.90
P14	9.63	8.34	5.59	1.08	1.84	3.80

LC_{50} represents the degradation product concentration that could result in 50% death of fish and *Daphnia* after 96 and 48 h of exposure, respectively. EC_{50} represents the degradation product concentration that could result in 50% growth inhibition of green algae after 96 h of exposure. Toxicity was classified based on the Globally Harmonized System of Classification and Labeling of Chemicals (https://unece.org/fileadmin/DAM/trans/danger/publi/ghs/ghs_rev04/English/ST-SG-AC10-30-Rev4e.pdf). Very toxic: $LC_{50}/EC_{50}/ChV \leq 1$ mg L^{-1}, Toxic: 1 mg $L^{-1} < LC_{50}/EC_{50}/ChV \leq 10$ mg L^{-1}, Harmful: 10 mg $L^{-1} < LC_{50}/EC_{50}/ChV \leq 100$ mg L^{-1}.

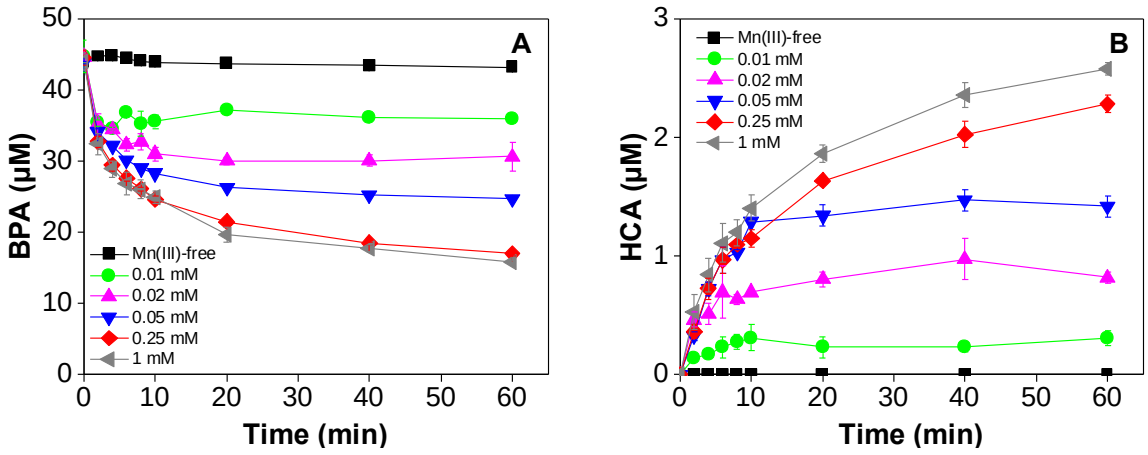

Figure 2.1. BPA degradation and HCA formation in the presence of various concentrations of soluble Mn(III). (A) Mn(III)-mediated BPA degradation in incubation vessels with 5 mM phosphate buffer (pH 7.2) initially containing 1.76 μmol of BPA. (B) HCA formation in the incubations vessels amended with Mn(III) and BPA. No BPA disappearance and HCA formation were observed in incubation vessels without Mn(III) additions. Error bars represent the standard deviation of duplicate samples and are not shown when smaller than the symbol size.

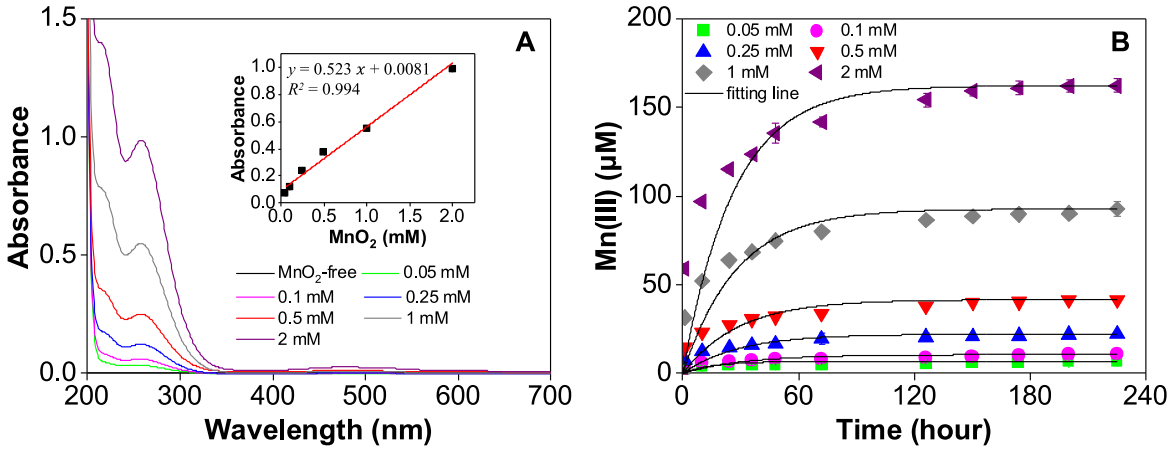

Figure 2.2. Extraction of Mn(III) from MnO_2 with pyrophosphate. (A) UV-vis spectra of Mn(III)-pyrophosphate generated by incubating different amounts of MnO_2 with pyrophosphate for 150 hours. The inset shows the relation between absorbance and the initial loading (nominal concentrations) of MnO_2. (B) Time courses of Mn(III)-pyrophosphate formation in incubation vessels with different initial MnO_2 loadings (nominal concentrations) at pH 7.2. Error bars represent the standard deviation of triplicate samples and are not shown when smaller than the symbol size.

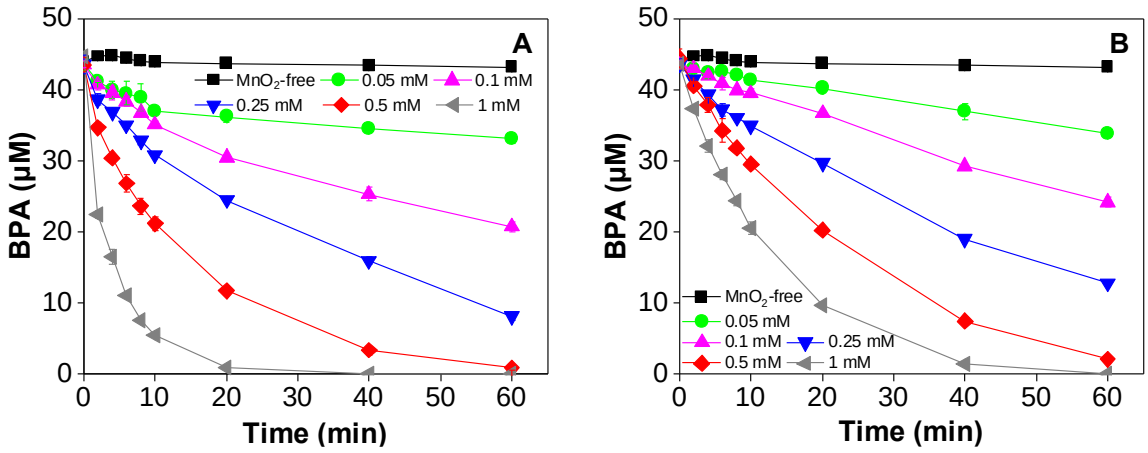

Figure 2.3. BPA removal in the presence of various nominal concentrations of MnO_2 and surface-Mn(III)-free MnO_2. (A) MnO_2-mediated BPA degradation in incubation vessels with 5 mM phosphate buffer (pH 7.2) initially containing 1.76 μmol of BPA. (B) Surface-Mn(III)-free MnO_2-mediated BPA degradation in incubation vessels with 5 mM phosphate buffer (pH 7.2) initially containing 1.76 μmol of BPA. MnO_2 is expressed as nominal concentration. Error bars represent the standard deviation of duplicate samples and are not shown when smaller than the symbol size.

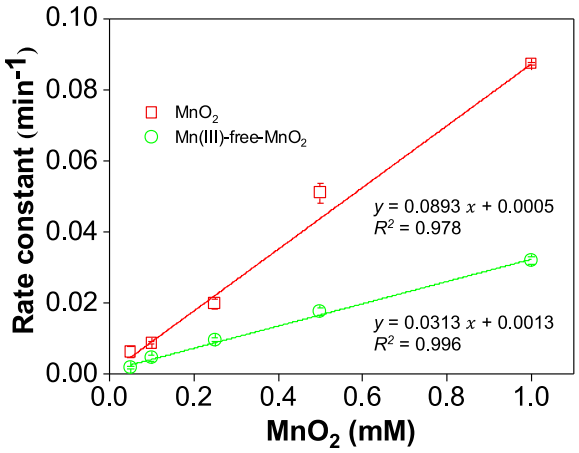

Figure 2.4. Effect of MnO_2 and surface-Mn(III)-free MnO_2 loadings on BPA degradation rate constants. MnO_2 and surface-Mn(III)-free MnO_2 are expressed as nominal concentrations. Error bars represent the standard deviation of duplicate samples.

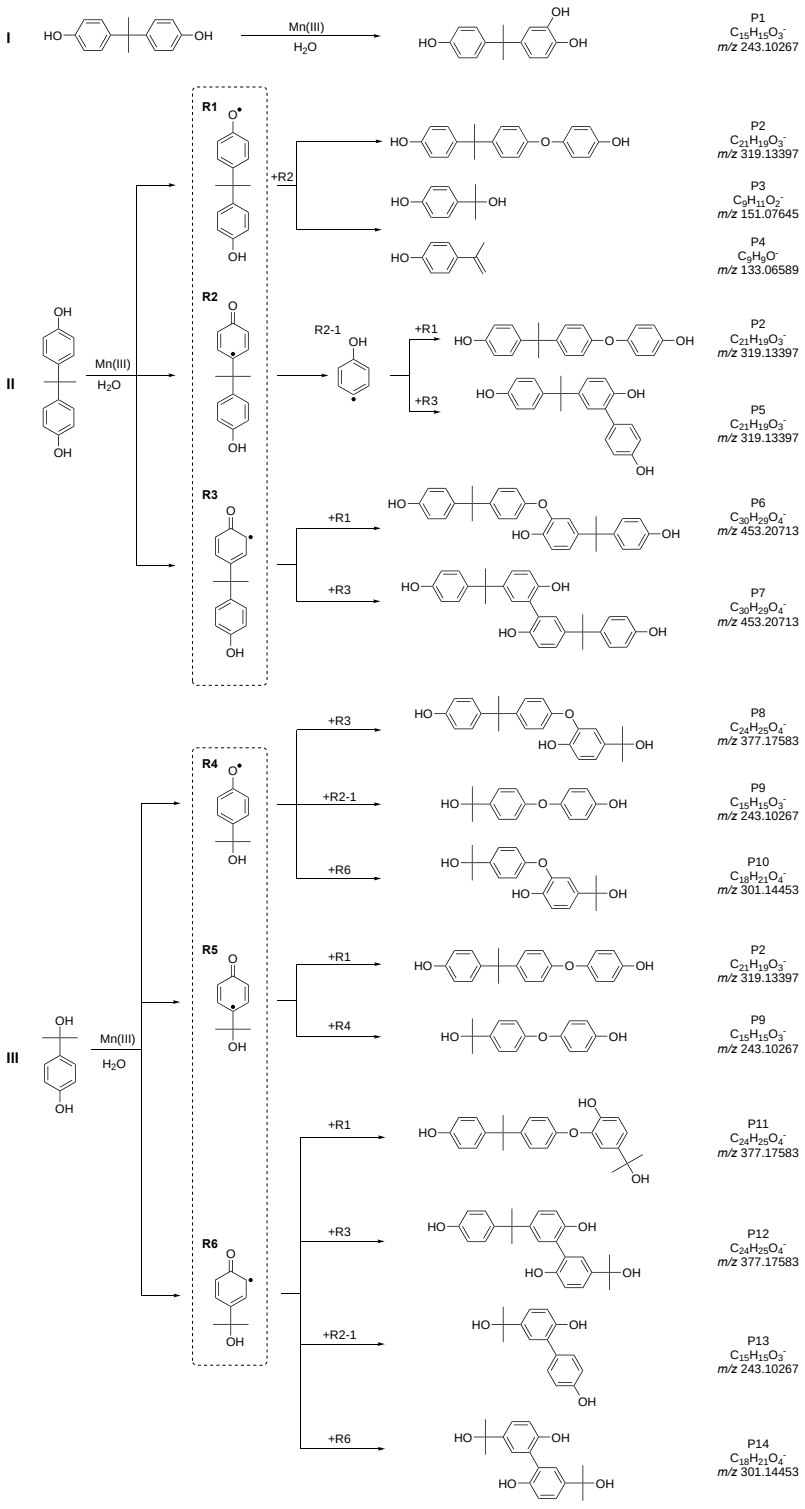

Figure 2.5. Proposed reaction pathways for BPA degradation by Mn(III) in phosphate buffer (pH 7.2).

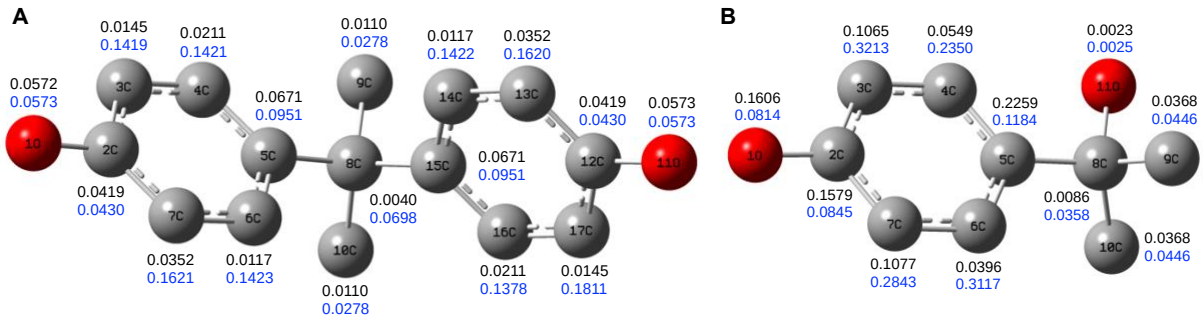

Figure 2.6. Frontier electron densities on carbon and oxygen atoms of BPA (A) and HCA (B) calculated by using Gaussian 09 program at the B3LYP/6-311** level. The numbers in black font indicate the $2FED^2_{HOMO}$ values, and numbers in blue font show the $FED^2_{HOMO} + FED^2_{LUMO}$ values. The red and grey spheres represent the oxygen and carbon atoms, respectively, in the BPA (left) and HCA (right) molecules. The hydrogen atoms are not shown.

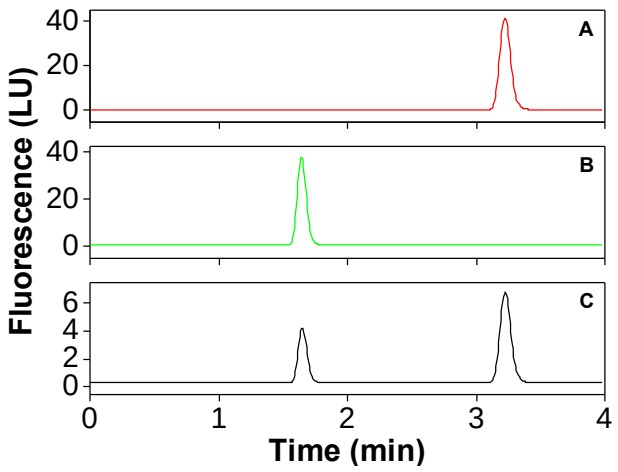

Figure S2.1. HPLC-FLD chromatograms documenting the degradation of BPA to HCA. (A) BPA standard (44 µM) in 5 mM phosphate buffer at pH 7.2 (B) Synthetic HCA standard (44.4 µM) in phosphate buffer at pH 7.2. (C) BPA (44 µM) after incubation with 0.5 mM Mn(III) at pH 7.2 for 20 min. LU=luminescence units.

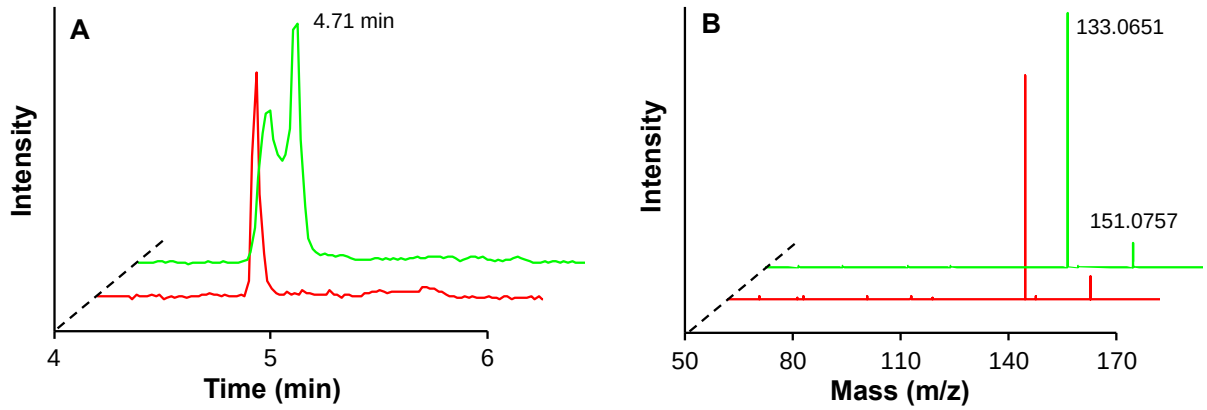

Figure S2.2. Evidence for the formation of HCA as transformation intermediate. (A) Total ion chromatogram and (B) mass spectra of authentic HCA (red) and HCA (green) generated from BPA following treatment with soluble Mn(III).

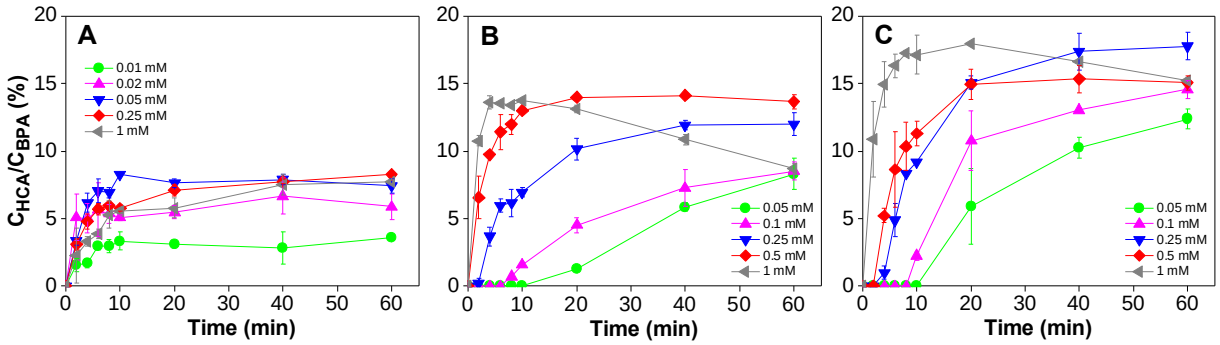

Figure S2.3. BPA conversion efficiency to HCA in the presence of different concentrations of oxidized Mn species. (A) Effect of Mn(III) loading on the conversion efficiency of BPA to HCA. (B) Conversion efficiency of BPA to HCA by MnO_2. (C) Conversion efficiency of BPA to HCA by surface-Mn(III)-free MnO_2. Incubations were performed in 60-mL glass vessels containing 5 mM phosphate buffer (pH 7.2) with an initial BPA concentration of 44 μM BPA over a 1-h incubation period. MnO_2 and surface-Mn(III)-free MnO_2 are expressed as nominal concentration. Error bars represent the standard deviation of duplicate samples and are not shown when smaller than the symbol size.

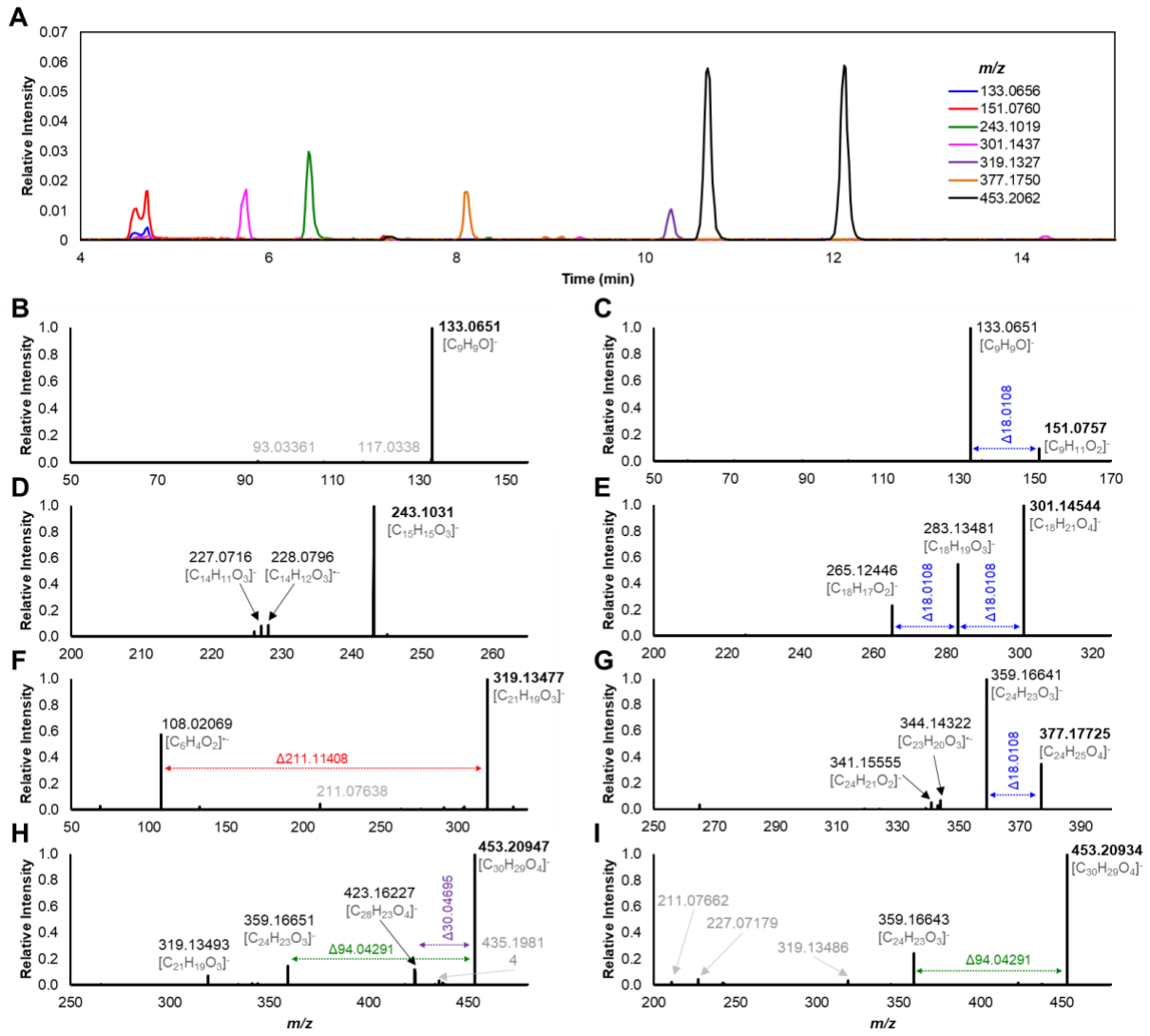

Figure S2.4. UHPLC-HRMS/MS detection of transformation intermediates (TI1-TI8) of BPA following Mn(III) treatment. Combined extracted ion chromatograms (EICs) for *m/z* associated with transformation intermediates are shown in panel A. Panels B-I show the mass spectrum of fragment ions for each *m/z* (indicated in bold text) shown in panel A. The Δ*m/z* are the neutral loss difference between fragments with a relative intensity >10%. Similar Δ*m/z* differences are depicted in the same color. Fragments in gray text have relative intensities <5%.

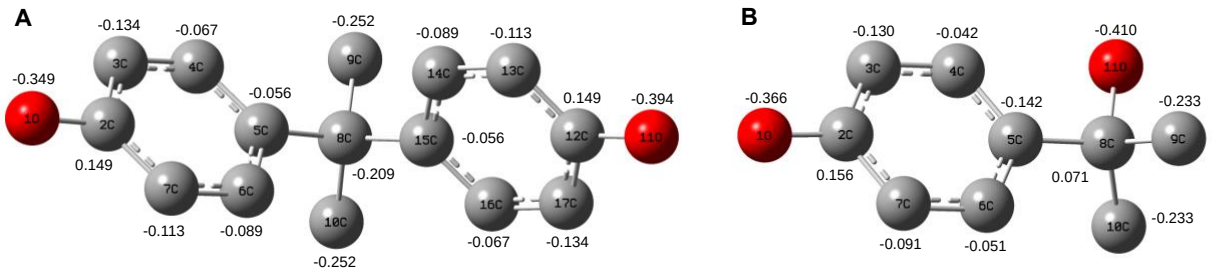

Figure S2.5. Charge densities on carbon and oxygen atoms of BPA (A) and HCA (B) calculated by using Gaussian 09 program at the B3LYP/6-311** level. The letters O and C represent the oxygen and carbon atoms, respectively, in BPA and HCA molecules. The hydrogen atoms are not shown. The unit of the charge density is e/Å^3.

Chapter 3. Degradation of Adsorbed Bisphenol A (BPA) by Soluble Mn(III)

The following chapter is modified from a manuscript published in 2021 in the journal Environmental Science & Technology, volume 55, issue 19, pages 13014-13023.

3.1 Abstract

Bisphenol A (BPA), a high production volume chemical and potential endocrine disruptor, is found associated with sediments and soils due to its hydrophobicity (log K_{OW} of 3.42). We used superfine powdered activated carbon (SPAC) with a particle size of 1.38 ± 0.03 μm as a BPA sorbent and assessed degradation of BPA by oxidized manganese (Mn) species. SPAC strongly sorbed BPA and desorption required organic solvents. No degradation of adsorbed BPA (278.7 ± 0.6 mg BPA g^{-1} SPAC) was observed with synthetic, solid α-MnO_2 with a particle size of 15.41 ± 1.35 μm; however, 89% mass reduction occurred following the addition of 0.5 mM soluble Mn(III). Small angle neutron scattering data suggested that both adsorption and degradation of BPA occurred in SPAC pores. The findings demonstrate that Mn(III) mediates oxidative transformation of dissolved and adsorbed BPA, the latter observation challenging the paradigm that contaminant desorption and diffusion out of pore structures are required steps for degradation. Soluble Mn(III) is abundant near oxic-anoxic interfaces and the observation that adsorbed BPA is susceptible to degradation has implications for predicting, and possibly managing, the fate and longevity of BPA in environmental systems.

Keywords: Bisphenol A degradation, manganese oxides, Mn(III), MnO_2, adsorption, activated carbon, small-angle neutron scattering (SANS)

3.2 Introduction

Bisphenol A (BPA) is widely used in manufacturing of polycarbonate plastics, epoxy resins, flame retardants, and other products (Staples et al., 1998). The global BPA market was about 8 million metric tons in 2016 and further increase is projected (Experts, 2016). BPA has been detected in numerous environmental matrices, ranging from 0.5−325 ng g^{-1} (dry weight) in soil (Huang et al., 2014), 0.20−39.1 μg g^{-1} (dry weight) in dust (Liao et al., 2012b). 1.49−13,370 ng g^{-1} (dry weight) in sediments (Liao et al., 2012a), and 0.5−776 ng L^{-1} in surface water bodies (Fromme et al., 2002). The presence of BPA in environmental systems has raised concerns due to estrogenic properties observed in laboratory studies (Kinch et al., 2015; Hernandez and Gore, 2017), and the environmental fate of BPA is, therefore, of significant interest (Im and Löffler, 2016). A number of studies have reported transformation and degradation of dissolved BPA under oxic conditions by bacteria (Im and Löffler, 2016), fungi (Chen et al., 2016), and algae (Eio et al., 2015) and, in addition to biotic processes, dissolved BPA is susceptible to abiotic degradation mediated by Mn(IV) dioxide mineral phases (Lin et al., 2009; Im et al., 2015), photodegradation (Ju et al., 2018), and advanced oxidation using hydroxyl radicals (Zhang et al., 2019).

Following iron and titanium, manganese (Mn) is the third most abundant transition metal in the earth's crust and commonly occurs in three oxidation states, Mn(II), Mn(III), and Mn(IV), in the environment (Sigel, 2000). Mn(IV) in the form of MnO_2 polymorphs are abundant in soils and sediments (Burdige, 1993; Post, 1999) and a strong oxidant ($E_H^o{}_{(Mn(IV)/Mn(II))}$ = 1.23 V) capable of oxidizing a variety of organic compounds (Stone, 1987; Chen et al., 2011), including BPA (Lin et al., 2009; Im et al., 2015). Mn(III) can be formed via the oxidation of Mn(II) (Webb et al., 2005), the one-electron reduction of Mn(IV) (Lin et al., 2012), and a conproportionation

reaction between Mn(II) and Mn(IV) (Liu et al., 2019). Mn(III) is found in the minerals bixbyite (Mn_2O_3), feitknechtite, groutite, and manganite (MnO[OH]), the mixed-charge phase hausmannite (Mn_3O_4), and in minerals with more complex chemistries. Free aqueous Mn(III) is prone to disproportionation to yield dissolved Mn(II) and solid Mn(IV) and is assumed to be short-lived in solution, which has led to a general underappreciation of Mn(III) in the traditional paradigm of Mn redox cycling (Johnson, 2006). Several studies have now demonstrated that soluble Mn(III) commonly occurs near oxic-anoxic interfaces (Trouwborst et al., 2006; Madison et al., 2013) and is an important environmental oxidant ($E_H^{o}{}_{(Mn(III)/Mn(II))}$ = 1.51 V) (Kostka et al., 1995). Both Mn(III) and Mn(IV) are environmentally relevant oxidants (Kostka et al., 1995; Im et al., 2015; Hu et al., 2017), but only Mn(IV) has been demonstrated to degrade BPA.

With an n-octanol-water partition coefficient log K_{OW} of 3.42 (Borrirukwisitsak et al., 2012), BPA has a tendency for sorption to hydrophobic matrices, which are major sinks for, and reservoirs of, BPA in the environment (Liao et al., 2012b; Huang et al., 2014). Although BPA sorbed to a porous matrix is considered stable, environmental perturbations could result in desorption and release of BPA (Li et al., 2008; Fei et al., 2014; Kim et al., 2015; Bele et al., 2016), thereby increasing the exposure risk. For example, the presence of co-contaminants (i.e., heavy metals) (Li et al., 2008), elevated temperatures (Kim et al., 2015), and elevated pH (Bele et al., 2016) have been shown to increase BPA desorption. Experiments using advanced chemical oxidation (e.g., Fenton) suggested that desorption and diffusion were required for degradation to occur (Kan and Huling, 2009; Kim et al., 2015), and the fate of adsorbed BPA within porous materials is unclear. The pore structure of solid matrices characteristically contains macro- (>50 nm), meso- (2-50 nm), and micropores (<2 nm), and represent the major zones for adsorption

(Fan et al., 2017). Sorptive processes diminish the pore size whereas desorption and diffusion cause the opposite effect.

Due to the widespread distribution of BPA in the environment and associated human health concerns, a detailed understanding of the fate and the longevity of BPA adsorbed to soils and sediments is needed. The objective of this study was to explore the reactivity of soluble Mn(III) towards BPA, and to investigate if Mn(III) and Mn(IV) species can initiate oxidation and degradation of adsorbed BPA. To do so, we have employed small-angle neutron scattering (SANS) to quantify changes in the structure of a porous matrix following BPA sorption and treatment with oxidized Mn species. SANS is an established technique to obtain pore geometry information at a mesoscopic scale in the range of 1 to 100 nm, and can provide information about the distribution of organic compounds within the solid matrix pore structure (Anovitz and Cole, 2015; Zhang et al., 2015).

3.3 Materials and Methods

3.3.1 Chemicals

BPA (>99% purity) was purchased from Sigma-Aldrich (St. Louis, MO, USA) and deuterated BPA-d16 (98% purity) was obtained from Cambridge Isotope Laboratories (Andover, MA, USA). Ethyl acetate, L-ascorbic acid, Leucoberbelin blue (LBB), potassium permanganate ($KMnO_4$), Mn(III) oxide (Mn_2O_3) (>98% purity), Mn(II) chloride tetrahydrate ($MnCl_2{\cdot}4\ H_2O$), and sodium pyrophosphate decahydrate ($Na_4P_2O_7 \times 10\ H_2O$) were obtained from Fisher Scientific (Waltham, MA, USA). All chemicals used were of reagent grade or higher purity.

Superfine powdered activated carbon (SPAC) composed of 1.38 ± 0.03 μm sized activated carbon particles was obtained from Regenesis (San Clemente, CA, USA).

3.3.2 Soluble Mn(III) and MnO_2 preparation and quantification

Soluble Mn(III) stock solutions were prepared according to an established procedure (Kostka et al., 1995). Briefly, eight grams of Mn_2O_3 was added to 100 mL of 40 mM $Na_4P_2O_7 \times 10\ H_2O$ solution and the pH was adjusted to 6.5 with 4 mM hydrochloric acid and 5 mM sodium hydroxide (NaOH). After 3 days of continuous stirring at room temperature, the mixture was centrifuged (6,000 × *g*, 10 min), and the supernatant was filtered through 0.22 μm polyethersulfone (PES) membrane (Nalgene, Rochester, NY, USA) to remove any remaining solids.

The synthesis of MnO_2 followed a described procedure (Kostka and Nealson, 1998). Briefly, 2.96 g of $KMnO_4$ was dissolved in 74.1 mL of Milli-Q water (at least 18.2 MΩ × cm) and heated to 90 °C on a hot plate under continuous stirring. With the solution at 90 °C, 3.71 mL of 5 M NaOH was added, and then 5.56 g of $MnCl_2 \cdot 4\ H_2O$ dissolved in 27.8 mL Milli-Q water was slowly added. The resulting suspension was stirred for 30 min and cooled to room temperature. The solids were collected by centrifugation at 6,000 × *g* for 10 min and washed five times with Milli-Q water. The MnO_2 precipitate was suspended in 100 mL deoxygenated Milli-Q water.

Mn(III) concentrations were measured at 258 nm with a PerkinElmer Lambda 35 UV-vis spectrophotometer in the presence of pyrophosphate (Figure S3.1) (Sun et al., 2015). A molar extinction coefficient of 6,750 $M^{-1}\ cm^{-1}$ was used to calculate Mn(III) concentrations (Liu et al., 2019). The Mn content of MnO_2 stock solutions was quantified by monitoring the absorbance following the addition of LBB at 623 nm (see the Supporting Information for details) (Krumbein

and Altmann, 1973). Standard curves were prepared with LBB and $KMnO_4$ (Figure S3.2). X-ray powder diffraction (XRD) analysis was performed to confirm that the crystal structure and chemical composition of the material matched α-MnO_2 (Figure S3.3).

3.3.3 Incubation conditions

The experiments were performed under ambient air conditions and at room temperature (~21°C), and all vessels were incubated in the dark on a rotary shaker (200 rpm, unless indicated otherwise) with the stoppers facing up.

3.3.4 Oxidative transformation of BPA by soluble Mn(III) and MnO_2

Experiments were performed in 60-mL glass serum bottles with a total volume of 40 mL of 5 mM potassium phosphate buffer, pH 7.2, containing 44 μM BPA. Sodium chloride (NaCl) was added to reach a constant ionic strength of 10 mM. The bottles were closed with black butyl rubber stoppers (Geo-Microbial Technologies, Ochelata, OK) and agitated at 120 rpm. To test the effect of Mn on the BPA transformation rate, Mn(III) and MnO_2 were added from stock solutions to achieve concentrations of 0.05, 0.1, 0.25, and 0.5 mM (nominal concentrations in the case of MnO_2). Aliquots (0.5 mL) were periodically collected after shaking and transferred to 1.5-mL plastic centrifuge tubes containing 20 μL of L-ascorbic acid solution (5 g L^{-1}) and immediately vortexed. The samples were then centrifuged at 10,000 × *g* (Eppendorf centrifuge 5415D, Hamburg, Germany) for 5 min, and the supernatant was transferred to 2-mL glass autosampler vials. The pseudo-first-order rate constants were obtained by plotting the natural log of BPA concentrations as a function of time using five early time points, where linear relationships were observed.

3.3.5 Adsorption experiments

The average size of the SPAC particles was determined by laser diffraction spectroscopy (Table S1). BPA sorption isotherms on SPAC were obtained using a batch equilibration method (Limousin et al., 2007). Briefly, 36 mg L^{-1} (dry weight) of SPAC was suspended in 5 mM phosphate buffer (pH 7.2) containing 10 mM NaCl. The adsorption experiment incubations received 1.5 mM sodium azide (NaN_3) to prevent microbial growth (Figueroa and MacKay, 2005). Glass serum bottles (60 mL total volume) received 40 mL of the SPAC suspension and 4−40 mg L^{-1} of BPA. The bottles were closed with black butyl rubber stoppers and agitated. All experiments were performed in triplicate. Aliquots (0.5 mL) were withdrawn over time, passed through 0.22 μm polytetrafluoroethylene (PTFE) membrane filters (Basix™, Fisher Scientific, Waltham, MA, USA), and the supernatant was subjected to high-performance liquid chromatography (HPLC) analysis. The aging of adsorbed BPA was determined by measuring the extracted amount of BPA after 2, 19, 40, 50 and 60 days. The amount of BPA adsorbed onto SPAC was calculated by subtracting the aqueous phase BPA from the initial amount of BPA. The Freundlich and Langmuir isotherm models (Eqs. [1] and [2]) were used to fit the BPA adsorption data (Kim et al., 2015).

Freundlich isotherm: $q_e = k_f \cdot C_e^{\frac{1}{n}}$ (1)

Langmuir isotherm: $q_e = \frac{Q_0 \cdot k_L \cdot C_e}{1 + k_L \cdot C_e}$ (2)

where q_e is the amount of BPA adsorbed per unit mass of SPAC at equilibrium (mg BPA g^{-1} SPAC), k_f is a constant of the Freundlich isotherm, C_e is the liquid-phase concentration of BPA at equilibrium (mg L^{-1}), $1/n$ is an indicator of adsorption intensity, Q_0 is the maximum adsorption capacity (mg g^{-1}), and k_L is a constant of the Langmuir isotherm (L g^{-1}).

3.3.6 Desorption kinetics

To assess the desorption kinetics, experiments were conducted with two types of SPAC with adsorbed BPA. To prepare SPAC with freshly adsorbed BPA, 1.76 µmol BPA dissolved in 40 mL of 5 mM phosphate buffer, pH 7.2, was incubated for 0.5 hours with 1.44 mg (dry weight) of SPAC in 60-mL glass serum bottles. The bottles were closed with black butyl rubber stoppers and agitated. Prolonged incubations for 60 days generated aged SPAC with adsorbed BPA. The suspensions were transferred to 50-mL Falcon conical centrifuge tubes (Oneonta, NY, USA) and centrifuged for 15 min at 15,000 × *g* before the supernatant was carefully removed with a pipette. Each SPAC pellet was suspended in 40 mL of freshly prepared sodium phosphate buffer solution (pH 6, 7.2 and 8.2) and the suspensions were transferred to 60-mL glass serum bottles. The bottles were closed with black butyl rubber stoppers and agitated in horizontal position. Desorption experiments using fresh and aged SPAC lasted 15 and 8 days, respectively. Suspension aliquots (0.5 mL) were withdrawn over time with plastic syringes, filtered, and the BPA concentration in the filtrate was then measured.

3.3.7 Degradation of BPA adsorbed to SPAC

Fresh and aged SPAC loaded with 278.7 ± 0.6 mg BPA g^{-1} were prepared to examine the degradation of adsorbed BPA by soluble Mn(III) and solid α-MnO_2. SPAC (1.44 mg) with adsorbed BPA was washed and then suspended in 40 mL of 5 mM phosphate buffer (pH 7.2) containing 10 mM NaCl, and 0.05, 0.1, 0.25, and 0.5 mM Mn(III) or 0.5 mM MnO_2 (nominal concentrations) was added to 60-ml glass serum bottles. Samples (1 mL) were withdrawn over time, extracted with ethyl acetate (see below), and BPA concentrations determined by HPLC.

3.3.8 Extraction procedures

The amount of BPA adsorbed to SPAC was measured following established liquid-liquid extraction procedures (Xu et al., 2008; Im et al., 2014). Each 1-mL aqueous sample was transferred to 10-mL vials and 3 mL of ethyl acetate was added. The closed vials were agitated for 12 hours and then centrifuged at 5,000 × *g* for 10 min. Longer extraction periods did not increase the recovery of BPA. The organic phases from three successive extractions were combined and dried under a gentle stream of nitrogen. Each residue was dissolved in 1 mL acetonitrile and water (1:1, v/v) and analyzed by HPLC. To test the recovery of BPA from SPAC, 1.76 µmol BPA was added to 60-mL serum bottles containing 1.44 mg SPAC suspended in 40 mL of a 5 mM phosphate buffer (pH 7.2) and agitated at 200 rpm. After 30 min, BPA was extracted with ethyl acetate as described above. All experiments were performed in triplicate and the recovery of BPA was 101 ± 1.3%.

3.3.9 SANS experiment and data analysis

SANS measures the changes in the scattering intensity as a function of scattering angle, and the comparative analysis of pore sizes derived from these data can be used to provide information about BPA adsorption, desorption, and degradation within the SPAC pore structure. Three samples including “neat” SPAC, SPAC with adsorbed BPA, and SPAC with adsorbed BPA after Mn(III) treatment were collected for SANS measurements. To facilitate the SANS measurements, deuterated BPA was used because its scattering length density (SLD) is very similar to that of SPAC carbon (i.e., 5.9×10^{-6} versus 6.0×10^{-6} Å^{-2}, respectively), and thus the scattering intensity from the SPAC/BPA interface would be expected to be very low (Zhang et al., 2015). Because of the contrast at this boundary, adsorption and degradation of BPA within the pores modulates the scattering intensities, and modelling of the scattering profile data can

provide information about pore size changes, and thus BPA adsorption and degradation. To generate SPAC with adsorbed BPA, 880 µmol of deuterated BPA was incubated with 1 g (dry weight) of SPAC in a total volume of 75 mL of 5 mM phosphate buffer, pH 7.2, on a rotary shaker (120 rpm) for 10 days. Preparation of SPAC samples without BPA followed identical procedures. Duplicate samples of SPAC with adsorbed deuterated BPA were analyzed with SANS to characterize the distribution of BPA within the SPAC matrix (i.e., pore size <100 nm) prior to and after treatment with 0.5 mM soluble Mn(III). To account for the effect of 2.5 mM pyrophosphate introduced with the soluble Mn(III), SPAC with adsorbed BPA was added to a solution with the same pyrophosphate concentration. All samples used in the degradation experiment were incubated on a shaker table (120 rpm) for 15 days. The three different SPAC suspensions were then transferred to individual 50-mL plastic tubes and centrifuged for 15 min at 15,000 × *g* before the supernatant was carefully removed with a pipette. The SPAC pellets were dried at 40 °C for 48 hours and homogenized with a porcelain mortar prior to the SANS measurements.

For SANS analysis, the samples were loaded into quartz cells with the flight path length of 1 mm (Hellma USA Inc., Plainview, NY, USA) on the General-Purpose SANS CG-2 beamline at Oak Ridge National Laboratory's High Flux Isotope Reactor (HFIR) (Heller et al., 2018). Three configurations with λ = 12 Å with a wavelength spread, $\Delta\lambda/\lambda$, of 0.13 and a sample-to-detector distance (SDD) of 19.2 m and λ = 4.75 Å with $\Delta\lambda/\lambda$ = 0.13 and SDDs of 6.8 m and 1.0 m were used to cover the scattering vector Q range between 0.0015−0.7 $Å^{-1}$. All measurements were conducted under ambient conditions. The total scattering cross sections were calibrated using porous silica and corrected for empty cell scattering, sample transmission, thickness, and detector sensitivity. The azimuthally isotropic two-dimensional scattering patterns were then

reduced to one-dimensional intensity *I* values as a function of *Q*. The data were analyzed with the polydisperse sphere (PDSP) model using PRINSAS, a software widely used to analyze small angle scattering (SAS) data of porous materials (Hinde, 2004; Ilavsky and Jemian, 2009). In addition, the unified model for the analysis of SAS data from hierarchical materials was used (see the Supporting Information for additional details) (Beaucage, 1995).

3.3.10 Analytical procedures

BPA was quantified using an Agilent 1200 Series HPLC system equipped with a diode array detector and a fluorescence detector (FLD) in serial configuration (Im et al., 2015). Separation was performed on an Agilent Eclipse XDB C18 column (4.6 mm × 150 mm, 5 μm) using isocratic elution at a flow rate of 1 mL min^{-1} of acetonitrile and Milli-Q water (50:50, v/v) at pH 7.2. The FLD was set at excitation and emission wavelengths of 226 nm and 310 nm, respectively. For standard curve preparation, vials containing 0.4, 1.1, 2.2, 11, 44, and 88 μM BPA and 50 mg mL^{-1} L-ascorbic acid were prepared in triplicates (Figure S3.4). The limit of detection and the limit of quantification were 0.4 μM and 1.1 μM BPA with signal-to-noise ratios of 3:1 and 10:1, respectively.

3.4 Results

3.4.1 BPA degradation by oxidized Mn species

Batch experiments demonstrated BPA degradation with solid phase MnO_2, a finding corroborating prior reports (Lin et al., 2009; Im et al., 2015). BPA degradation was also observed in incubation vessels with soluble Mn(III) indicating that both solid phase MnO_2 and soluble Mn(III) degrade BPA (Figure 3.1). No BPA loss was observed in incubations lacking oxidized

Mn species indicating that sorption of BPA to the experimental vessels was negligible (Figure 3.1).

The initial MnO_2 loading significantly affected the rate of BPA degradation, an effect that was less pronounced with Mn(III) as oxidant (Figure 3.1 and Figure S3.5). The initial BPA concentration decreases followed pseudo-first order reaction kinetics, but the rates declined after about 8 min in both systems that received with MnO_2 or Mn(III) (Figure 3.1). An initial BPA removal rate of 0.04 ± 0.003 min^{-1} was measured with 0.05 mM Mn(III), and a slightly higher rate of 0.05 ± 0.002 min^{-1} was observed with 0.5 mM Mn(III) (Figure S3.5A). While the initial degradation rate data suggested BPA removal was not sensitive to the Mn(III) loading, the limited temporal resolution of the discontinuous analytical approach may have masked initial rate differences (Figure 3.1A). Over longer incubation periods, the amount of BPA removed was clearly Mn(III) loading dependent (Figure S3.6). Increased MnO_2 loadings resulted in progressively higher initial BPA degradation rates (Figure 3.1B). In vessels with 0.05, 0.1, 0.25 and 0.5 mM MnO_2, BPA removal rates of 0.02 ± 0.003, 0.03 ± 0.001, 0.06 ± 0.004, and 0.10 ± 0.01 min^{-1}, respectively, were measured (Figure S3.5B). The maximum BPA degradation rate observed with MnO_2 was 2.0 ± 0.03-fold faster than the maximum rate observed in vessels with soluble Mn(III) (Figure S3.5). Over a 1-hour reaction period, 49.7 ± 1.20% of the initial 1.76 µmol BPA was removed with 0.05 mM MnO_2, and nearly complete removal (98.8 ± 0.01%) was achieved with 0.5 mM MnO_2. In contrast, approximately half (59%) of the initial 1.76 µmol BPA was degraded within 1 hour in vessels with 0.5 mM Mn(III) (Figure 3.1A). To achieve the same BPA removal with Mn(III), longer incubation periods were required (e.g., 4 days in the presence of 0.5 mM Mn[III]) (Figure S3.6).

3.4.2 Adsorption isotherms

The adsorption of BPA to SPAC reached equilibrium within 0.5 hours, indicating that BPA sorption is a fast process. Analysis of the data showed that a Langmuir isotherm (R^2 = 0.99) fit the adsorption data slightly better than did the Freundlich isotherm (R^2 = 0.96) (Figure S3.7). Using the Langmuir model, a maximum adsorption capacity of 357 mg BPA per g of SPAC was determined. The amount of BPA that could be extracted with ethyl acetate gradually decreased as a function of time, whereas the fraction of non-extractable BPA increased (Figure S3.8). The aging process followed pseudo-first-order reaction kinetics and occurred at a rate of 5.54 ± 0.02 day^{-1}. Following a 60-day incubation, only 20.1 ± 0.2% of the initial 1.76 (± 0.02) μmol of BPA adsorbed to SPAC could be extracted with ethyl acetate (Figure S3.8).

3.4.3 Degradation of BPA adsorbed to SPAC

To explore if adsorbed BPA is susceptible to oxidative transformation, SPAC with adsorbed BPA was incubated with Mn(III) or MnO_2. Both Mn(III) and MnO_2 degraded dissolved BPA (Figure 3.1); however, only soluble Mn(III) degraded fresh and aged BPA adsorbed to SPAC (Figure 3.2). Following a 15-day incubation period, only about 11% of the initial 1.76 ± 0.02 μmol of freshly adsorbed BPA remained in incubations with 0.5 mM soluble Mn(III) (Figure 3.2B). In incubations with aged adsorbed BPA and 0.5 mM Mn(III), the initial 0.37 ± 0.01 μmol of solvent-extractable BPA was completely degraded during an 8-day incubation (Figure 3.2C). Degradation of adsorbed BPA followed pseudo-first-order reaction kinetics and rates of 0.27 ± 0.01 day^{-1} and 0.78 ± 0.03 day^{-1} were observed for freshly prepared and aged adsorbed BPA, respectively, in the presence of 0.5 mM soluble Mn(III). In contrast, no BPA degradation was observed with up to 2 mM MnO_2 (nominal concentrations) (Figure 3.2A). In control incubations

without oxidized Mn species, no BPA was detected in the aqueous phase over a 15-day incubation period (Figure S3.9), indicating that no BPA desorption had occurred.

Addition of 0.05 and 0.1 mM Mn(III) into vessels with 44 μM (1.76 μmol) dissolved BPA caused removal of 59 ± 1.7 and 86 ± 0.6% of BPA, respectively, after 4 days. Complete (100%) removal was observed with 0.25 and 0.5 mM Mn(III) (Figure S3.6). In vessels with the same amount of BPA freshly adsorbed to SPAC and the same Mn(III) concentrations, smaller amounts of BPA, ranging from 9.1−88.8%, were removed over the same period (Figure 3.2B). Apparently, Mn(III) degraded adsorbed BPA at lower rates than dissolved BPA indicating that adsorption affects the rate and extent of BPA degradation.

3.4.4 Changes in pore size due to BPA adsorption and degradation

To develop an understanding of BPA adsorption and degradation within the SPAC pore structure, SANS analysis was performed and the data analyzed with the PDSP model. Figure 3.3A shows the SANS curves in log-log space where $I(Q)$ is the scattering intensity, and Q is the scattering vector related to the neutron wavelength (λ) and the scattering angle (θ) as $Q = \left(\frac{4\pi}{\lambda}\right)\sin\left(\frac{\theta}{2}\right)$, which is a restatement of Bragg's Law (Bragg and Bragg, 1913). Nanoporous materials often exhibit hierarchical structures, which are reflected in these data by the two Guinier "knees" indicated by the arrows on the SANS curves in Figure 3.3A. These knees result from separate distributions of scatterers (pores in this case) with similar sizes, and their locations correlate with the radii of gyration (R_g) of the size limits of those distributions where $R_g \sim 2\pi/Q$ (Krzysko et al., 2020; Weston et al., 2020). R_g was used to represent the pore size because the pores of SPAC have irregular and tortuous shapes. The volume-weighted pore size distributions (Figure 3.3B) indicate the presence of two major populations of pores in all three samples

(Figure 3.3A). One is represented by micropores with an average size of ~ 8 Å and a noticeable shoulder at ~ 13 Å. The other population exhibits a broad size range from 100 to 900 Å in diameter (i.e., macropores). Adsorption of BPA caused little change to the micropore population other than a slight increase in the intensity of the ~13 Å shoulder (green line in Figure 3.3B, Figure S3.10). In contrast, the average size of the macropores decreased suggesting that the BPA molecules adsorbed on the internal walls of these larger pores and formed a surface layer. As a result, the pores became smaller, an effect that was measurable with SANS because the SLD of deuterated BPA is close to that of activated carbon (green line in Figure 3.3B, Figure S3.10). Addition of soluble Mn(III) shifted the position of the main micropore peak from 8 to 7 Å and its intensity decreased (blue line in Figure 3.3B). This shift was attributed to the migration of smaller BPA transformation products into the micropores. The shoulder also shifted from 13 to 11 Å and its intensity increased significantly, presumably also a result of the penetration of BPA transformation products into micropores, or due to a layer of BPA (approximately 11 Å in size) on the surface of the macropores. The SANS analysis further suggested that the average size of the larger pore population (level 2) declined following Mn(III) treatment (blue line in Figure 3.3B and Figure S3.10).

Results obtained using the unified fit model, which was developed for modelling hierarchical materials (Beaucage, 1995), support these conclusions. In this model, each structural level is defined by an equation with two parts: with a Guinier section defining a maximum intensity (G) and R_g defining the upper size limit of the level (see the SI for details), below which (e.g., at higher Q) the intensity of the Guinier section of the curve drops off rapidly (Guinier et al., 1955). The rapid drop of intensity corresponds to the position of the knees mentioned above. A structurally limited power-law term contains a prefactor B governing its intensity and a power

law slope P related to surface roughness, as well as the same R_g used in the Guinier section. This power law term defines the slope and intensity at Q values above each knee. The prefactor B is often defined in terms of G, R_g and P, and thus is not an independent variable.

Based on the observation of two knees in the log-log scattering plots (Figure 3.3 and Figure S3.11), the SPAC appears to consist of two structural levels (i =2) within the size range analyzed by SANS. Level 1 corresponds to the micropores, and level 2 corresponds to the population of pores ranging from 100 to 900 Å (Figure 3.3B). The scattering contributions from the different structural levels are decomposed in Figure S3.11 and the parameters obtained through the model fitting are shown in Table 3.3. The average R_g values for the macropores and micropores are 728.1 ± 0.3 and 7.9 ± 0.1 Å, respectively (Table 3.1). Upon sorption of deuterated BPA, the size of the macropores declined by ~10%, indicating adsorption of BPA (Figure S3.10). A 6% size increase in the micropores (level 1 structure) was also observed, which presumably reflects the adsorption of 11 Å BPA molecules in the macropores (Wei and Hore, 2021), an interpretation supported by the PDSP fitting results.

After addition of soluble Mn(III), the larger pores experienced a further reduction in diameter by ~24%, while the R_g values for the micropores showed a measurable increase of 4%. These observations suggest migration of BPA transformation products into the micropores, as well as a continuation of the processes adding an adsorbed layer to the macropores. Overall, the SANS data provide direct evidence for adsorption of transformation products of deuterated BPA throughout the SPAC pore structure.

3.5 Discussion

Sediments are major sinks for and reservoirs of BPA in the environment, and an understanding of the processes that affect the fate and the longevity of BPA is relevant to predicting potential human exposure. MnO_2 is a reactive phase with a high oxidation potential capable of oxidizing various types of organic and inorganic compounds, including BPA (Nico and Zasoski, 2001; Beal et al., 2009; Im et al., 2015). A primary source of natural MnO_2 minerals is microbial oxidation of Mn(II), a process that can occur under both oxic (Hansel, 2017; Shobnam et al., 2021) and anoxic conditions (Daye et al., 2019; Yu and Leadbetter, 2020). MnO_2 polymorphs occur commonly in natural sediments, and 26−348 mg L^{-1} of MnO_2 has been reported in freshwater sediments (Kepkay, 1985; Sigg et al., 1987) and 2−16 mg L^{-1} in the surface layer of marine sediments (Vandieken et al., 2012). In addition to Mn(IV), Mn(III) is a strong oxidant, which has been recognized to play a role in biogeochemical cycling (Wesolowski et al., 2004; Chen et al., 2013; Wang et al., 2014; Jones et al., 2018), and is an intermediate in biotic Mn(II) oxidation (Glenn and Gold, 1985), biotic MnO_2 reduction (Lin et al., 2012), and abiotic permanganate reduction (Adler and Noyes, 1955). Free aqueous Mn(III) is short-lived and undergoes disproportionation to soluble Mn(II) and solid Mn(IV) (Webb et al., 2005), but commonly occurs in environmental systems such as soils (Jones et al., 2018), natural water bodies (Trouwborst et al., 2006), and sediments (Madison et al., 2013). This is due to the formation of stable, water-soluble Mn(III) complexes with natural ligands, including pyrophosphate (Kostka et al., 1995), oxalate (Chen et al., 2013), citrate (Wright et al., 2018), and siderophores (Webb et al., 2005).

3.5.1 BPA degradation by oxidized Mn species

The experimental efforts reported here have demonstrated that, in addition to MnO_2, Mn(III) mediates BPA degradation. Reactivity with BPA was observed at Mn(III) and MnO_2 (nominal) concentrations as low as 50 µM. Mn concentrations in this range have been reported in various environmental settings (Kepkay, 1985; Sigg et al., 1987; Vandieken et al., 2012), suggesting that BPA degradation by oxidized Mn can occur *in situ*, and Mn-mediated oxidation may be a relevant natural attenuation process (Im et al., 2015; Im and Löffler, 2016). The BPA degradation rates in experimental vessels with Mn(III) decreased over time (Figure 3.1A), similar to what was observed in MnO_2-bearing systems (Figure 3.1B) (Lin et al., 2009; Im et al., 2015). The highest BPA degradation rates with Mn(III) were observed during the initial reaction phase, and were largely independent of the initial Mn(III) loading (Figure 3.1A and Figure S3.5), but then declined within minutes (Figure 3.1A). A possible explanation for the decreasing rates over time is the formation of transformation products, such as 4-hydroxycumyl alcohol (HCA), that are also susceptible to oxidation by Mn(III). Further, Mn(II) may affect the reactivity of Mn(III), and passivation of solid MnO_2 by Mn(II) has been described (Zhang and Huang, 2003; Im et al., 2015).

3.5.2 Adsorption of BPA to activated carbon (SPAC) nanopores

With a log K_{ow} of 3.42 (Borrirukwisitsak et al., 2012), an aqueous solubility of 300 mg L^{-1} at 25°C (Shareef et al., 2006), and a Henry's Law constant of 1.0×10^{-10} atm m^3 mol^{-1} (Staples et al., 1998), BPA is not volatile at ambient temperature and has a tendency to adsorb on hydrophobic surfaces. In our experiments, BPA sorption to SPAC reached the capacity expected for carbon-based porous materials (Figure S3.7) (Kim et al., 2015; Bhatnagar and Anastopoulos, 2017), and SANS analysis confirmed the adsorption of BPA within the macropores of the SPAC

pore structure. BPA adsorption could be described by a Langmuir isotherm indicative of monolayer adsorption (Butt et al., 2013). A decrease in organic solvent extractable BPA was observed with increasing incubation time (i.e., aging) (Figure S3.8), suggesting that BPA adsorption changed from physisorption based on Van der Waals forces to chemisorption. In support of this hypothesis, prolonged extraction periods (e.g., 3 days) to recover more sorbed BPA were not successful. Previous work demonstrated increases in macropore and micropore porosity following organic solvents extraction (DiStefano et al., 2016), suggesting that the extraction solvent can reach BPA adsorbed in the SPAC macropores. Most likely, the formation of bound residues (i.e., covalent bond formation between SPAC and BPA) limited extractability of aged BPA adsorbed to SPAC, a phenomenon that has been described for a variety of organic compounds, including BPA and tetrabromobisphenol A, adsorbed to solid matrices (Fent et al., 2003; Li et al., 2015).

3.5.3 SANS analysis of Mn(III)-treated SPAC

Treatment with Mn(III) decreased the amount of extractable BPA, and SANS analysis revealed that this process was coupled with changes to the sizes of macro- and micropores of SPAC. The observed pore size changes suggest that adsorbed BPA degradation mainly occurred in the larger SPAC pores in the 100-900 Å size range. BPA has a molecular size of ~11 Å (Agenson et al., 2003), which makes it physically impossible for BPA molecules to penetrate the SPAC micropores. Degradation of BPA molecules led to a shift of the shoulder peak from 13 to 11 Å and increased its volume fraction (Figure 3.3B). In addition, the intensity of the smaller micropore peak decreased and shifted from 8 to 7 Å. The latter is presumably due to the formation of BPA transformation products of smaller molecular size (e.g., HCA, 4-isopropenylphenol) (Huang and Weber, 2005; Im et al., 2015) that can diffuse out of the larger

pores and migrate into the micropores (Figure S3.10). The 4% increase of the average size of level 1 structures obtained with the unified modelling method was attributed to the significant increase in the volume fraction of the shoulder peak (Figure 3.3B).

The SANS analysis also suggested a decrease in the size of the larger pores following Mn(III) treatment. This shift of the average macropore size (indicated by the blue line in Figure 3.3B) is much larger than the size of a single BPA molecule, suggesting the formation of molecules that are larger than BPA (e.g., BPA dimers) in response to the Mn(III) treatment (Huang and Weber, 2005; Lin et al., 2009). The macropores also provide diffusion channels for Mn(III), and thus a pore size reduction may hinder the deeper penetration of soluble Mn(III) into the SPAC, a possible explanation for the observed incomplete degradation of adsorbed BPA (Figure 3.2).

The discussion above presents a sensible interpretation of the SANS data focused on the changes in pore size of SPAC caused by BPA and its transformation products; however, a few uncertainties should be considered. For example, the reduction of adsorption of Mn(III) leads to the formation of Mn(II), and adsorption to different types of activated carbon has been demonstrated (Ahmad et al., 2005; Stafiej and Pyrzynska, 2007). The SPAC used in our experiments was loaded with adsorbed BPA, and the BPA transformation products formed following Mn(III) treatment also adsorb to SPAC, possibly limiting the adsorption sites for Mn(II) (Fent et al., 2003; Li et al., 2015). Further, the Mn(II) ion is much smaller than a BPA molecule (Agenson et al., 2003), and it is unlikely that Mn(II) adsorption affected the experimental results. Another potential issue is the formation of Mn(II) phosphate (i.e., $Mn_3[PO_4]_2$) precipitate. We never observed precipitate formation presumably because the reaction conditions were not conducive for precipitate formation (Massa et al., 2005), and

interference by $Mn_3(PO_4)_2$ precipitate is unlikely. Pyrophosphate was present in all experiments and was therefore not a variable, indicating that adsorption of pyrophosphate was not a factor complicating the interpretation of the SANS data. Further, it is theoretically possible that Mn(III) oxidizes SPAC, causes dissolution, and alters the pore size structure; however, experimental evidence for such processes is lacking.

Degradation of dissolved BPA by MnO_2 is an established process (Lin et al., 2009; Im et al., 2015); however, our results demonstrated that the α-MnO_2 particles used in our experiments could not mediate degradation of BPA adsorbed to activated carbon (i.e., SPAC). The α-MnO_2 particle size exceeded that of a SPAC particle by more than 10-fold (i.e., 15.41 ± 1.35 versus 1.38 ± 0.03 μm, respectively) and was much larger than the pores of the SPAC particles (Table 3.2). The experimental data indicated strong adsorption of BPA to SPAC, as no BPA was released over time. As a result, physical separation prevented oxidation of BPA by solid-phase MnO_2. In contrast, soluble Mn(III), which could enter the pore structure of the SPAC, mediated the degradation of adsorbed BPA. Generally, desorption of hydrophobic compounds and their diffusion out of the pore structure are thought to be required steps for degradation (Kan and Huling, 2009; Kim et al., 2015; Fan et al., 2017); however, the findings reported here indicate that diffusion of BPA out of the SPAC pore structure was not required for degradation to occur. It remains to be determined if Mn(III) directly interacts with adsorbed BPA or if desorption within the pore structure is required for oxidative attack within the pores.

3.5.4 Environmental implications

Adsorbed BPA occurs in a number of environmental systems, and has been reported in soils (0.5−325 ng BPA g^{-1}, dry weight) (Huang et al., 2014), sediments (1.49−13,370 ng BPA g^{-1}, dry weight) (Liao et al., 2012b), and sewage sludge (4−1,363 ng BPA Kg^{-1}, dry weight) (Fromme et

al., 2002), which are considered major sinks and reservoirs for BPA. Although these materials have unique physicochemical properties that distinguish them from SPAC (Fan et al., 2017; Ren and Santamarina, 2018), they often possess broadly similar hydrophobic pore structures in the nanometer to micrometer size range (Kuzyakov and Mason-Jones, 2018; Ren and Santamarina, 2018). Mn(III) also occurs in various environmental systems and the finding that Mn(III) contributes to BPA degradation, including the degradation of adsorbed BPA, advances our understanding of natural attenuation processes that affect the fate and longevity of BPA, as well as other hydrophobic compounds susceptible to Mn(III) degradation. By extension, these findings also suggest a possible method for treating BPA-contaminated environments. Areas with elevated Mn(III) concentrations and active Mn cycling, such as oxic-anoxic transition zones are, therefore, likely hotspot zones for oxidized Mn-mediated BPA degradation. Such transition zones may function as natural barriers controlling the release of BPA to the overlying water column, minimizing human exposure risk. The new findings can inform models that more accurately predict BPA behavior in sediments and soils, and generate opportunities for engineering solutions aimed at reducing BPA release to surface waters, thereby mitigating human health concerns.

Acknowledgements

This work was supported by the Polycarbonate/BPA Global Group of the American Chemistry Council (ACC), Washington, DC. Effort by L. M. Anovitz was supported by research sponsored by the Division of Chemical Sciences, Geosciences, and Biosciences, Office of Basic Energy Sciences, U.S. Department of Energy.

References

Adler, S.J. and Noyes, R.M. 1955. The mechanism of the permanganate-oxalate reaction. JACS 77(8), 2036-2042.

Agenson, K.O., Oh, J.-I. and Urase, T. 2003. Retention of a wide variety of organic pollutants by different nanofiltration/reverse osmosis membranes: controlling parameters of process. J. Membr. Sci. 225(1-2), 91-103.

Ahmad, b.J., Cheng, W., Low, W., Nora'aini, A. and Noor, M.M.M. 2005. Study on the removal of iron and manganese in groundwater by granular activated carbon. Desalination 182(1-3), 347-353.

Anovitz, L.M. and Cole, D.R. 2015. Characterization and analysis of porosity and pore structures. Rev. Mineral. Geochem. 80(1), 61-164.

Beal, E.J., House, C.H. and Orphan, V.J. 2009. Manganese- and iron-dependent marine methane oxidation. Science 325(5937), 184-187.

Beaucage, G. 1995. Approximations leading to a unified exponential/power-law approach to small-angle scattering. J. Appl. Crystallogr. 28(6), 717-728.

Bele, S., Samanidou, V. and Deliyanni, E. 2016. Effect of the reduction degree of graphene oxide on the adsorption of bisphenol A. Chem. Eng. Res. Des. 109, 573-585.

Bhatnagar, A. and Anastopoulos, I. 2017. Adsorptive removal of bisphenol A (BPA) from aqueous solution: A review. Chemosphere 168, 885-902.

Borrirukwisitsak, S., Keenan, H.E. and Gauchotte-Lindsay, C. 2012. Effects of salinity, pH and temperature on the octanol-water partition coefficient of bisphenol A. Int. J. Environ. Sci. Technol. 3(5), 460.

Bragg, W.H. and Bragg, W.L. 1913. The reflection of X-rays by crystals. Proc. Math. Phys. Eng. Sci. 88(605), 428-438.

Burdige, D.J. 1993. The biogeochemistry of manganese and iron reduction in marine sediments. Earth-Sci. Rev. 35(3), 249-284.

Butt, H.-J., Graf, K. and Kappl, M. (2013) Physics and chemistry of interfaces, John Wiley & Sons Press.

Chen, G., Zhao, L. and Dong, Y.-h. 2011. Oxidative degradation kinetics and products of chlortetracycline by manganese dioxide. J. Hazard. Mater. 193, 128-138.

Chen, W., Liu, C., Boyd, S.A., Teppen, B.J. and Li, H. 2013. Reduction of carbadox mediated by reaction of Mn(III) with oxalic acid. Environ. Sci. Technol. 47(3), 1357-1364.

Chen, Y., Stemple, B., Kumar, M. and Wei, N. 2016. Cell surface display fungal laccase as a renewable biocatalyst for degradation of persistent micropollutants bisphenol A and sulfamethoxazole. Environ. Sci. Technol. 50(16), 8799-8808.

Daye, M., Klepac-Ceraj, V., Pajusalu, M., Rowland, S., Farrell-Sherman, A., Beukes, N., Tamura, N., Fournier, G. and Bosak, T. 2019. Light-driven anaerobic microbial oxidation of manganese. Nature 576(7786), 311-314.

DiStefano, V.H., McFarlane, J., Anovitz, L.M., Stack, A.G., Gordon, A.D., Littrell, K.C., Chipera, S.J., Hunt, R.D., Lewis Sr, S.A. and Hale, R.E. 2016. Extraction of organic compounds from representative shales and the effect on porosity. J. Nat. Gas Sci. Eng. 35, 646-660.

Eio, E.J., Kawai, M., Niwa, C., Ito, M., Yamamoto, S. and Toda, T. 2015. Biodegradation of bisphenol A by an algal-bacterial system. Environ. Sci. Pollut. Res. 22(19), 15145-15153.

Experts, I. 2016. Bisphenol-A - A Global Market Overview.

Fan, D., Gilbert, E.J. and Fox, T. 2017. Current state of in situ subsurface remediation by activated carbon-based amendments. J. Environ. Manage. 204, 793-803.

Fei, Y., Leung, K.M. and Li, X. 2014. Adsorption and desorption behaviors of selected endocrine disrupting chemicals in simulated gastrointestinal fluids. Mar. Pollut. Bull. 85(2), 363-369.

Fent, G., Hein, W.J., Moendel, M.J. and Kubiak, R. 2003. Fate of ^{14}C-bisphenol A in soils. Chemosphere 51(8), 735-746.

Figueroa, R.A. and MacKay, A.A. 2005. Sorption of oxytetracycline to iron oxides and iron oxide-rich soils. Environ. Sci. Technol. 39(17), 6664-6671.

Fromme, H., Küchler, T., Otto, T., Pilz, K., Müller, J. and Wenzel, A. 2002. Occurrence of phthalates and bisphenol A and F in the environment. Water Res. 36(6), 1429-1438.

Glenn, J.K. and Gold, M.H. 1985. Purification and characterization of an extracellular Mn (II)-dependent peroxidase from the lignin-degrading basidiomycete, Phanerochaete chrysosporium. Arch. Biochem. Biophys. 242(2), 329-341.

Guinier, A., Fournet, G. and Yudowitch, K.L. (1955) Small-angle scattering of X-rays, John Wiley & Sons Press.

Hansel, C.M. (2017) Adv. Microb. Physiol., pp. 37-83, Elsevier.

Heller, W.T., Cuneo, M., Debeer-Schmitt, L., Do, C., He, L., Heroux, L., Littrell, K., Pingali, S.V., Qian, S. and Stanley, C. 2018. The suite of small-angle neutron scattering instruments at Oak Ridge National Laboratory. J. Appl. Crystallogr. 51(2), 242-248.

Hernandez, M.E. and Gore, A.C. 2017. Endocrine disruptors: Chemical contaminants—A toxic mixture for neurodevelopment. Nat. Rev. Endocrinol. 13(6), 322.

Hinde, A.L. 2004. PRINSAS–a Windows-based computer program for the processing and interpretation of small-angle scattering data tailored to the analysis of sedimentary rocks. J. Appl. Crystallogr. 37(6), 1020-1024.

Hu, E., Zhang, Y., Wu, S., Wu, J., Liang, L. and He, F. 2017. Role of dissolved Mn(III) in transformation of organic contaminants: non-oxidative versus oxidative mechanisms. Water Res. 111, 234-243.

Huang, D., Zhao, H., Liu, C. and Sun, C. 2014. Characteristics, sources, and transport of tetrabromobisphenol A and bisphenol A in soils from a typical e-waste recycling area in South China. Environ. Sci. Pollut. Res. 21(9), 5818-5826.

Huang, Q. and Weber, W.J. 2005. Transformation and removal of bisphenol A from aqueous phase via peroxidase-mediated oxidative coupling reactions: efficacy, products, and pathways. Environ. Sci. Technol. 39(16), 6029-6036.

Ilavsky, J. and Jemian, P.R. 2009. Irena: tool suite for modeling and analysis of small-angle scattering. J. Appl. Crystallogr. 42(2), 347-353.

Im, J. and Löffler, F.E. 2016. Fate of bisphenol A in terrestrial and aquatic environments. Environ. Sci. Technol. 50(16), 8403-8416.

Im, J., Prevatte, C.W., Campagna, S.R. and Löffler, F.E. 2015. Identification of 4-hydroxycumyl alcohol as the major MnO_2-mediated bisphenol A transformation product and evaluation of its environmental fate. Environ. Sci. Technol. 49(10), 6214-6221.

Im, J., Prevatte, C.W., Lee, H.G., Campagna, S.R. and Löffler, F.E. 2014. 4-Methylphenol produced in freshwater sediment microcosms is not a bisphenol A metabolite. Chemosphere 117, 521-526.

Johnson, K.S. 2006. Manganese redox chemistry revisited. Science 313(5795), 1896-1897.

Jones, M.E., Nico, P.S., Ying, S., Regier, T., Thieme, J.r. and Keiluweit, M. 2018. Manganese-driven carbon oxidation at oxic–anoxic interfaces. Environ. Sci. Technol. 52(21), 12349-12357.

Ju, L., Wu, P., Yang, Q., Ahmed, Z. and Zhu, N. 2018. Synthesis of ZnAlTi-LDO supported C60@ AgCl nanoparticles and their photocatalytic activity for photo-degradation of bisphenol A. Appl. Catal. B. 224, 159-174.

Kan, E. and Huling, S.G. 2009. Effects of temperature and acidic pre-treatment on fenton-driven oxidation of MTBE-spent granular activated carbon. Environ. Sci. Technol. 43(5), 1493-1499.

Kepkay, P.E. 1985. Kinetics of microbial manganese oxidation and trace metal binding in sediments: Results from an in situ dialysis technique. Limnol. Oceanogr. 30(4), 713-726.

Kim, J.R., Huling, S.G. and Kan, E. 2015. Effects of temperature on adsorption and oxidative degradation of bisphenol A in an acid-treated iron-amended granular activated carbon. Chem. Eng. J. 262, 1260-1267.

Kinch, C.D., Ibhazehiebo, K., Jeong, J.-H., Habibi, H.R. and Kurrasch, D.M. 2015. Low-dose exposure to bisphenol A and replacement bisphenol S induces precocious hypothalamic neurogenesis in embryonic zebrafish. Proc. Natl. Acad. Sci. U. S. A. 112(5), 1475-1480.

Kostka, J. and Nealson, K.H. (1998) Techniques in Microbial Ecology, pp. 58-78, Oxford University Press.

Kostka, J.E., Luther III, G.W. and Nealson, K.H. 1995. Chemical and biological reduction of Mn(III)-pyrophosphate complexes: potential importance of dissolved Mn(III) as an environmental oxidant. Geochim. Cosmochim. Acta. 59(5), 885-894.

Krumbein, W. and Altmann, H. 1973. A new method for the detection and enumeration of manganese oxidizing and reducing microorganisms. Helgoländer Wissenschaftliche Meeresuntersuchungen 25(2), 347.

Krzysko, A.J., Nakouzi, E., Zhang, X., Graham, T.R., Rosso, K.M., Schenter, G.K., Ilavsky, J., Kuzmenko, I., Frith, M.G. and Ivory, C.F. 2020. Correlating inter-particle forces and particle shape to shear-induced aggregation/fragmentation and rheology for dilute anisotropic particle suspensions: A complementary study via capillary rheometry and in-situ small and ultra-small angle X-ray scattering. J. Colloid Interface Sci. 576, 47-58.

Kuzyakov, Y. and Mason-Jones, K. 2018. Viruses in soil: Nano-scale undead drivers of microbial life, biogeochemical turnover and ecosystem functions. Soil Biol. Biochem. 127, 305-317.

Li, F., Wang, J., Jiang, B., Yang, X., Nastold, P., Kolvenbach, B., Wang, L., Ma, Y., Corvini, P.F.o.-X. and Ji, R. 2015. Fate of tetrabromobisphenol A (TBBPA) and formation of ester-and ether-linked bound residues in an oxic sandy soil. Environ. Sci. Technol. 49(21), 12758-12765.

Li, J., Zhou, B., Liu, Y., Yang, Q. and Cai, W. 2008. Influence of the coexisting contaminants on bisphenol A sorption and desorption in soil. J. Hazard. Mater. 151(2-3), 389-393.

Liao, C., Liu, F., Guo, Y., Moon, H.-B., Nakata, H., Wu, Q. and Kannan, K. 2012a. Occurrence of eight bisphenol analogues in indoor dust from the United States and several Asian countries: implications for human exposure. Environ. Sci. Technol. 46(16), 9138-9145.

Liao, C., Liu, F., Moon, H.-B., Yamashita, N., Yun, S. and Kannan, K. 2012b. Bisphenol analogues in sediments from industrialized areas in the United States, Japan, and Korea: spatial and temporal distributions. Environ. Sci. Technol. 46(21), 11558-11565.

Limousin, G., Gaudet, J.-P., Charlet, L., Szenknect, S., Barthes, V. and Krimissa, M. 2007. Sorption isotherms: A review on physical bases, modeling and measurement. Appl. Geochem. 22(2), 249-275.

Lin, H., Szeinbaum, N.H., DiChristina, T.J. and Taillefert, M. 2012. Microbial Mn(IV) reduction requires an initial one-electron reductive solubilization step. Geochim. Cosmochim. Acta. 99, 179-192.

Lin, K., Liu, W. and Gan, J. 2009. Oxidative removal of bisphenol A by manganese dioxide: efficacy, products, and pathways. Environ. Sci. Technol. 43(10), 3860-3864.

Liu, W., Sun, B., Qiao, J. and Guan, X. 2019. Influence of pyrophosphate on the generation of soluble Mn (III) from reactions involving Mn oxides and Mn(VII). Environ. Sci. Technol. 53(17), 10227-10235.

Madison, A.S., Tebo, B.M., Mucci, A., Sundby, B. and Luther, G.W. 2013. Abundant porewater Mn(III) is a major component of the sedimentary redox system. Science 341(6148), 875-878.

Massa, W., Yakubovich, O.V. and Dimitrova, O.V. 2005. A novel modification of manganese orthophosphate $Mn_3(PO_4)_2$. Solid State Sci. 7(8), 950-956.

Nico, P.S. and Zasoski, R.J. 2001. Mn(III) center availability as a rate controlling factor in the oxidation of phenol and sulfide on δ-MnO_2. Environ. Sci. Technol. 35(16), 3338-3343.

Post, J.E. 1999. Manganese oxide minerals: Crystal structures and economic and environmental significance. Proc. Natl. Acad. Sci. U. S. A. 96(7), 3447-3454.

Ren, X. and Santamarina, J. 2018. The hydraulic conductivity of sediments: A pore size perspective. Eng. Geol. 233, 48-54.

Shareef, A., Angove, M.J., Wells, J.D. and Johnson, B.B. 2006. Aqueous solubilities of estrone, 17β-estradiol, 17α-ethynylestradiol, and bisphenol A. J. Chem. Eng. Data 51(3), 879-881.

Shobnam, N., Sun, Y., Mahmood, M., Löffler, F.E. and Im, J. 2021. Biologically mediated abiotic degradation (BMAD) of bisphenol A by manganese-oxidizing bacteria. J. Hazard. Mater., 125987.

Sigel, H. (2000) Met. Ions Biol. Syst., pp. 49-82, CRC Press.

Sigg, L., Sturm, M. and Kistler, D. 1987. Vertical transport of heavy metals by settling particles in Lake Zurich. Limnol. Oceanogr. 32(1), 112-130.

Stafiej, A. and Pyrzynska, K. 2007. Adsorption of heavy metal ions with carbon nanotubes. Sep. Purif. Technol. 58(1), 49-52.

Staples, C.A., Dome, P.B., Klecka, G.M., Oblock, S.T. and Harris, L.R. 1998. A review of the environmental fate, effects, and exposures of bisphenol A. Chemosphere 36(10), 2149-2173.

Stone, A.T. 1987. Reductive dissolution of manganese (III/IV) oxides by substituted phenols. Environ. Sci. Technol. 21(10), 979-988.

Sun, B., Guan, X., Fang, J. and Tratnyek, P.G. 2015. Activation of manganese oxidants with bisulfite for enhanced oxidation of organic contaminants: the involvement of Mn(III). Environ. Sci. Technol. 49(20), 12414-12421.

Trouwborst, R.E., Clement, B.G., Tebo, B.M., Glazer, B.T. and Luther, G.W. 2006. Soluble Mn(III) in suboxic zones. Science 313(5795), 1955-1957.

Vandieken, V., Pester, M., Finke, N., Hyun, J.-H., Friedrich, M.W., Loy, A. and Thamdrup, B. 2012. Three manganese oxide-rich marine sediments harbor similar communities of acetate-oxidizing manganese-reducing bacteria. ISME J. 6(11), 2078-2090.

Wang, Z., Xiong, W., Tebo, B.M. and Giammar, D.E. 2014. Oxidative UO_2 dissolution induced by soluble Mn(III). Environ. Sci. Technol. 48(1), 289-298.

Webb, S.M., Dick, G.J., Bargar, J.R. and Tebo, B.M. 2005. Evidence for the presence of Mn(III) intermediates in the bacterial oxidation of Mn (II). Proc. Natl. Acad. Sci. U. S. A. 102(15), 5558-5563.

Wei, Y. and Hore, M.J. 2021. Characterizing polymer structure with small-angle neutron scattering: A Tutorial. J. Appl. Phys. 129(17), 171101.

Wesolowski, D.J., Ziemniak, S.E., Anovitz, L.M., Machesky, M.L., Bénézeth, P. and Palmer, D.A. (2004) Aqueous Systems at Elevated Temperatures and Pressures, pp. 493-595, Elsevier.

Weston, J.S., Chun, J., Schenter, G., Weigandt, K., Zong, M., Zhang, X., Rosso, K.M. and Anovitz, L. 2020. Connecting particle interactions to agglomerate morphology and rheology of boehmite nanocrystal suspensions. J. Colloid Interface Sci. 572, 328-339.

Wright, M.H., Geszvain, K., Oldham, V.E., Luther III, G.W. and Tebo, B.M. 2018. Oxidative formation and removal of complexed Mn(III) by Pseudomonas species. Front. Microbiol. 9, 560.

Xu, J., Wu, L., Chen, W. and Chang, A.C. 2008. Simultaneous determination of pharmaceuticals, endocrine disrupting compounds and hormone in soils by gas chromatography–mass spectrometry. J. Chromatogr. A 1202(2), 189-195.

Yu, H. and Leadbetter, J.R. 2020. Bacterial chemolithoautotrophy via manganese oxidation. Nature 583(7816), 453-458.

Zhang, H. and Huang, C. 2003. Oxidative transformation of triclosan and chlorophene by manganese oxides. Environ. Sci. Technol. 37(11), 2421-2430.

Zhang, R., Liu, S., Bahadur, J., Elsworth, D., Melnichenko, Y., He, L. and Wang, Y. 2015. Estimation and modeling of coal pore accessibility using small angle neutron scattering. Fuel 161, 323-332.

Zhang, Y., Tang, Y., Qin, Z., Luo, P., Ma, Z., Tan, M., Kang, H. and Huang, Z. 2019. A novel manganese oxidizing bacterium-*Aeromonas hydrophila* strain DS02: Mn (II) oxidization and biogenic Mn oxides generation. J. Hazard. Mater. 367, 539-545.

Appendix

Table 3.1. Radii of pore structure levels of SPAC, SPAC with adsorbed deuterated BPA, and SPAC after Mn(III)-mediated degradation of adsorbed deuterated BPA.

Structure level	R_g (Å)		
	SPAC	**SPAC-BPA**	**SPAC-BPA-Mn(III)**
Level 1	7.9 ± 0.1	8.5 ± 0.1	8.9 ± 0.1
Level 2	728.1 ± 0.3	653.8 ± 0.2	494.2 ± 0.1

Table 3.2. Particle size distribution of SPAC and MnO_2.

Size distribution	Particle size (μm)	
	SPAC	**MnO_2**
Mean	1.376 ± 0.032	15.408 ± 1.350
Median	1.134 ± 0.018	4.775 ± 0.534
d10	0.557 ± 0.004	0.788 ± 0.028
d90	2.448 ± 0.051	44.004 ± 3.312

d10 and d90 represent size ranges with 10% and 90% of the particles smaller than the values indicated, respectively.

Table 3.3. Modeling parameters of SANS profiles.

Parameter	SPAC	SPAC-BPA	SPAC-BPA-Mn(III)
G_1 (cm^{-1})	3.9e5 ± 146	3.3e5 ± 110	3.4e5 ± 82.7
$R_{g,1}$ (Å)	728.1 ± 0.1	653.8 ± 0.1	494.7 ± 0.1
B_1 (cm^{-1})	2.0e-5 ± 2.1e-9	2.4e-5 ± 2.6e-9	7.1e-5 ± 7.8e-9
P_1	3.9 ± 2.4e-5	3.9 ± 2.4e-5	3.9 ± 2.5e-5
G_2 (cm^{-1})	1.2 ± 0.1	1.6 ± 0.1	4.7 ± 0.1
$R_{g,2}$ (Å)	7.9 ± 0.1	8.5 ± 0.1	8.9 ± 0.1
B_2 (cm^{-1})	1.0e-3 ± 3.8e-6	1.6e-3 ± 3.6e-6	5.3e-3 ± 9.0e-6
P_2	4.1 ± 0.1	4.1 ± 0.1	4.0 ± 0.1
Bkgd (cm^{-1})	0.203 ± 4.8e-5	0.267 ± 6.0e-5	0.829 ± 1.9e-4

G_i and B_i are pre-factors for the Guinier exponential and power law terms. i is the structural level. R_g is the radius of gyration, which represents the pore size. Bkgd is incoherent scattering background.

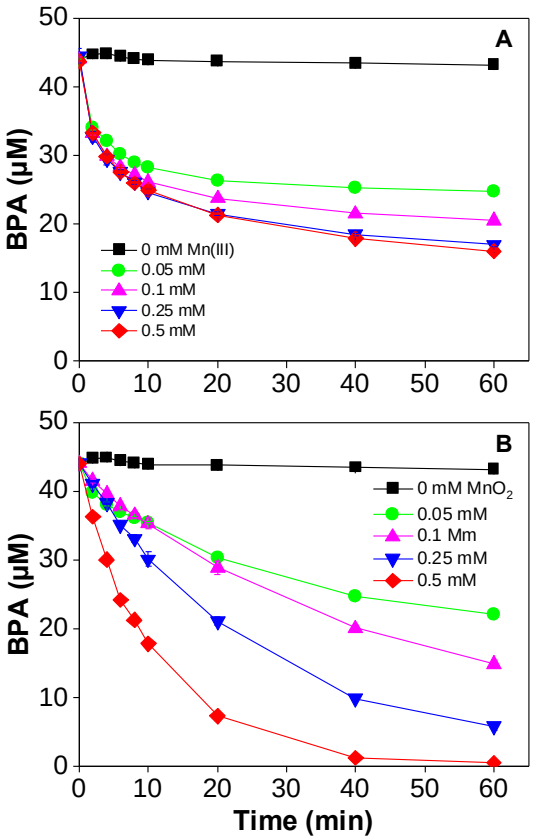

Figure 3.1. BPA concentration profiles in the presence of different concentrations of oxidized Mn species. (A) Mn(III)-mediated BPA degradation in incubation vessels with 5 mM phosphate buffer (pH 7.2) initially containing 44 μM BPA over a 1-hour incubation period. (B) α-MnO_2-mediated BPA degradation in incubation vessels with phosphate buffer (pH 7.2) initially containing 44 μM BPA. MnO_2 is expressed as nominal concentration. Error bars represent the standard deviation of duplicate samples and are not depicted when smaller than the symbol size.

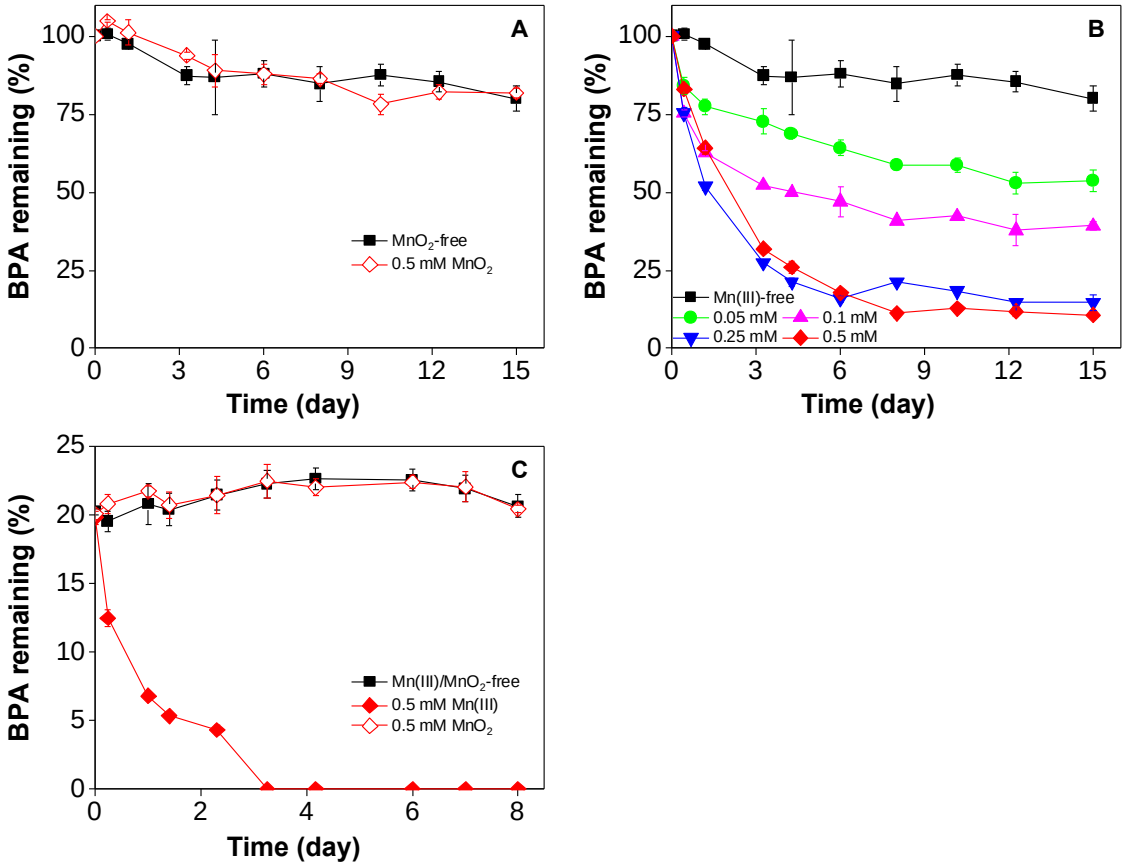

Figure 3.2. Degradation of BPA adsorbed to SPAC by oxidized Mn species. (A) Lack of removal of freshly adsorbed BPA in incubation vessels amended with solid α-MnO_2. BPA was incubated with SPAC for 30 min before the initiation of the experiments. (B) Soluble Mn(III)-mediated degradation of freshly adsorbed BPA. (C) Degradation of aged BPA adsorbed to SPAC by 0.5 mM soluble Mn(III) and 0.5 mM MnO_2. BPA was incubated with SPAC for 60 days before initiation of the experiment. Experiments were performed using 1.44 mg SPAC with 401 µg of adsorbed BPA. The amount of BPA remaining was determined by HPLC following ethyl acetate extraction of suspension samples. α-MnO_2 is a solid and indicated are the nominal concentrations. Error bars represent the standard deviations of triplicate vessels and are not depicted when smaller than the symbol size.

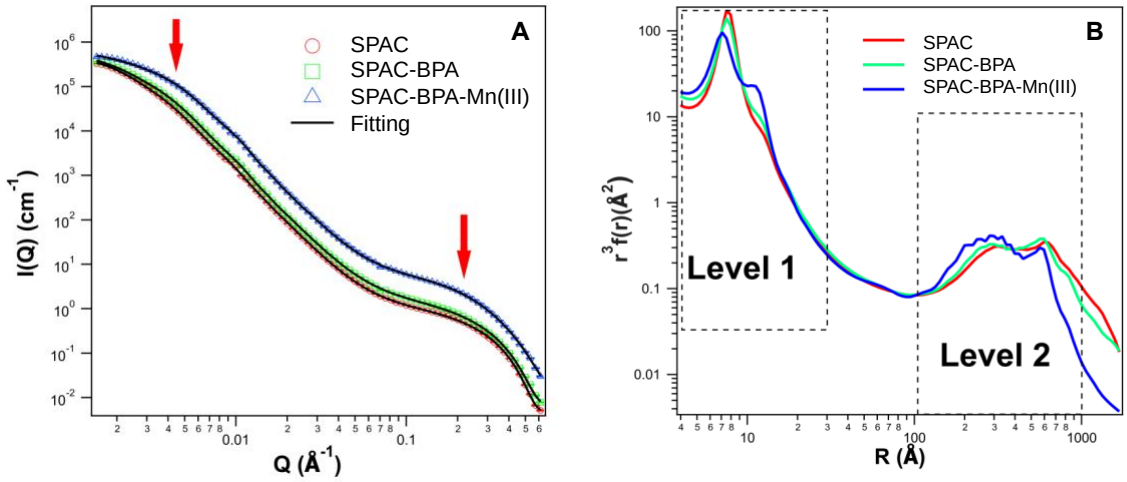

Figure 3.3. SANS profiles and data modelling. Panel (A) shows the background-subtracted SANS profiles for dried SPAC, dried SPAC with adsorbed deuterated BPA, and dried SPAC with adsorbed deuterated BPA after Mn(III)-mediated degradation. The solid black lines represent the best fit based on the PDSP model (see SI for details). The arrows indicate the locations of knees where the slopes of the scattering curves change significantly. Panel (B) illustrates the volume-weighted $f(r)$ distributions of three samples obtained from the PDSP model. $f(r)$ represents the probability density of the pore size distribution, which is defined as the number of pores within an interval between r and $r + dr$ normalized to the total number of pores. A two-level unified model was also applied to fit SANS data and the results are shown in Table 3.1 and Figure S3.11.

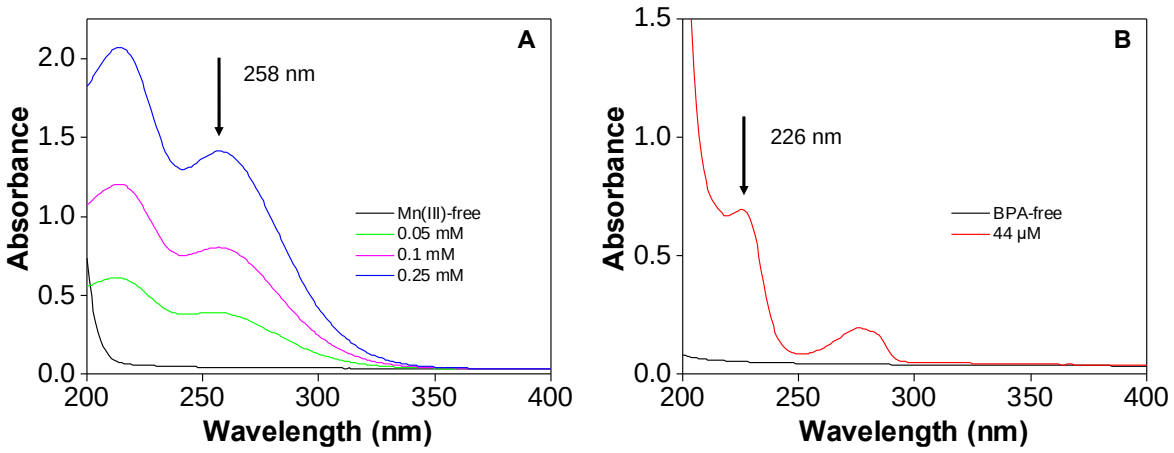

Figure S3.1. UV spectra of soluble Mn(III) (A) and BPA (B) analyzed with a PerkinElmer Lambda 35 UV-vis spectrophotometer. Solutions with different concentrations of Mn(III) were prepared by diluting a 9 mM Mn(III) stock solution with 5 mM potassium phosphate buffer (pH 7.2). The Mn(III) stock solution was prepared using Mn_2O_3 and pyrophosphate as described in the Methods section of the main manuscript. A 44 µM BPA solution was prepared in 5 mM phosphate buffer (pH 7.2). Arrows point to characteristic absorption maxima of Mn(III) and BPA.

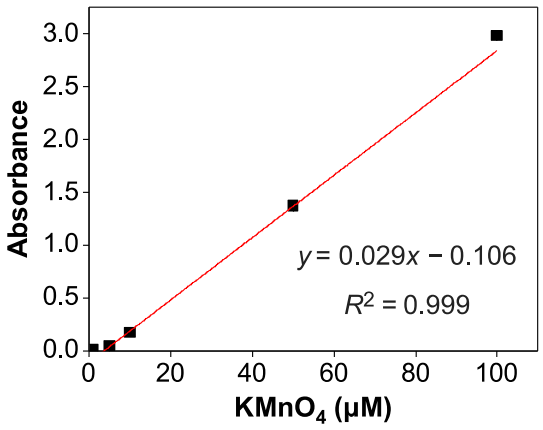

Figure S3.2. Representative standard curve used to determine nominal MnO_2 concentrations in the incubation vessels. Triplicates of each standard were analyzed. The error bars are smaller than the symbol size and not visible.

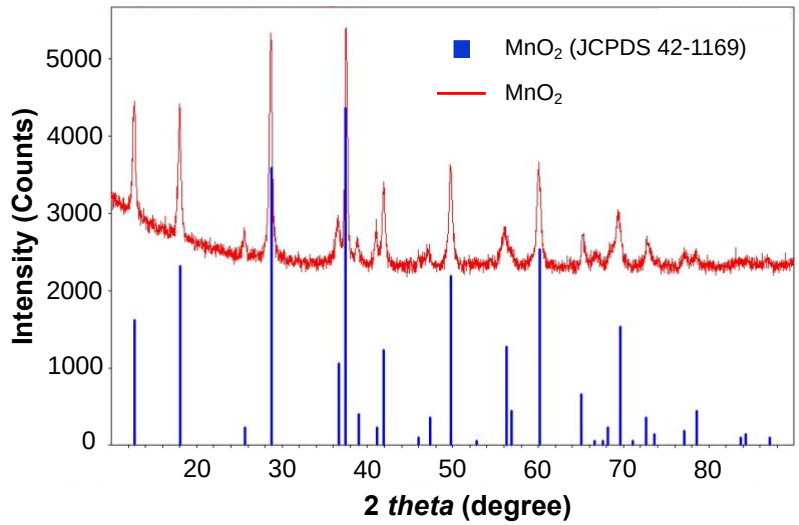

Figure S3.3. XRD pattern of α-MnO_2 synthesized in the present study (red) and the standard XRD spectrum of α-MnO_2 (JCPDS 42-1169) (blue).

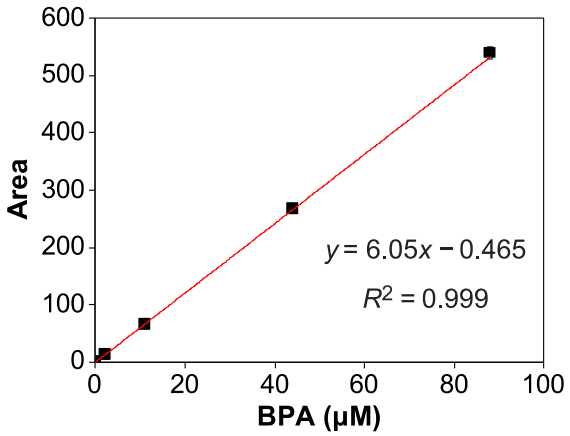

Figure S3.4. Representative standard curve for determining BPA concentrations. BPA was measured by HPLC equipped with a fluorescence detector at excitation and emission wavelengths of 226 nm and 310 nm, respectively. Error bars are smaller than the symbol size and not visible.

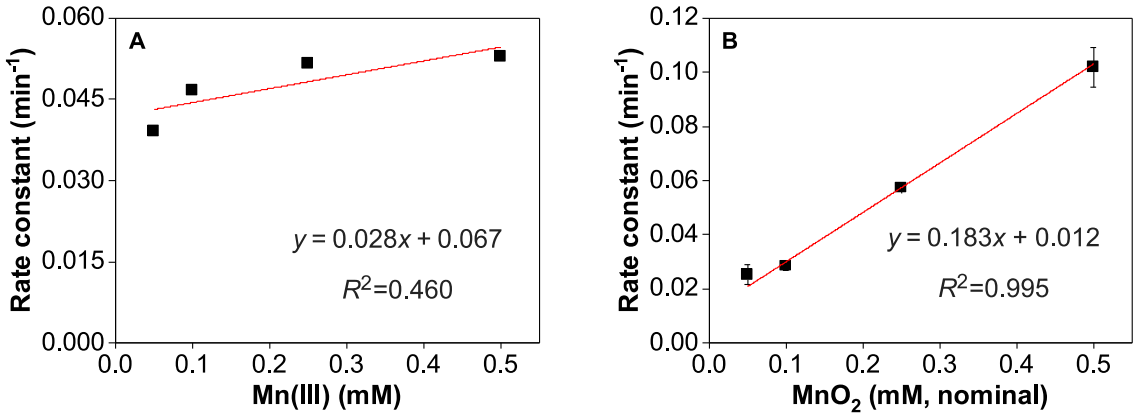

Figure S3.5. Effect of dissolved Mn(III) (A) and MnO_2 (B) loadings on initial BPA degradation rate constants. The rate constants were obtained by plotting the natural log of BPA concentrations as a function of time using five early time points, where linear relationships were observed. Error bars represent the standard deviation of duplicate samples and are not depicted when smaller than the symbol size.

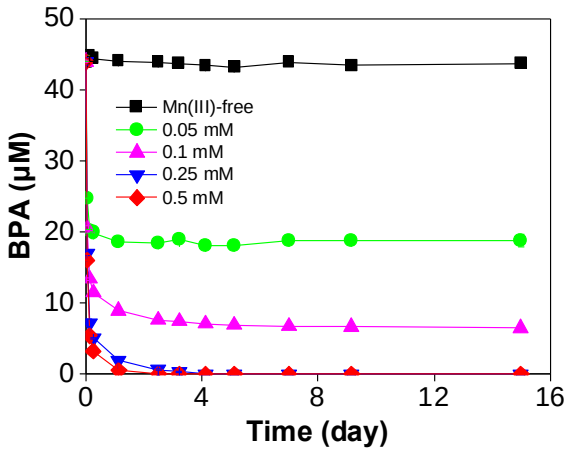

Figure S3.6. Mn(III)-mediated BPA degradation in incubation vessels with phosphate buffer (pH 7.2) with a starting concentration of 44 μM BPA monitored over a 15-day incubation period. Error bars are smaller than the symbol size and not shown.

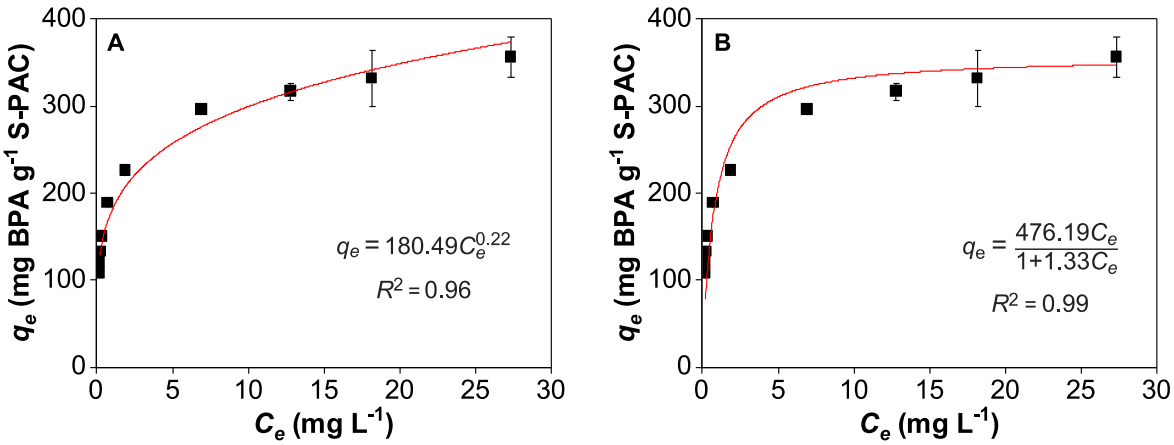

Figure S3.7. Adsorption characteristics of BPA to SPAC in systems without Mn. Freundlich (panel A) and Langmuir (panel B) isotherms for the adsorption of BPA to SPAC. Error bars represent the standard deviation of samples collected from triplicate incubation vessels and are not depicted when smaller than the symbol size.

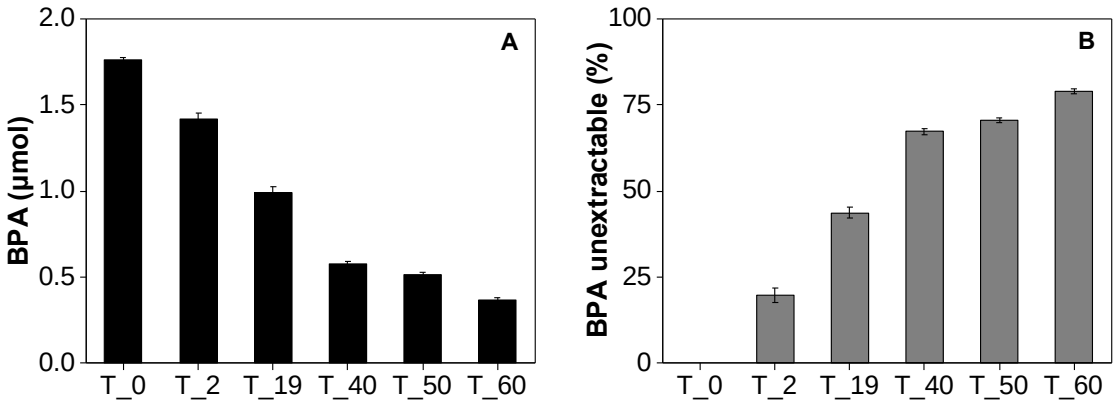

Figure S3.8. Recovery of BPA from SPAC following organic solvent extraction as a function of time. Panel A shows the amount (µmol) of BPA recovered by extraction with ethyl acetate after 2, 19, 40, 50, and 60 days of incubation at room temperature. Panel B shows the amount (%) of BPA adsorbed to SPAC that cannot be extracted with ethyl acetate after 2, 19, 40, 50, and 60 days of incubation at room temperature. The error bars represent the standard deviation of samples collected and analyzed from triplicate incubation vessels.

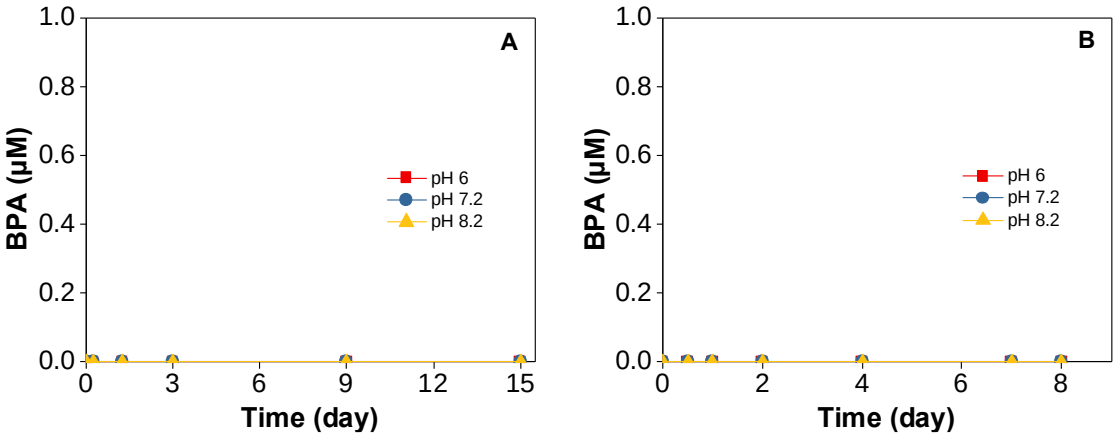

Figure S3.9. Desorption kinetics of BPA from SPAC at pH 6.0, 7.2 and 8.2. Panel A shows the lack of BPA desorption from SPAC with freshly adsorbed BPA. SPAC with freshly adsorbed BPA was prepared by incubating 1.76 μmol BPA with SPAC for 30 min, centrifugation, and suspending the pellets in phosphate buffer as described in the Methods section. Panel B shows the lack of desorption of aged BPA adsorbed to SPAC. Aged SPAC adsorbed BPA was prepared by incubating 1.76 μmol BPA with SPAC for 60 days. Each datum point represents the average of three independent experiments.

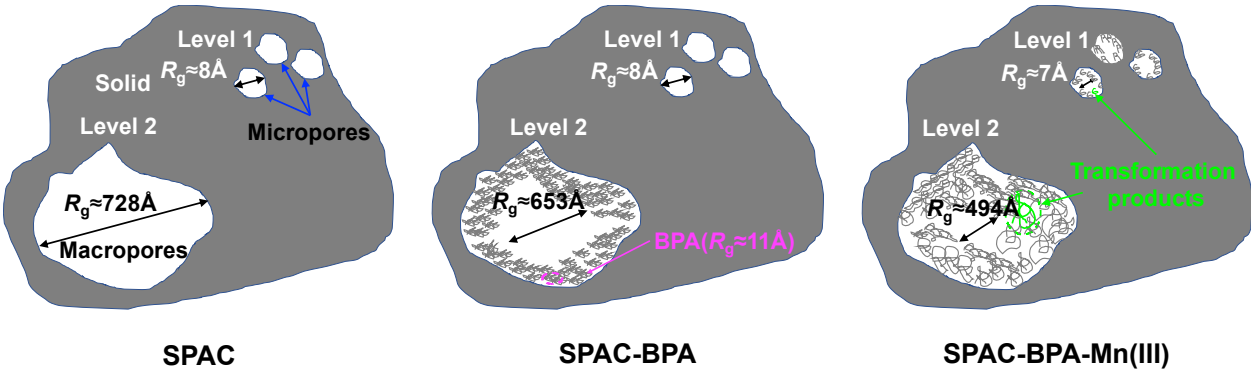

Figure S3.10. Schematics of a SPAC particle featuring three micropores (level 1) and one macropore (level 2). The left illustration represents a ”neat” SPAC particle, the illustration in the middle depicts an SPAC particle with adsorbed deuterated BPA, and the illustration on the right shows the SPAC particle with adsorbed deuterated BPA and BPA transformation products after Mn(III) treatment. The R_g values indicate the average size of the irregular shaped pores.

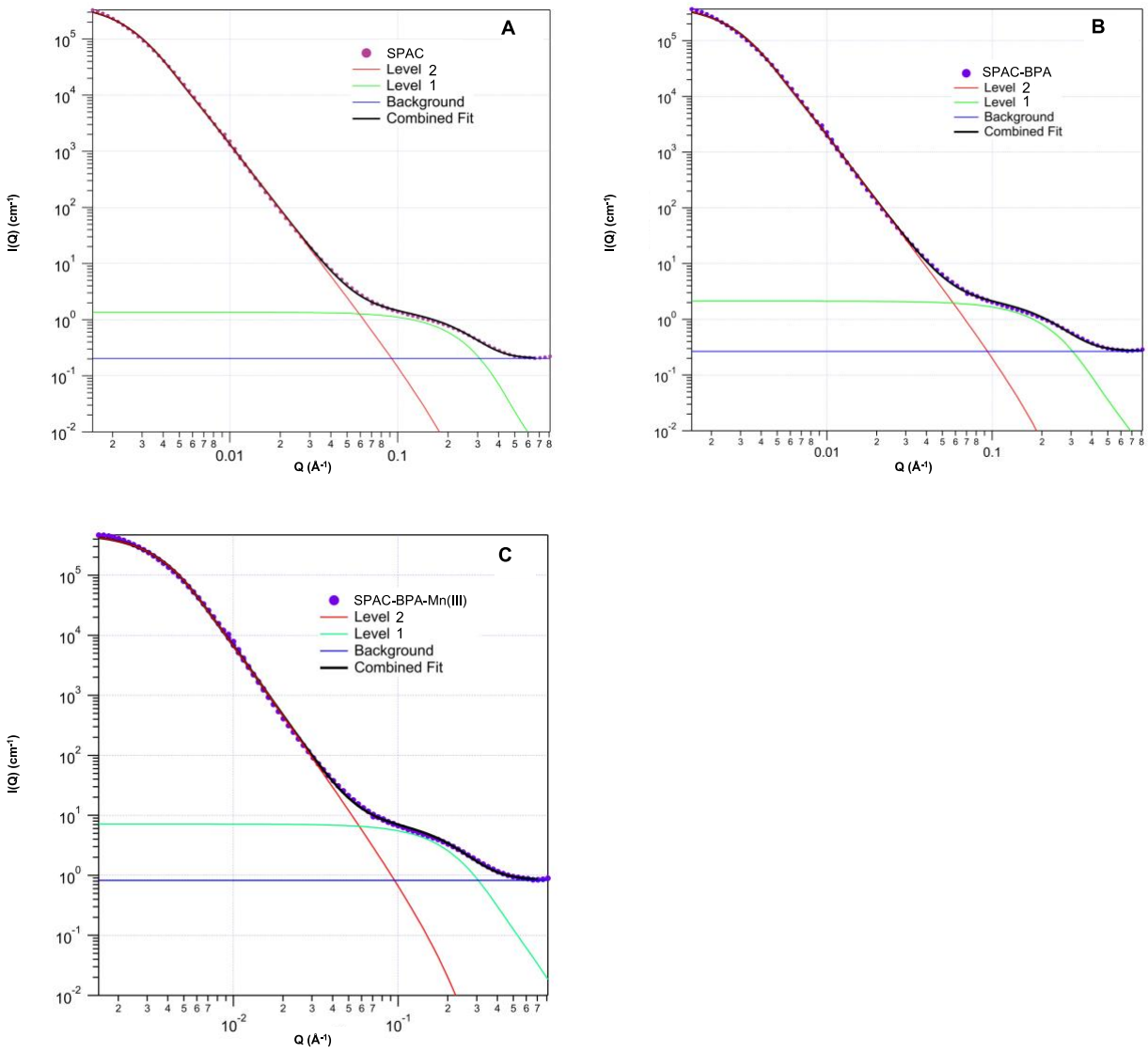

Figure S3.11. Decomposition of total scattering intensity into micropore and macropore levels. Panel A shows the decomposition of total scattering intensity into level structures of SPAC. Panel B shows SPAC with adsorbed deuterated BPA. Panel C depicts SPAC with adsorbed deuterated BPA after Mn(III) treatment. The green curve represents the scattering of level 1 structure based on the unified model fits. The red curve in each panel represents the calculated scattering from the level 2 structure based on the unified model fits. The blue line arises from incoherent scattering background, which is independent of the wave vector Q.

Chapter 4. Biotransformation of Bisphenols by *Erythrobacter* sp. Strain SD21 in the Absence of Manganese

The information presented in the following chapter is being incorporated into a manuscript for submission to the journal Environmental Science & Technology.

4.1 Abstract

The large-scale production and utilization of polycarbonate plastic and epoxy resins introduces bisphenols with potential estrogenic effects into environmental systems. Oxidized manganese (Mn) species mediate the abiotic degradation of bisphenols and this process has been studied extensively. We demonstrate that *Erythrobacter* sp. strain SD21, a Mn-oxidizing bacterium, effectively transforms bisphenol A (BPA), bisphenol S (BPS), and bisphenol AF (BPAF) in the absence of Mn. Complete removal of 0.78 ± 0.001 μmol BPA and 1.03 ± 0.015 μmol BPS was observed in 50-mL strain SD21 cultures within a 7-day incubation period, and approximately 67% of initial 0.04 ± 0.002 μmol of BPAF was consumed over the same period. Growth of strain SD21 was sensitive to BPS and BPAF, and the organism showed increased maximum OD600 values with BPS < 20 μM but BPS > 36 μM decreased the maximum bacterial OD600 values; however, BPAF inhibited strain SD21 growth regardless of different initial loadings. Hydroxylated transformation products of bisphenols were detected in cultures amended with bisphenols. The genome of strain SD21 harbors genes encoding monooxygenases and no hydroxylation of bisphenols was not observed in cultures amended with azide of 1 mM, a known inhibitor of phenylalanine 4-monooxygenase. Apparently, strain SD21 mediates the oxidation of bisphenols indirectly via the oxidation of Mn(II) to reactive Mn(III) and Mn(IV) species, and also has the ability to co-metabolize BPA, BPS, and BPAF.

Keywords: bisphenol A, bisphenol S, bisphenol AF, *Erythrobacter* sp. strain SD21, biotransformation, monooxygenase, hydroxylation.

4.2 Introduction

Bisphenol S (BPS) and bisphenol AF (BPAF), two major substitutes of bisphenol A (BPA), are used to gradually replace BPA in the production of thermal receipts, the packaging of food and drink, and the coating of food cans (NITE, 2003; Stout, 2008; Simoneau et al., 2011; Grignard et al., 2012). The global BPAF production is unknown, but the annual production in the US reached 230 tons in 2008 (Stout, 2008). The global BPS market in 2020 was 45,000 tons with further increase projected (ChemAnalyst, 2022). BPAF and BPS have been detected in numerous environmental matrices and up to 2,010 and 1,970 ng g^{-1} and 250 and 20 ng L^{-1} were detected in sediment (dry weight) and freshwater bodies, respectively (Liao et al., 2012; Yang et al., 2014). BPAF and BPS are used in the production of "BPA-free" products; however, there is concern that structural analogues also have estrogenic properties (Fic et al., 2015; Kinch et al., 2015; Gingrich et al., 2019).

The high-volume production BPA and other bisphenols and the possible risks of human exposure triggered environmental fate investigations of BPS and BPAF (Choi and Lee, 2017; Li et al., 2018; Zhou et al., 2020). BPAF and BPS are susceptible to abiotic degradation by photo-degradation (Kondrakov, 2015; Shao et al., 2017b; Wang et al., 2020), UV-based oxidation (Cao et al., 2012; Park and Kim, 2012; Kovačič et al., 2019), sulfate radical-based oxidation (Shao et al., 2017a; Wang et al., 2020), as well as other processes (Li et al., 2018). On the other hand, a number of studies have reported the biological transformation and degradation of BPS and BPAF in soils, freshwater bodies, and wastewater treatment plants (Choi and Lee, 2017; Sun et al., 2017; Frankowski et al., 2020; Zhou et al., 2020). Previous experimental efforts also suggested that BPAF is more recalcitrant to biodegradation than BPA and BPS (Choi and Lee, 2017). The biologically-mediated transformation and degradation of BPS and BPAF were mainly

investigated in complex systems with diverse microorganisms, and no studies have reported the degradation of BPAF by any axenic cultures yet. A single axenic culture, *Sphingobium fuliginis* OMI, has been reported to degrade BPS, but no degradation products have been identified and mechanistic understanding has not been attained (Ogata et al., 2013).

Biotic BPA transformation and degradation have been well-documented, and several bacterial enzymes, including cytochrome P450 monooxygenase (Sasaki et al., 2005a), laccase (Telke et al., 2009), and *p*-hydroxybenzoate hydroxylase (Zhou et al., 2015) have been implicated in BPA hydroxylation, the initial step preceding further degradation. A recent study demonstrated that BPA transformation in an axenic culture of *Erythrobacter* sp. SD-21 (Shobnam et al., 2021). *Erythrobacter* sp. SD-21 is a model organism for studying manganese (II) (Mn[II]) oxidation and the formation of Mn(III) and Mn(IV) species, which are strong oxidants and can mediate the transformation and degradation of BPA (Im et al., 2015; Shobnam et al., 2021; Sun et al., 2021).

Due to the widespread distribution of BPS and BPAF in the environment, a detailed understanding of the fate of these BPA substitutes is needed. The objective of this study was to investigate the biotransformation capability of BPA substitutes, BPS and BPAF, by the bacterium *Erythrobacter* sp. SD-21, which was identified with the capability to transform BPA recently (Shobnam et al., 2021). A series of incubation experiments were conducted to investigate the biotransformation of products of BPA, BPS and BPAF, respectively, and to explore the transformation mechanisms.

4.3 Materials and Methods

4.3.1 Chemicals

BPA (>99% purity), BPS (>98% purity), and BPAF (>99% purity) were purchased from Sigma-Aldrich (St. Louis, MO, USA). Sodium chloride, yeast extract, peptone, methanol, acetonitrile, acetic acid, and HEPES were obtained from Fisher Scientific (Waltham, MA, USA). All chemicals used were of reagent grade or higher purity.

4.3.2 Bacterial strain and growth condition

Strain SD21 was isolated from the sediment of San Diego Bay, San Diego, USA, which is a well-characterized Mn-oxidizing bacterium (Francis and Tebo, 2001). Strain SD21 was grown in an organic-rich K-medium containing 0.5 g L^{-1} yeast extract, 2 g L^{-1} peptone, 20 mM HEPES, and the artificial seawater at pH 7.4 (Francis and Tebo, 2001). The artificial seawater comprises 0.3 M NaCl, 0.05 M $MgSO_4$, 0.01 M $CaCl_2$, and 0.01 M KCl (Francis and Tebo, 2001). The optimum growth occurs at 30 °C with continuously agitation at 120 rpm. Cell growth was monitored at 600 nm with a PerkinElmer Lambda 35 UV−vis spectrophotometer and cell yields were determined with the Bradford assay (see the Supporting Information for details). The growth of SD21 was also checked by using a defined medium. Strain SD21 was grown in 100 mL flask bottles with 50 mL of completely synthetic, defined mineral salt medium that comprised 1.5 mM KH_2PO_4, 5 mM NH_4Cl, the trace metal solution (Löffler et al., 2005), the Wolin vitamin mix (Wolin et al., 1963), 20 mM HEPES (pH 7.4) and 100% artificial seawater (see above). Acetate or pyruvate of 5 mM was added as sole carbon source and electron donor.

4.3.3 Biotransformation experiments

The biotransformation of three bisphenols, BPA, BPS, and BPAF, by strain SD21 was investigated. Briefly, strain SD21 was grown in 100 mL flask bottles with 50 mL of the K-medium, and the bottles were loosely closed with filter screw caps for exchanging of oxygen. Bisphenols were added to the bottles containing medium using plastic syringes (BD, Franklin Lakes, NJ, USA) to achieve final concentrations of 8-32 μM for BPA, 11-36 μM for BPS, and 0.4-1.6 μM for BPAF, respectively. Culture vessels were continuously agitated at 120 rpm in an upright position at 30 °C. Aliquots (0.3 mL) were withdrawn over time and bisphenols were extracted using the same volume of methanol following an established procedure (Im et al., 2016). The samples were then centrifuged at 10,000 g (Eppendorf centrifuge 5415D, Hamburg, Germany) for 15 min, and the supernatant was transferred to 2 mL glass HPLC autosampler vials. The transformation rates of bisphenols were determined from the progression curves and the linear regression analysis included four data points at least.

4.3.4 Intracellular or extracellular transformation

The oxidation of Mn(II) to MnO_2 occurred in the extracellular of the strain SD21 by Mn peroxidase (Estes et al., 2017; Medina et al., 2018), which may react with bisphenols (Huang and Weber, 2005). To distinguish the transformation of bisphenols occurred in the intracellular or the extracellular of the strain SD21, the resting cell and the cell-free filtrate were prepared for transformation experiments, respectively. Strain SD21 was precultured in a 2 L glass bottle containing 1.6 L K-medium. The cells of SD21 were harvested at the late exponential phase (OD_{600} ~ 0.5) by centrifugation at 10,000 g at 4 °C for 30 min. For the transformation experiment using resting cells, the cell pellets were resuspended in 100 mL of the sterile K-medium after carefully removing the supernatant using a pipette, and 10 mL of the cell suspension was

transferred to three sets of 50 mL glass vials, each set receiving 15 μM BPA, 16 μM BPS, and 1 μM BPAF, respectively. The supernatant was filtered using a 0.22 μm PVDF filter (Thermo Fisher Scientific, Pittsburgh, PA, USA) and resulting in the cell-free filtrate. Transformation experiments of bisphenols in the extracellular were performed in 50 mL glass vials with a total volume of 10 mL of cell-free filtrate, containing 15 μM BPA, 16 μM BPS, and 1 μM BPAF, respectively. Bottles that received the same concentration of bisphenols as the corresponding treatment and 10 mL of the sterile K-medium instead of cell suspension or cell-free filtrate served as negative controls. The bottles were loosely capped and agitated at 120 rpm at 30 °C. All experiments were performed in triplicate vessels. Aliquots (0.3 mL) were withdrawn over time with sterile pipettes and incubated with the same volume of methanol for 30 min for extraction, and the bisphenols concentrations were measured by HPLC after centrifuging at 10,000g for 15 min.

4.3.5 Transformation products identification

Strain SD-21 cultures were grown with 15 μM BPA, 16 μM BPS, and 1 μM BPAF, respectively, in 100 mL flask bottles containing 50 mL of the K-medium at the same incubation conditions (see above). Following a 7-day incubation period, the entire vessels were extracted using an equal volume of ethyl acetate, agitated for 12 h, and then centrifuged at 5,000 g for 10 min (Sun et al., 2021). The organic phases from three successive extractions were combined and dried under a gentle stream of nitrogen gas. Each residue was dissolved in 1 mL of acetonitrile and water (1:1, v/v) and stored at 4 °C for further analysis. The transformation intermediates of three bisphenols in the extracts were analyzed using the ultra-high performance liquid chromatography-high resolution mass spectrometry (UHPLC-HRMS/MS) with a modified method (see the Supporting Information for details) (Choi and Lee, 2017).

4.3.6 Functional analysis of the genome of the strain SD21

The genome of strain SD-21 has been sequenced previously and downloaded from the NCBI (PRJNA19305). Protein-coding sequences present in the genome were predicted using Prodigal v2.6.3 (Hyatt et al., 2010), and assigned KEGG orthologs (KOs) using KofamScan v1.3.0 against HMM profiles from the KEGG database (released on 24-Feb-2021) (Aramaki et al., 2020). The metabolic pathway was constructed using KEGG Mapper and the completeness of various metabolic pathways was assessed using KEGG-Decoder v1.32.0 (Graham et al., 2018; Kanehisa et al., 2022), and interest pathways (e.g., tricarboxylic acid [TCA], pyruvate metabolism pathway) or enzymes (e.g., monooxygenase) were manually selected from KEGG Mapper results.

4.3.7 Phylogenetic analysis of the phenylalanine 4-monooxygenase

Strain SD21 harbors one gene encoding phenylalanine 4-monooxygenase (EC 1.14.16.1), which is likely involved in bisphenols transformation. Six protein sequences of biochemically characterized bacterial phenylalanine 4-monooxygenase and 23 amino acid sequences of closest relatives of the phenylalanine 4-monooxygenase harbored by strain SD21 were retrieved from the Uniprot database. Protein sequences of phenylalanine 4-monooxygenase were aligned using ClustaloΩ with default settings (Sievers et al., 2011). The alignment was used to build a maximum likelihood reference tree in RAxML V8.2.12 with '-f a' algorithm, gamma parameter optimization, and a general time-reversible model option (Stamatakis, 2014). The generated tree files were visualized with iTOL (Letunic and Bork, 2016).

4.3.8 Monooxygenase inhibition experiments

To investigate the role of monooxygenase in bisphenols biotransformation, azide was used as the inhibitor (Aregbesola et al., 2022). Specifically, the cell pellets were collected by

centrifugation of 3 L strain SD21 culture at late exponential phase (see above) and washed using sterile 10 mM phosphate buffer solution three times. The cell pellets were resuspended in 200 mL using the same phosphate buffer solution after carefully removing the supernatant using a pipette, and 10 mL of the cell suspension was transferred into three sets of 50 mL glass vials, each set receiving 15 μM of BPA, 16 μM of BPS, or 1 μM of BPAF, respectively. In addition, the same series of three sets were set up without adding azide as the positive control. The potential effect of azide on the abiotic transformation of three bisphenols was assessed by adding 1 mM azide into 10 mL of the sterile phosphate buffer solution with 15 μM of BPA, 16 μM of BPS, or 1 μM of BPAF, respectively. Bottles that received the same concentration of bisphenols as the corresponding treatment in 10 mL of the sterile phosphate buffer solution served as negative controls. The bottles were loosely capped and agitated at 120 rpm at 30 °C. All experiments were performed in triplicate vessels. Aliquots (0.3 mL) were withdrawn over time and extracted using methanol, and the bisphenols concentrations were measured after centrifugation.

4.3.9 Analytical procedures

BPA, BPS, and BPAF were quantified using an Agilent 1100 Series HPLC system equipped with a diode array detector and a fluorescence detector (FLD) (Sun et al., 2021). For BPA and BPS, separation was performed on an Agilent Eclipse XDB C18 column (4.6 mm × 150 mm, 5 μm) using isocratic elution at a flow rate of 1 mL min^{-1} of acetonitrile and Milli-Q water (50:50, v/v) at pH 7.2. For BPAF, separation was performed on the same column but using 80:20 at a flow rate of 0.5 mL min^{-1} of acetonitrile and Mill-Q water (v/v). The FLD was set at excitation and emission wavelengths of 226 nm and 310 nm, respectively. The DAD was set at the wavelength of 246 nm. For standard curve construction, vials containing 0.4, 1.1, 2.2, 11, 44, and

88 μM BPA were prepared in triplicates. BPS standard curves were created using solutions of 0.55, 2.2, 5.5, 11, and 40 μM. BPAF standard curves were created using solutions of 0.2, 0.5, 1, and 2 μM.

4.3.10 Toxicity prediction

Acute and chronic toxicity of BPA, BPS, and BPAF as well as their degradation products were predicted using the US EPA Ecological Structure Activity Relationships (ECOSAR) software (Version 2.0) (USEPA, 2017). The ECOSAR software evaluates the exposure risks of organic compounds to fish, *Daphnia*, and green algae, by using quantitative structure activity relationships model. The prediction results include the half-maximum effective concentrations (EC_{50}), half-maximum lethal concentrations (LC_{50}), and chronic toxicity (ChV) of each compound.

4.4 Results

4.4.1 Bisphenols biotransformation by the strain SD21

In the presence of strain SD21, BPA was effectively transformed (Figure 4.1A). In addition, BPS and BPAF transformation were observed with strain SD21, indicating that an axenic culture mediates transformation of both BPA substitutes (Figure 4.1). BPA, BPS, and BPAF concentrations remained constant in medium and heat-inactivated controls, indicating that the sorption of three bisphenols to the experimental vessels and cells was negligible (Figure 4.1).

The initial loadings of BPA, BPS, and BPAF significantly affected the rates and extents of their transformation by strain SD21 (Figure 4.1 and Figure S4.1). A BPA transformation rate of 2.21 ± 0.01 μM BPA day^{-1} was measured at an initial 8 μM BPA, and a significant higher

transformation rate of 3.70 ± 0.21 μM BPA day^{-1} was observed at higher initial BPA concentrations of up to 32 μM. Though BPA transformation rates by SD21 increased with initial loadings, incubation periods for the complete transformation of different initial BPA loadings showed a negative relation with the transformation rate. Specifically, nearly complete removal of BPA of 8 and 16 μM were achieved by the strain SD21 within 4 and 6-day incubations, respectively; however, to achieve the same BPA removal, approximately a 12-day incubation period was required for 32 μM BPA (Figure 4.1A).

Increasing initial BPS and BPAF loadings also resulted in progressively higher transformation rates (Figure S4.1). In treatments with 11, 20, and 36 μM BPS, BPS transformation rates of 3.55 ± 0.08, 3.71 ± 0.45, and 5.78 ± 0.14 μM BPS day^{-1} were measured (Figure S4.1B). Over 4, 6, and 8-day incubations, respectively, all the initial 11, 20, and 36 μM BPS were transformed by strain SD21. The transformation rates of BPAF by SD21 were also sensitive to its initial loadings. The transformation rates of BPAF increased from 0.06 (± 0.00) to 0.14 (± 0.01) μM BPAF day^{-1} when the initial BPAF increased from 0.4 to 1.6 μM (Figure S4.1C). However, incomplete removal of BPAF by strain SD21 was observed with the maximum removal extent of 84.30 ± 2.07% over a 14-day incubation.

4.4.2 Inhibitory effects of BPS and BPAF on strain SD21

BPA, BPS, and BPAF exhibited different effects on the growth of strain SD21 (Figure S4.2). BPA has no significant ($p > 0.05$) effect on cell growth of strain SD21 (Figure S4.2A); however, BPS and BPAF showed different effects. Compared with the positive control incubations, relative lower initial BPS loadings (< 20 μM) promoted the growth of strain SD21 with the maximum OD600 value increased by approximately 40% and 24% in the presence of 12 and 20 μM BPS, respectively. In contrast, 38 μM BPS reduced the maximum OD600 value of strain

SD21 (Figure S4.2B). BPAF also impacted the growth of strain SD21. Compared to the positive control incubations, the maximum OD600 value of strain SD21 decreased by approximately 10% with 0.4 μM BPAF and by about 45% with 1.6 μM BPAF increased (Figure S4.2C).

4.4.3 Intracellular biotransformation of bisphenols

To determine if extracellular and intracellular fractions of strain SD21 responsible for the transformation of bisphenols, BPA, BPS, and BPAF transformation were investigated using cell-free filtrate and washed resting cell suspensions. Bisphenol concentrations remained constant in cell-free filtrate, indicating that the transformation of BPA, BPS and BPAF were not mediated by extracellular reactive species or catalysts (Figure 4.2). In contrast, BPA and BPS were effectively transformed by resting cells over a 12-hour incubation period at rates of 3.11 ± 0.15 μM BPA h^{-1} and 3.56 ± 0.02 μM BPS h^{-1}. In addition, transformation of BPAF was observed in the presence of resting cells at the rate of 0.009 ± 0.001 μM BPAF h^{-1} and 71.78 ± 2.29% of the initial 0.96 ± 0.01 μM BPAF was transformed in 3-day incubation (Figure 4.2C).

4.4.4 Biotransformation products of bisphenols

Bisphenols biotransformation intermediates by strain SD21 were identified using UHPLC-HRMS based analysis. Four transformation intermediates were identified in the biotransformation of BPA (Figure 4.3). Intermediate 1 (BPA-T1) with an *m/z* of 243.1021 ($[M-H]^-$) eluted at 5.9 min, which is 16 atomic mass units (i.e., O) more than the parent molecular mass of BPA, and likely represents a BPA analogue through hydroxylation (Figure 4.3). Intermediate 2 (BPA-T2) with an *m/z* of 121.0290 was eluted at 45.7 min, which had a molecular formula of $C_7H_5O_2^-$. Intermediate 3 (BPA-T3) with an *m/z* of 133.0656 ($[M-H]^-$) eluted at 4.7 min, and two other fragment ions with *m/z* ratios of 117.0340 and 93.0336, respectively. The MS information suggests that the intermediate could be formed by breaking the bond between the

propane-2,2-diyl group and one 4-hydroxyphenyl group, and had a molecular formula of $C_9H_{10}O$. Intermediate 4 (BPA-T4) had a molecular mass of 137.0239 ($[M-H]^-$) with the molecular formula of $C_7H_5O_3^-$. Combined with previous studies (Zhang et al., 2007; Nakamura et al., 2011; Choi and Lee, 2017), intermediates 1, 2, 3, and 4 were identified as *o*-monohydroxylated BPA, *p*-hydroxybenzaldehyde, *p*-isopropenylphenol, and *p*-hydroxybenzoate.

BPS transformation by strain SD21 yielded four products. The first intermediate (BPS-T1) eluted at 5.2 min had an *m/z* of 265.0171 and a predictive molecular formula of $C_{12}H_9O_5S^-$, and likely represents an oxidized BPS analogue with an O atom addition. Intermediate 2 (BPS-T2) had a molecular mass of 281.0120, which is 32 and 16 atomic mass units (i.e., O) more than the parent molecular mass of BPS and BPS-T1, respectively. BPS-T3 with the *m/z* of 313.0018 had a molecular formula of $C_{12}H_9O_8S^-$. Intermediate BPS-T4 eluted at 7.2 min with an *m/z* of 199.0065. The four intermediates BPS-T1-T4 likely represent the monohydroxylated BPS, the dihydroxylated BPS, the meta-cleavage product of dihydroxylated BPS, and one further transformation product.

In the case of BPAF, intermediate 1 (BPAF-T1) with an *m/z* of 351.0456 eluted at 7.4 min which is 16 atomic mass units (i.e., O) more than the parent molecular mass of BPAF, and likely represents a mono-hydroxylated BPAF product (Figure 4.3). The second and the third intermediates (BPAF-T2 and BPAF-T3) have the molecular weights of 259.0194 and 243.0245, respectively with the formula of $C_9H_5F_6O_2^-$ and $C_9H_5F_6O^-$, respectively. Intermediate 4 (BPAF-T4) with an *m/z* of 112.9850 eluted at 5.3 min. BPAF-T4 has the molecular formula of $C_2F_3O_2^-$, which same as the trifluoroacetate ($[M-H]^-$).

Transformation pathways of BPA, BPS, and BPAF were proposed based on the identified products, EAWAG-Biocatalysis/Biodegradation Database (Gao et al., 2010). Bisphenols were

initially hydroxylated to mono-hydroxylated bisphenols, and further transformed through meta-cleavage (Figure 4.3).

4.4.5 Functional analysis of strain SD21

The genome of strain SD21 comprises 19 DNA scaffolds with G+C content of 62.9%. The genome contains 2,992 genes, including 2,941 protein-coding genes and 2 16S rRNA genes. Strain SD21 encodes the complete gene sets for pyruvate oxidation and TCA cycle based on KEGG annotation (Figure S4.3), indicating a diverse metabolic potential. However, no growth was observed of strain SD21 in a defined mineral salts medium with acetate or pyruvate as sole carbon source. Therefore, the above biotransformation experiments of bisphenols by strain SD21 were conducted using the K-medium. In addition, the genome of strain SD21 encodes 21 putative hydroxylase/monooxygenase based on the RefSeq annotation (Table 4.1) and 13 of 21 assigned KEGG orthologs. Further analysis of 13 hydroxylase/monooxygenase found that one monooxygenase, phenylalanine 4-monooxygenase (k00500), is likely involved in the hydroxylation of bisphenols. Phylogenetic analysis of the 30 phenylalanine 4-monooxygenase amino acid sequences revealed high sequence similarity (> 81.5%) between the closed relatives of strain SD21, but a relatively lower similarity (42-51%) to biochemically characterized bacterial phenylalanine 4-monooxygenases (Figure S4.4). In contrast, phenylalanine 4-monooxygenase in strain SD21 showed no similarity to the three known bacterial enzymes, cytochrome P450 monooxygenase, laccase, and *p*-hydroxybenzoate hydroxylase, for BPA transformation.

4.4.6 Azide inhibit bisphenols biotransformation

To explore the enzyme(s) involved in the transformation of bisphenols, BPA, BPS, and BPAF was incubated with dense SD21 cells in phosphate buffer solutions containing 1 mM

azide, respectively. BPA, BPS, and BPAF were stable in the negative and azide abiotic controls, indicating that the sorption of three bisphenols to the experimental vessels and azide induced abiotic transformation were negligible (Figure 4.4). Without azide, approximately 64% of initial 15 μM BPA was transformed at the rate of 0.009 ± 0.0003 μM BPA h^{-1} by strain SD21 within 1-day incubation (Figure 4.4A). No further transformation of BPA was observed over a 3-day incubation period. In contrast, the addition of 1 mM azide completely inhibited the transformation of BPA in strain SD21 cultures over the same period. In the case of BPS, more than 68% of initial 16 μM BPS were transformed by strain SD21 within 1-day incubation; however, only 32% of initial the amount of BPS was transformed over the same period in the presence of 1 mM azide (Figure 4.4B). In the case of BPAF, approximately 75% of initial 1.1 μM BPAF was transformed by strain SD21 within 3-day incubation. In contrast, only about 37% of initial amount of BPAF was transformed over the same period in the presence of 1 mM azide (Figure 4.4C).

4.5 Discussion

BPA substitutes have been widely used and frequently detected in various environmental systems (Liao et al., 2012; Yang et al., 2014; Karsauliya et al., 2021; Liu et al., 2021). Bacteria transformation and degradation of BPA has been well demonstrated (Im and Löffler, 2016; Shobnam et al., 2021); however, to date, the axenic culture mediated biological transformation of BPS and BPAF are still limiting. In the present study, *Erythrobacter* sp. strain SD21 effectively transforms BPA and its substitutes BPS and BPAF through enzymatic reactions. Apparently, strain SD21 is the first axenic culture identified as capable of transforming multiple bisphenols.

4.5.1 Biotransformation of BPA, BPS, and BPAF by strain SD21

The experimental efforts here demonstrated that, in addition to BPA, strain SD21 transforms BPAF and BPS. The growth studies also demonstrated that strain SD21 only grows in the nutrient-rich medium and the biotransformation of three bisphenols was dependent on the complex medium not a defined medium with specific organic substrates (i.e.., pyruvate, acetate). These experimental efforts are inconsistent with the genomic evidence that strain SD21 has diverse metabolic potential for a number of organic compounds (e.g., pyruvate, acetate) (Figure S4.3), indicating that strain SD21 is possibly an auxotrophic bacterium.

The transformation rates of BPA, BPS, and BPAF in strain SD21 demonstrated a positive relationship with initial concentrations, which can be explained by Michaelis-Menten kinetics ($V_0 = \frac{V_{max}[S]}{K_m+[S]}$). Similar to prior work studying BPA and BPS biotransformation (Sasaki et al., 2005b; Choi and Lee, 2017; Shobnam et al., 2021), rapid and complete biotransformation (Figure 4.1) of BPA and BPS suggests that these two bisphenols would not be likely to accumulate in environmental systems. In contrast, BPAF resisted transformation in strain SD21 cultures. A plausible explanation for the slow and incomplete transformation of BPAF is that the two electronegative trifluoromethyl groups in BPAF make the transformation (e.g., hydroxylation) less favorable (Choi and Lee, 2017; Frankowski et al., 2020; Zhou et al., 2020). Therefore, the increasing production as a BPA substitute and further inputs of BPAF to environmental systems would result in an increased level of BPAF.

Strain SD21 attained the same maximum OD600 values in the presence of different initial BPA loadings, similar to a prior study (Shobnam et al., 2021), indicating that BPA has no inhibitory effects on strain SD21. Compared to BPA, BPS and BPAF exhibited different effects on strain SD21 growth (Figure S4.2). Apparently, the lower level of BPS (≤ 20 μM) promoted

the growth of SD21, suggesting that BPS is likely a substrate for the growth of strain SD21. An alternative explanation is that BPS attenuates the inhibition of bacterial growth by toxins secreted by strain SD21, a similar phenomenon has been described in previous studies (Tebo et al., 2004; Shobnam et al., 2021). However, excess BPS (≥ 32μM) inhibited bacterial growth, which has been reported by affecting the synthesis of the cell membrane (Schäpe et al., 2020). In the case of BPAF, BPAF has the highest log K_{OW} of 4.47 (USEPA, 2011) among the three bisphenols studied in the present study and thus high lipophilicity, which could result in increased toxicity to the bacterium (Tišler et al., 2016).

4.5.2 Mechanisms of bisphenols biotransformation by strain SD21

The analysis of BPA, BPS, and BPAF transformation pathways demonstrated that hydroxylation should be the initial step for SD21 mediated transformation of three bisphenols, similar to what was observed in prior studies (Kolvenbach et al., 2007; Zhou et al., 2015; Choi and Lee, 2017). The biological hydroxylation of the aromatic ring is typically catalyzed by monooxygenase/hydroxylase (Ullrich and Hofrichter, 2007; Husain and Qayyum, 2013). Although known enzymes catalyzing the transformation of BPS and BPAF are lacking, the enzymatic transformation of BPA has been well studied. Prior work have identified three BPA transformation enzymes, including cytochrome P450 monooxygenase in *Sphingomonas* sp. strain AO1 (Sasaki et al., 2005a), laccase in *Pseudomonas* sp. strain LBC1 (Telke et al., 2009), and *p*-hydroxybenzoate hydroxylase in *Sphingobium* sp. strain BiD32 (Zhou et al., 2015), respectively. The functional analysis only identified the putative P450 monooxygenase in strain SD21 (Table 4.1) but failed to assign a KEGG ortholog, and no evidence concerning the involvement of the P450 enzyme systems was observed in a previous study (Shobnam et al., 2021). Furthermore, strain SD21 synthesizes and excretes a heme peroxidase responsible for Mn(II) oxidation outside

the cell (Anderson et al., 2009; Estes et al., 2017), which has been linked with the capability to transform BPA (Hirano et al., 2000; Shobnam et al., 2021); however, we observed that BPA, BPS and BPAF were not transformed in the cell-free filtrate. Collectively, these findings demonstrate that strain SD21 encodes other types of the enzyme(s) for transforming BPA, BPS, and BPAF.

Strain SD21 harbors a number of genes encoding monooxygenase/hydroxylase in addition to the putative P450 monooxygenase, but one enzyme, phenylalanine 4-monooxygenase, is likely to be involved in BPA, BPS, and BPAF transformation. Phenylalanine 4-monooxygenase has been reported to be involved in the hydroxylation of phenolic compounds (Aregbesola et al., 2020). The phenylalanine 4-monooxygenase inhibitor, azide, has been shown to inhibit its activity through binding to the iron in phenylalanine 4-monooxygenase (Mitic, 2001) and completely inhibited phenylalanine 4-monooxygenase activity concentration of azide as low as 1 mM (Aregbesola et al., 2022). The experimental efforts here demonstrated that 1 mM azide inhibited bisphenol transformation in strain SD21 resting cell suspensions. Growth of strain SD21 in the cell suspension assays in the presence of azide and in phosphate buffer without nutrients is not expected. These findings suggest that phenylalanine 4-monooxygenase is most likely involved in bisphenols transformation by strain SD21.

4.5.3 Toxicity evaluation of bisphenols transformation products

Bisphenols are potential estrogenic agents and transformation should result in reduced endocrine-disrupting activity; however, the human health concerns associated with the transformation products are not clear. Some BPA transformation products have been documented to impact human cancer cells more than the parent compound (Suzuki et al., 2004; McCormick et al., 2011; Nakamura et al., 2011). BPA and BPAF are assessed to be toxic to very toxic

(LC50/EC50/ChV<10 mg L^{-1}) to aquatic organisms (Table 4.2), but BPS is only categorized into the harmful level (LC_{50}/EC_{50}/ChV > 10 mg L^{-1}). Most of the BPA transformation products were predicted with lower toxicity (i.e., BPA-T2, BPA-T3, and BPA-T4); however, only one (i.e., BPA-T1) is predicted with comparable toxicity to BPA. In the case of BPS, all the four transformation products are predicted with lower toxicity than BPS, indicating that the biotransformation would detoxify the BPS. SD21-mediated BPAF transformation yielded two products (BPAF-T1 and BPAF-T3) with the same level of toxicity, but the remaining 2 products were categorized as the harmful level. Therefore, the fate of bisphenols transformation products should be understood for a meaningful and comprehensive risk assessment.

4.5.4 Environmental implications

The need to replace BPA has led to increased production of substitutes compounds, which has introduced BPS and BPAF to various environmental systems (Liao et al., 2012; Catenza et al., 2021). The study demonstrated that *Erythrobacter* sp. strain SD21 transforms BPA, BPS, and BPAF through enzymatic hydroxylation reactions. These observations suggest that attenuation of BPA and its substitutes in natural systems can occur. BPA and BPS were rapidly and efficiently transformed by strain SD21, but BPAF was not, indicating that BPAF is more likely to accumulate in environmental systems. The biotransformation of BPA and BPS yielded less toxic products, which are likely to be mineralized (Fent et al., 2003; Choi and Lee, 2017); however, the transformation of BPAF generated products with trifluoromethyl groups, and the trifluoromethyl group is resistant to further biotransformation (Yu et al., 2022). Based on the available data demonstrating that BPAF is a source of more toxic transformation products, the use of BPAF as a BPA substitute should be reconsidered.

Acknowledgments

This work was supported by the Polycarbonate/BPA Global Group of the American Chemistry Council (ACC), Washington, DC. Samples were processed in the Biological and Small Molecule Mass Spectrometry Core (BSMMSC), University of Tennessee, Knoxville, TN (RRID: SCR_021368).

References

Anderson, C., Johnson, H., Caputo, N., Davis, R., Torpey, J. and Tebo, B.M. 2009. Mn (II) oxidation is catalyzed by heme peroxidases in "*Aurantimonas manganoxydans*" strain SI85-9A1 and *Erythrobacter* sp. strain SD-21. Appl. Environ. Microbiol. 75(12), 4130-4138.

Aramaki, T., Blanc-Mathieu, R., Endo, H., Ohkubo, K., Kanehisa, M., Goto, S. and Ogata, H. 2020. KofamKOALA: KEGG ortholog assignment based on profile HMM and adaptive score threshold. Bioinformatics 36(7), 2251-2252.

Aregbesola, O.A., Kumar, A., Mokoena, M.P. and Olaniran, A.O. 2020. Role of tetrachloro-1, 4-benzoquinone reductase in phenylalanine hydroxylation system and pentachlorophenol degradation in *Bacillus cereus* AOA-CPS1. Int. J. Biol. Macromol. 161, 875-890.

Aregbesola, O.A., Kumar, A., Mokoena, M.P. and Olaniran, A.O. 2022. Classic pentachlorophenol hydroxylating phenylalanine 4-monooxygenase from indigenous *Bacillus tropicus* strain AOA-CPS1: cloning, overexpression, purification, characterization and structural homology modelling. Appl. Biochem. Biotechnol. 194(2), 635-658.

Cao, G., Lu, J. and Wang, G. 2012. Photolysis kinetics and influencing factors of bisphenol S in aqueous solutions. J. Environ. Sci. 24(5), 846-851.

Catenza, C.J., Farooq, A., Shubear, N.S. and Donkor, K.K. 2021. A targeted review on fate, occurrence, risk and health implications of bisphenol analogues. Chemosphere 268, 129273.

ChemAnalyst 2022. Global Bisphenol S Market Analysis 2015-2030. https://www.researchandmarkets.com/reports/5232464/global-bisphenol-s-market-analysis-plant (accessed Mar, 2022).

Choi, Y.J. and Lee, L.S. 2017. Aerobic soil biodegradation of bisphenol (BPA) alternatives bisphenol S and bisphenol AF compared to BPA. Environ. Sci. Technol. 51(23), 13698-13704.

Estes, E., Andeer, P., Nordlund, D., Wankel, S. and Hansel, C. 2017. Biogenic manganese oxides as reservoirs of organic carbon and proteins in terrestrial and marine environments. Geobiology 15(1), 158-172.

Fent, G., Hein, W.J., Moendel, M.J. and Kubiak, R. 2003. Fate of ^{14}C-bisphenol A in soils. Chemosphere 51(8), 735-746.

Fic, A., Mlakar, S.J., Juvan, P., Mlakar, V., Marc, J., Dolenc, M.S., Broberg, K. and Mašič, L.P. 2015. Genome-wide gene expression profiling of low-dose, long-term exposure of human osteosarcoma cells to bisphenol A and its analogs bisphenols AF and S. Toxicol. In Vitro 29(5), 1060-1069.

Francis, C.A. and Tebo, B.M. 2001. Enzymatic manganese (II) oxidation by a marine α-proteobacterium. Appl. Environ. Microbiol. 67(9), 4024-4029.

Frankowski, R., Zgoła-Grześkowiak, A., Smułek, W. and Grześkowiak, T. 2020. Removal of bisphenol A and its potential substitutes by biodegradation. Appl. Biochem. Biotechnol., 1-11.

Gao, J., Ellis, L.B. and Wackett, L.P. 2010. The University of Minnesota biocatalysis/biodegradation database: improving public access. Nucleic Acids Res. 38(suppl_1), D488-D491.

Gingrich, J., Pu, Y., Ehrhardt, R., Karthikraj, R., Kannan, K. and Veiga-Lopez, A. 2019. Toxicokinetics of bisphenol A, bisphenol S, and bisphenol F in a pregnancy sheep model. Chemosphere 220, 185-194.

Graham, E., Heidelberg, J. and Tully, B. 2018. Potential for primary productivity in a globally-distributed bacterial phototroph. The ISME journal 12(7), 1861-1866.

Grignard, E., Lapenna, S. and Bremer, S. 2012. Weak estrogenic transcriptional activities of bisphenol A and bisphenol S. Toxicol. In Vitro 26(5), 727-731.

Hirano, T., Honda, Y., Watanabe, T. and Kuwahara, M. 2000. Degradation of bisphenol A by the lignin-degrading enzyme, manganese peroxidase, produced by the white-rot basidiomycete, *Pleurotus ostreatus*. Biosci. Biotechnol. Biochem. 64(9), 1958-1962.

Huang, Q. and Weber, W.J. 2005. Transformation and removal of bisphenol A from aqueous phase via peroxidase-mediated oxidative coupling reactions: efficacy, products, and pathways. Environ. Sci. Technol. 39(16), 6029-6036.

Husain, Q. and Qayyum, S. 2013. Biological and enzymatic treatment of bisphenol A and other endocrine disrupting compounds: a review. Crit. Rev. Biotechnol. 33(3), 260-292.

Hyatt, D., Chen, G.-L., LoCascio, P.F., Land, M.L., Larimer, F.W. and Hauser, L.J. 2010. Prodigal: prokaryotic gene recognition and translation initiation site identification. BMC Bioinform. 11(1), 1-11.

Im, J. and Löffler, F.E. 2016. Fate of bisphenol A in terrestrial and aquatic environments. Environ. Sci. Technol. 50(16), 8403-8416.

Im, J., Prevatte, C.W., Campagna, S.R. and Löffler, F.E. 2015. Identification of 4-hydroxycumyl alcohol as the major MnO_2-mediated bisphenol A transformation product and evaluation of its environmental fate. Environ. Sci. Technol. 49(10), 6214-6221.

Im, J., Yip, D., Lee, J. and Löffler, F.E. 2016. Simplified extraction of bisphenols from bacterial culture suspensions and solid matrices. J. Microbiol. Methods 126, 35-37.

Kanehisa, M., Sato, Y. and Kawashima, M. 2022. KEGG mapping tools for uncovering hidden features in biological data. Protein Sci. 31(1), 47-53.

Karsauliya, K., Bhateria, M., Sonker, A. and Singh, S.P. 2021. Determination of bisphenol analogues in infant formula products from India and evaluating the health risk in infants asssociated with their exposure. J. Agric. Food Chem. 69(13), 3932-3941.

Kinch, C.D., Ibhazehiebo, K., Jeong, J.-H., Habibi, H.R. and Kurrasch, D.M. 2015. Low-dose exposure to bisphenol A and replacement bisphenol S induces precocious hypothalamic neurogenesis in embryonic zebrafish. Proc. Natl. Acad. Sci. U. S. A. 112(5), 1475-1480.

Kolvenbach, B., Schlaich, N., Raoui, Z., Prell, J., Zühlke, S., Schäffer, A., Guengerich, F. and Corvini, P. 2007. Degradation pathway of bisphenol A: does *ipso* substitution apply to phenols containing a quaternary α-carbon structure in the *para* position? Appl. Environ. Microbiol. 73(15), 4776-4784.

Kondrakov, A.O. (2015) Heterogeneous Photocatalysis and Sensitized Photolysis for Enhanced Degradation of Bisphenol A and its Analogues, Lehrstuhl für Wasserchemie und Wassertechnologie am Engler-Bunte-Inst.

Kovačič, A., Česen, M., Laimou-Geraniou, M., Lambropoulou, D., Kosjek, T., Heath, D. and Heath, E. 2019. Stability, biological treatment and UV photolysis of 18 bisphenols under laboratory conditions. Environ. Res. 179, 108738.

Letunic, I. and Bork, P. 2016. Interactive tree of life (iTOL) v3: an online tool for the display and annotation of phylogenetic and other trees. Nucleic Acids Res. 44(W1), W242-W245.

Li, J., Pang, S., Zhou, Y., Sun, S., Wang, L., Wang, Z., Gao, Y., Yang, Y. and Jiang, J. 2018. Transformation of bisphenol AF and bisphenol S by manganese dioxide and effect of iodide. Water Res. 143, 47-55.

Liao, C., Liu, F., Moon, H.-B., Yamashita, N., Yun, S. and Kannan, K. 2012. Bisphenol analogues in sediments from industrialized areas in the United States, Japan, and Korea: spatial and temporal distributions. Environ. Sci. Technol. 46(21), 11558-11565.

Liu, J., Zhang, L., Lu, G., Jiang, R., Yan, Z. and Li, Y. 2021. Occurrence, toxicity and ecological risk of Bisphenol A analogues in aquatic environment–A review. Ecotoxicol. Environ. Saf. 208, 111481.

Löffler, F.E., Sanford, R.A. and Ritalahti, K.M. 2005. Enrichment, cultivation, and detection of reductively dechlorinating bacteria. Methods Enzymol. 397, 77-111.

McCormick, J.M., Es, T.V., Cooper, K.R., White, L.A. and Häggblom, M.M. 2011. Microbially mediated *O*-methylation of bisphenol A results in metabolites with increased toxicity to the developing zebrafish (*Danio rerio*) embryo. Environ. Sci. Technol. 45(15), 6567-6574.

Medina, M., Rizo, A., Dinh, D., Chau, B., Omidvar, M., Juarez, A., Ngo, J. and Johnson, H.A. 2018. MopA, the Mn oxidizing protein from *Erythrobacter* sp. SD-21, requires heme and NAD^+ for Mn (II) oxidation. Front. Microbiol., 2671.

Mitic, N. (2001) Investigation of the active site structure of non-heme iron dependent phenylalanine hydroxylase: spectroscopic studies and their implications for reaction mechanism, Yale University.

Nakamura, S., Tezuka, Y., Ushiyama, A., Kawashima, C., Kitagawara, Y., Takahashi, K., Ohta, S. and Mashino, T. 2011. *Ipso* substitution of bisphenol A catalyzed by microsomal cytochrome P450 and enhancement of estrogenic activity. Toxicol. Lett. 203(1), 92-95.

NITE 2003. Summary of the Interim Report - Bisphenol A, National Institute of Technology and Evaluation, Japan.

Ogata, Y., Goda, S., Toyama, T., Sei, K. and Ike, M. 2013. The 4-*tert*-butylphenol-utilizing bacterium *Sphingobium fuliginis* OMI can degrade bisphenols via phenolic ring hydroxylation and *meta*-cleavage pathway. Environ. Sci. Technol. 47(2), 1017-1023.

Park, C. and Kim, J. 2012. Effects of nitrate on the advanced UV photolysis of di (2-ethylhexyl) phthalate degradation in aqueous solution. Desalination Water Treat. 47(1-3), 163-170.

Sasaki, M., Akahira, A., Oshiman, K.-i., Tsuchido, T. and Matsumura, Y. 2005a. Purification of cytochrome P450 and ferredoxin, involved in bisphenol A degradation, from *Sphingomonas* sp. strain AO1. Appl. Environ. Microbiol. 71(12), 8024-8030.

Sasaki, M., Maki, J.-i., Oshiman, K.-i., Matsumura, Y. and Tsuchido, T. 2005b. Biodegradation of bisphenol A by cells and cell lysate from *Sphingomonas* sp. strain AO1. Biodegradation 16(5), 449-459.

Schäpe, S.S., Krause, J.L., Masanetz, R.K., Riesbeck, S., Starke, R., Rolle-Kampczyk, U., Eberlein, C., Heipieper, H.-J., Herberth, G. and von Bergen, M. 2020. Environmentally relevant concentration of bisphenol S shows slight effects on SIHUMIx. Microorganisms 8(9), 1436.

Shao, P., Duan, X., Xu, J., Tian, J., Shi, W., Gao, S., Xu, M., Cui, F. and Wang, S. 2017a. Heterogeneous activation of peroxymonosulfate by amorphous boron for degradation of bisphenol S. J. Hazard. Mater. 322, 532-539.

Shao, P., Ren, Z., Tian, J., Gao, S., Luo, X., Shi, W., Yan, B., Li, J. and Cui, F. 2017b. Silica hydrogel-mediated dissolution-recrystallization strategy for synthesis of ultrathin α-Fe_2O_3 nanosheets with highly exposed (1 1 0) facets: a superior photocatalyst for degradation of bisphenol S. Chem. Eng. J. 323, 64-73.

Shobnam, N., Sun, Y., Mahmood, M., Löffler, F.E. and Im, J. 2021. Biologically mediated abiotic degradation (BMAD) of bisphenol A by manganese-oxidizing bacteria. J. Hazard. Mater., 125987.

Sievers, F., Wilm, A., Dineen, D., Gibson, T.J., Karplus, K., Li, W., Lopez, R., McWilliam, H., Remmert, M. and Söding, J. 2011. Fast, scalable generation of high-quality protein multiple sequence alignments using Clustal Omega. Mol. Syst. Biol. 7(1), 539.

Simoneau, C., Valzacchi, S., Morkunas, V. and Van den Eede, L. 2011. Comparison of migration from polyethersulphone and polycarbonate baby bottles. Food Addit. Contam.: Part A 28(12), 1763-1768.

Stamatakis, A. 2014. RAxML version 8: a tool for phylogenetic analysis and post-analysis of large phylogenies. Bioinformatics 30(9), 1312-1313.

Stout, M. 2008. Chemical Information Profile for Bisphenol AF.

Sun, Q., Wang, Y., Li, Y., Ashfaq, M., Dai, L., Xie, X. and Yu, C.-P. 2017. Fate and mass balance of bisphenol analogues in wastewater treatment plants in Xiamen City, China. Environ. Pollut. 225, 542-549.

Sun, Y., Im, J., Shobnam, N., Fanourakis, S.K., He, L., Anovitz, L.M., Erickson, P.R., Sun, H., Zhuang, J. and Löffler, F.E. 2021. Degradation of adsorbed bisphenol A by soluble Mn(III). Environ. Sci. Technol. 55(19), 13014-13023.

Suzuki, T., Nakagawa, Y., Takano, I., Yaguchi, K. and Yasuda, K. 2004. Environmental fate of bisphenol A and its biological metabolites in river water and their xeno-estrogenic activity. Environ. Sci. Technol. 38(8), 2389-2396.

Tebo, B.M., Bargar, J.R., Clement, B.G., Dick, G.J., Murray, K.J., Parker, D., Verity, R. and Webb, S.M. 2004. Biogenic manganese oxides: properties and mechanisms of formation. Annu. Rev. Earth Planet. Sci. 32, 287-328.

Telke, A.A., Kalyani, D.C., Jadhav, U.U., Parshetti, G.K. and Govindwar, S.P. 2009. Purification and characterization of an extracellular laccase from a *Pseudomonas* sp. LBC1 and its application for the removal of bisphenol A. J. Mol. Catal. B: Enzym. 61(3-4), 252-260.

Tišler, T., Krel, A., Gerželj, U., Erjavec, B., Dolenc, M.S. and Pintar, A. 2016. Hazard identification and risk characterization of bisphenols A, F and AF to aquatic organisms. Environ. Pollut. 212, 472-479.

Ullrich, R. and Hofrichter, M. 2007. Enzymatic hydroxylation of aromatic compounds. Cell. Mol. Life Sci. 64(3), 271-293.

USEPA 2011. Estimation Program Interface (EPI) Suite, US EPA Washington, DC.

USEPA 2017. USEPA ECOSAR (Ecological Structure Activity Relationships) v.2.0. https://www.epa.gov/tsca-screening-tools/ecological-structure-activity-relationships-ecosar-predictive-model (accessed Aug 31, 2021).

Wang, J., Wang, C., Guo, H., Ye, T., Liu, Y., Cheng, X., Li, W., Yang, B. and Du, E. 2020. Crucial roles of oxygen and superoxide radical in bisulfite-activated persulfate oxidation of bisphenol AF: Mechanisms, kinetics and DFT studies. J. Hazard. Mater. 391, 122228.

Wolin, E., Wolin, M.J. and Wolfe, R. 1963. Formation of methane by bacterial extracts. J. Biol. Chem. 238(8), 2882-2886.

Yang, Y., Lu, L., Zhang, J., Yang, Y., Wu, Y. and Shao, B. 2014. Simultaneous determination of seven bisphenols in environmental water and solid samples by liquid chromatography–electrospray tandem mass spectrometry. J. Chromatogr. A 1328, 26-34.

Yu, Y., Che, S., Ren, C., Jin, B., Tian, Z., Liu, J. and Men, Y. 2022. Microbial defluorination of unsaturated per-and polyfluorinated carboxylic acids under anaerobic and aerobic conditions: a structure specificity study. Environ. Sci. Technol. 56(8), 4894-4904.

Zhang, C., Zeng, G., Yuan, L., Yu, J., Li, J., Huang, G., Xi, B. and Liu, H. 2007. Aerobic degradation of bisphenol A by *Achromobacter xylosoxidans* strain B-16 isolated from compost leachate of municipal solid waste. Chemosphere 68(1), 181-190.

Zhou, N., Liu, Y., Cao, S., Guo, R., Ma, Y. and Chen, J. 2020. Biodegradation of bisphenol compounds in the surface water of Taihu Lake and the effect of humic acids. Sci. Total Environ. 723, 138164.

Zhou, N.A., Kjeldal, H., Gough, H.L. and Nielsen, J.L. 2015. Identification of putative genes involved in bisphenol A degradation using differential protein abundance analysis of *Sphingobium* sp. BiD32. Environ. Sci. Technol. 49(20), 12232-12241.

Appendix

Table 4.1. The putative hydroxylase/monooxygenase encoded by *Erythrobacter* sp. strain SD21.

RefSeq Locus Tag	Product	AA Length	KO number
ED21_17782	putative oxidoreductase, nitronate monooxygenase family	238	k02371
ED21_17967	Phenylalanine-4-monooxygenase	313	k00500
ED21_18787	Luciferase-like monooxygenase YhbW	324	-
ED21_18817	Putative cytochrome P450 hydroxylase	446	-
ED21_19052	Fatty acid hydroxylase family (carotene hydroxylase/sterol desaturase)	238	k00227
ED21_19697	2-polyprenyl-3-methyl-6-methoxy-1,4-benzoquinol hydroxylase, coq7 type	180	k06134
ED21_20174	Fatty acid hydroxylase family (carotene hydroxylase/sterol desaturase)	314	-
ED21_20339	Fatty acid hydroxylase family (carotene hydroxylase/sterol desaturase)	279	-
ED21_22108	Monooxygenase, flavin-binding family	505	k10215
ED21_22643	Fatty acid hydroxylase family (carotene hydroxylase/sterol desaturase)	260	-
ED21_23611	putative oxidoreductase, nitronate monooxygenase family	325	k23948
ED21_23836	Beta-carotene hydroxylase	172	k15746
ED21_24651	Putative hydroxylase	260	k06996
ED21_25006	Similar to eukaryotic Peptidyl prolyl 4-hydroxylase, alpha subunit	224	k00472
ED21_25397	Similar to eukaryotic Peptidyl prolyl 4-hydroxylase, alpha subunit	211	k00472
ED21_26928	Fatty acid hydroxylase family (carotene hydroxylase/sterol desaturase)	274	-
ED21_28978	putative oxidoreductase, nitronate monooxygenase family	322	k00459
ED21_30549	2-polyprenyl-6-methoxyphenol hydroxylase	404	k03185
ED21_32029	Cyclohexanone monooxygenase	440	-
ED21_32064	putative oxidoreductase, nitronate monooxygenase family	287	k00459
ED21_32074	Putative cytochrome P450 hydroxylase	420	-

Table 4.2. Predicted acute and chronic toxicity of BPA, BPS, and BPAF, and their transformation products using the ECOSAR program.

Compounds	Acute toxicity (mg L^{-1})			Chronic toxicity (mg L^{-1})		
	Fish (LC_{50})	Daphnid (LC_{50})	Green algae (EC_{50})	Fish	Daphnid	Green algae
BPA	1.28	5.24	1.33	0.550	1.77	0.227
BPA-T1	2.65	13.1	2.07	1.22	4.57	0.329
BPA-T2	17.3	17.0	9.19	3.61	0.165	3.20
BPA-T3	15.1	9.35	10.1	1.64	1.17	3.21
BPA-T4	3.97E+3	2.13E+3	1.26E+3	363	178	291
BPS	427	235	153	40.2	20.9	37.2
BPS-T1	1.23E+3	645	349	109	50.7	77.1
BPS-T2	4.57E+3	2.27E+3	976	382	153	190
BPS-T3	2.78E+6	1.16E+6	2.37E+5	1.88E+5	4.73E+4	3.10E+4
BPS-T4	9.98E+3	4.71E+3	1.64E+3	785	276	286
BPAF	1.66	1.18	2.26	0.212	0.218	0.986
BPAF-T1	4.68	3.20	5.10	0.569	0.520	2.01
BPAF-T2	115	67.4	56.2	11.7	7.09	15.7
BPAF-T3	4.85	3.25	4.81	0.576	0.503	1.83
BPAF-T4	2.07E+4	1.02E+4	4.31E+3	1.72E+3	680	830

LC_{50} represents the degradation product concentration that could result in 50% death of fish and *Daphnia* after 96 and 48 h of exposure, respectively. EC_{50} represents the degradation product concentration that could result in 50% growth inhibition of green algae after 96 h of exposure. Toxicity was classified based on the Globally Harmonized System of Classification and Labeling of Chemicals (https://unece.org/fileadmin/DAM/trans/danger/publi/ghs/ghs_rev04/English/ST-SG-AC10-30-Rev4e.pdf). Very toxic: $LC_{50}/EC_{50}/ChV \leq 1$ mg L^{-1}, Toxic: 1 mg $L^{-1} < LC_{50}/EC_{50}/ChV \leq 10$ mg L^{-1}, Harmful: 10 mg $L^{-1} < LC_{50}/EC_{50}/ChV \leq 100$ mg L^{-1}.

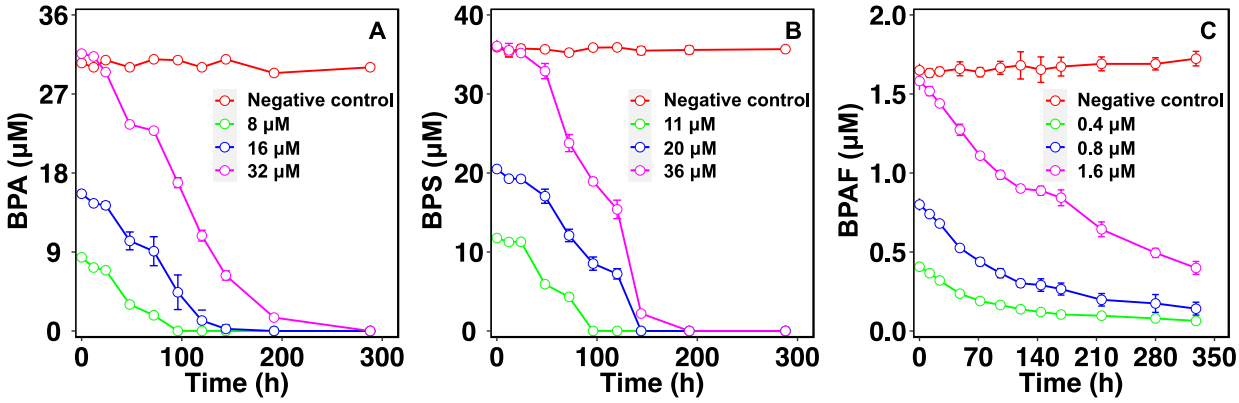

Figure 4.1. BPA, BPS, and BPAF concentration profiles in strain SD21. (A) Strain SD21 mediated BPA transformation in K-medium at pH 7.4 initially containing 8, 16, and 32 μM BPA over a 12-day incubation period. (B) Strain SD21 mediated BPS transformation in K-medium initially containing 11, 20, and 36 μM BPS. (C) Strain SD21 mediated BPAF transformation in K-medium initially containing 0.4, 0.8, and 1.6 μM BPAF over a 14-day incubation period. Error bars represent the standard deviation of triplicate samples and are not depicted when smaller than the symbol size.

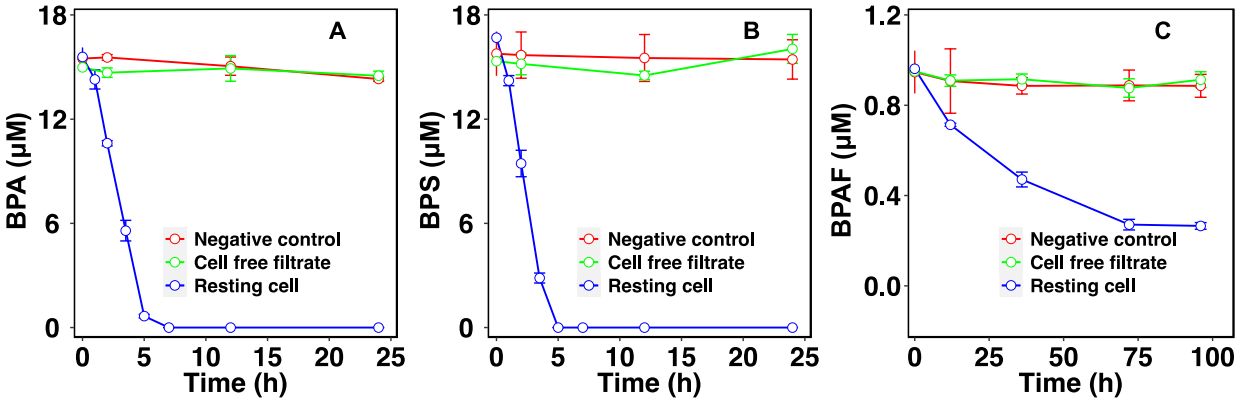

Figure 4.2. BPA, BPS, and BPAF concentration profiles in resting cell suspension and cell-free filtrate. (A) Transformation of 15 μM BPA in resting cell suspension assay using strain SD21 cells grown in K-medium at pH 7.4. (B) Transformation of 16 μM BPS in resting cell suspension assay using strain SD21 cells grown in K-medium. (C) Transformation of 1 μM BPAF in resting cell suspension assay using strain SD21 cells grown in K-medium. Error bars represent the standard deviations of triplicate vessels and are not depicted when smaller than the symbol size.

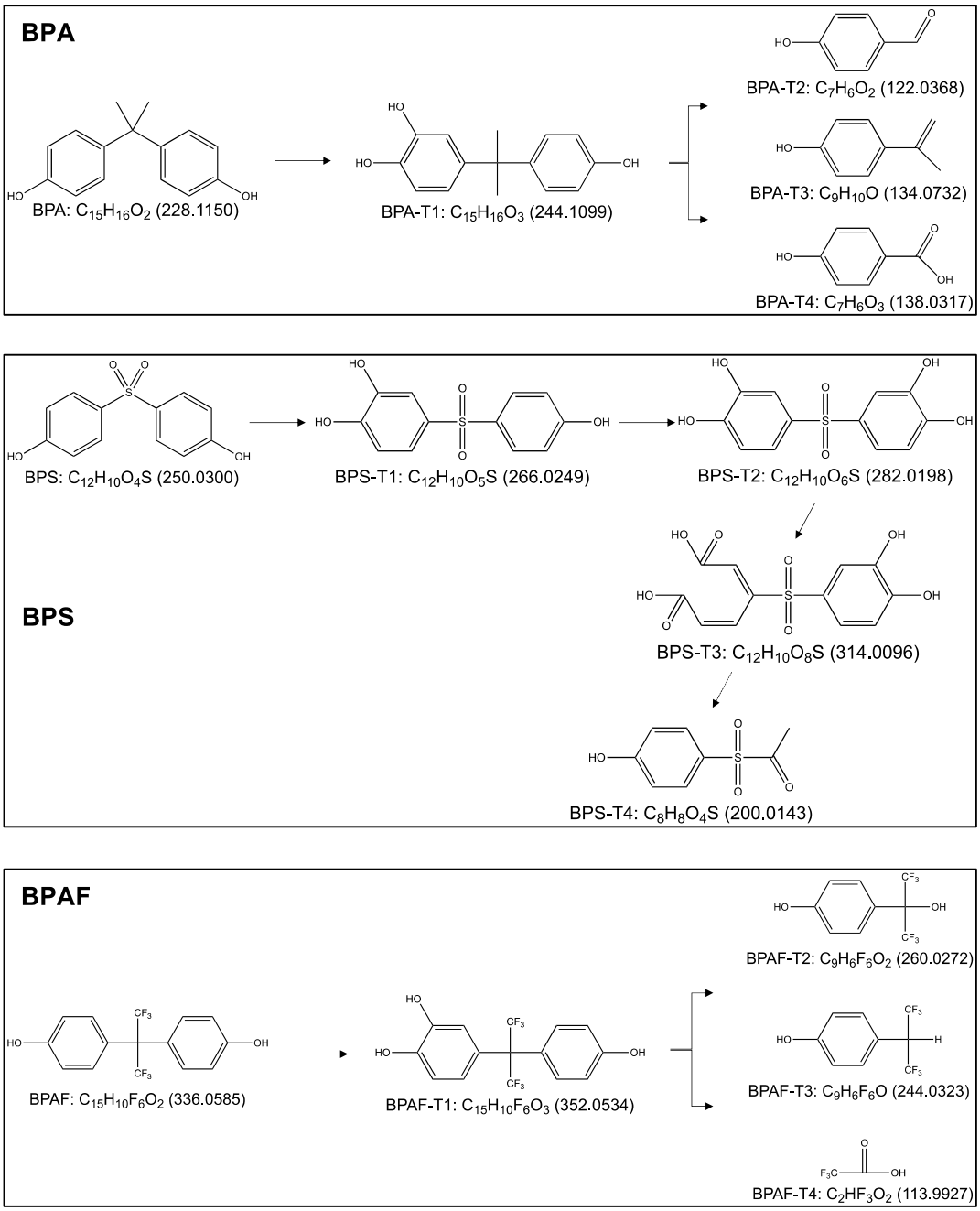

Figure 4.3. Biotransformation pathways of BPA, BPS, and BPAF by strain SD21.

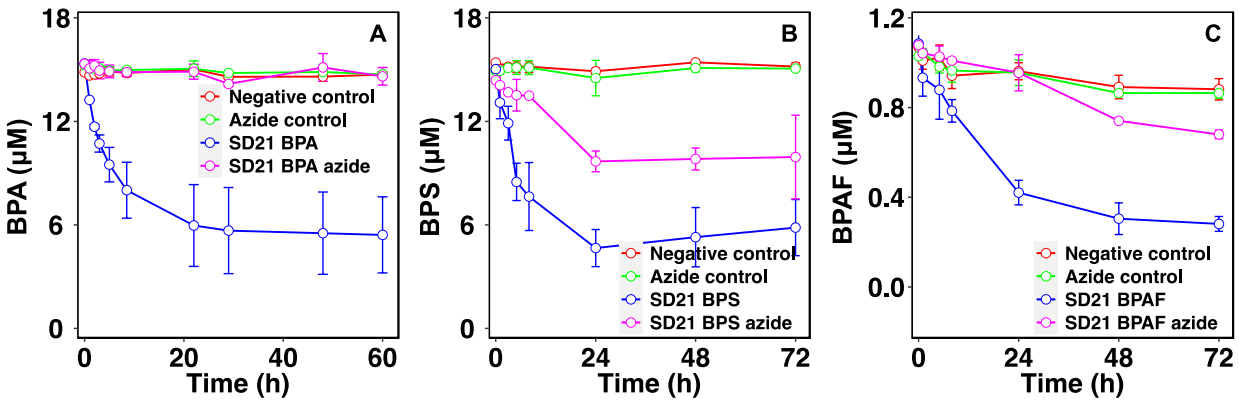

Figure 4.4. Azide inhibits transformation of BPA, BPS, and BPAF. (A) Transformation of initial 15 μM BPA in phosphate buffer (pH 7.4) by strain SD21 was inhibited by 1 mM azide. (B) Azide of 1 mM inhibited BPS transformation by strain SD21 in phosphate buffer initially containing 16 μM BPS. (C) Azide inhibited BPAF transformation by strain SD21 in phosphate buffer. Error bars represent the standard deviations of triplicate vessels and are not depicted when smaller than the symbol size.

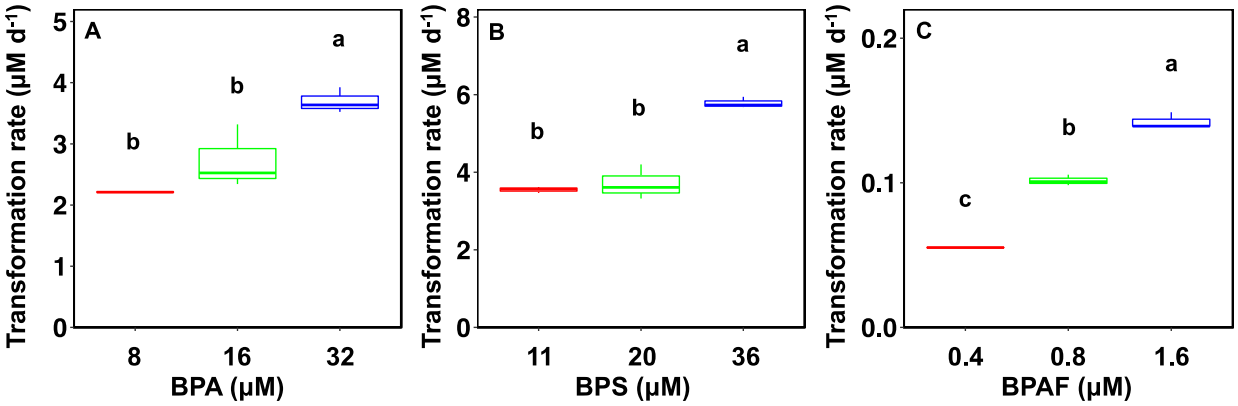

Figure S4.1. Transformation rates of BPA, BPS, and BPAF by strain SD21. (A) The initial BPA concentrations affect its transformation rate. BPA transformation were conducted in 50 mL K-medium with initial BPA concentration of 8, 16, and 32 μM, respectively. (B) The transformation rate of BPS by strain SD21 with 11, 20, and 36 μM of initial BPS, respectively. (C) Transformation rates of BPAF by strain SD21. Error bars represent the standard deviation of triplicate samples and are not depicted when smaller than the symbol size.

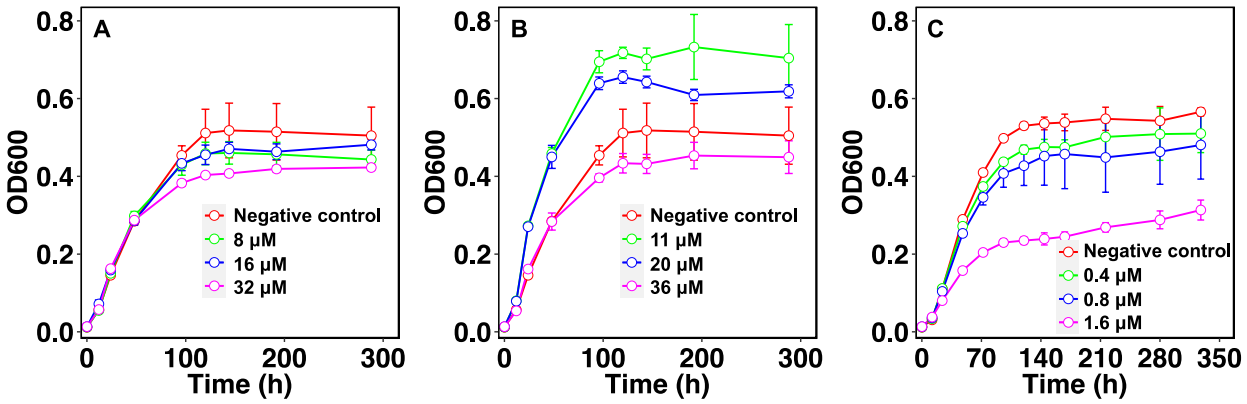

Figure S4.2. SD21 growth profiles in the presence of BPA, BPS, and BPAF. (A) Strain SD21 grew in K-medium at pH 7.4 initially containing 8, 16, and 32 µM BPA, respectively, over a 12-day incubation period. (B) BPS affected the strain SD21 growth in K-medium initially containing 11, 20, and 36 µM BPS, respectively. (C) BPAF of 0.4, 0.8, and 1.6 µM, respectively, inhibited strain SD21 growth yields over a 14-day incubation period. Error bars represent the standard deviation of triplicate samples and are not depicted when smaller than the symbol size.

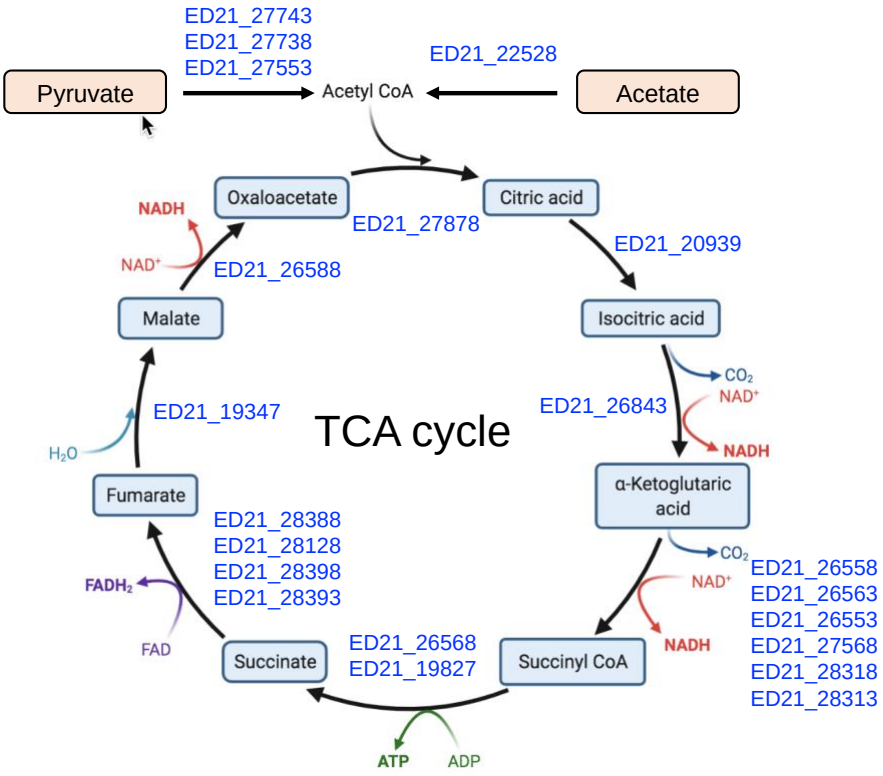

Figure S4.3. Metabolic potential of strain SD21 to pyruvate and acetate based on the KEGG annotation. The fonts in blue color indicate the gene locus tags of each protein identified in the genome of strain SD21.

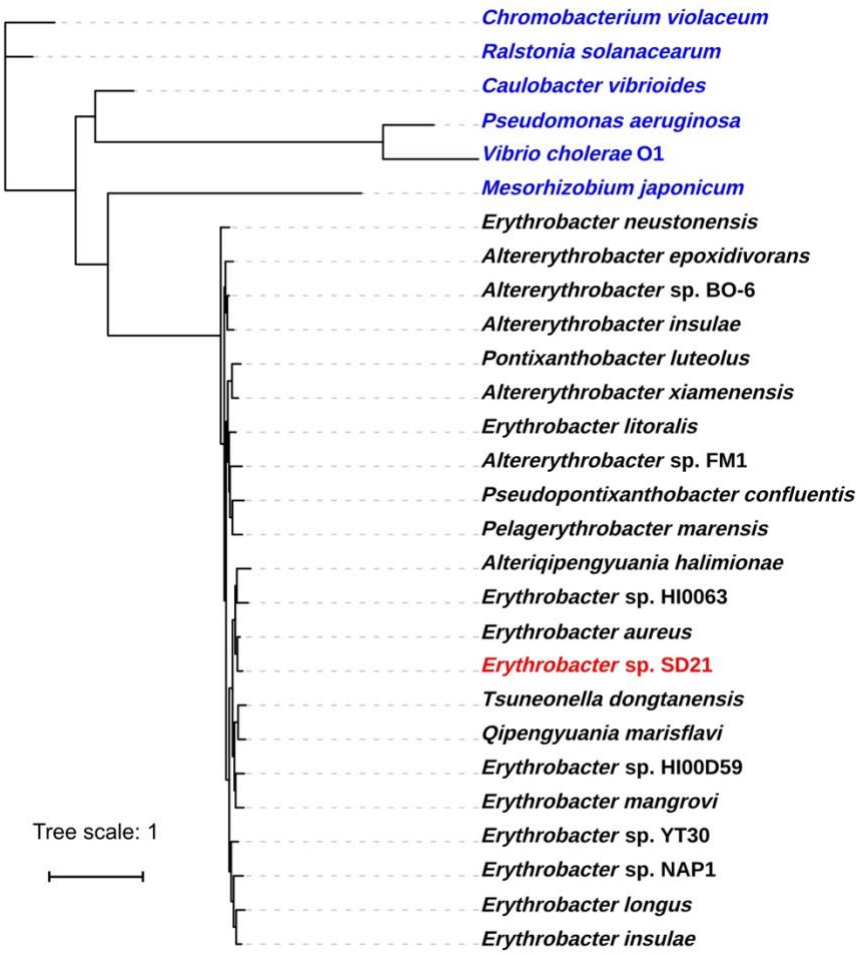

Figure S4.4. Amino acid sequence-based phylogenetic tree of selected phenylalanine 4-monooxygenase. Phenylalanine 4-monooxygenase harbored by strain SD21 is shown in red font. Biochemically characterized bacterial phenylalanine 4-monooxygenase downloaded from the Swiss-Protein database are shown in blue font.

Chapter 5. Summary and Conclusion

Bisphenol A (BPA) is a widely used industrial chemical for the production of polycarbonates and epoxy resins. The global BPA market reached a value of nearly $11 billion in 2020 and is projected to reach $30.62 billion by 2026. High production volume and widespread use introduced BPA to various environmental systems. Laboratory studies suggested estrogenic effects of BPA, what has triggered research exploring the fate of BPA. In addition, a number of BPA substitutes have been developed to generate "BPA-free" products. Two common BPA substitutes are bisphenol S (BPS) and bisphenol AF (BPAF); however, recent studies suggested estrogenic effects of BPS and BPAF comparable to those of BPA, environmental fate studies for the BPA substitutes.

Manganese (Mn) cycling is driven by Mn(II)-oxidizing bacteria and Mn(IV)-reducing bacteria. MnO_2 and Mn(III) are the major oxidized Mn species in Mn cycling. Previous experimental efforts demonstrated that synthetic MnO_2 and biogenic MnO_2 effectively react with BPA and potentially other bisphenols. Recent efforts showed that Mn(III) is also an environmentally relevant oxidant with potentially substantial contributions to the degradation of bisphenols. In addition to oxidized Mn species, the Mn(II)-oxidizing bacteria can directly contribute to transforming BPA. Therefore, the environmental fate of bisphenols has close relation with Mn-cycling.

Several studies have now demonstrated that soluble Mn(III) commonly occurs in environmental systems and is an environmentally relevant oxidant, which may affect the fate of BPA. Chapter 2 demonstrates that MnO_2-mediated BPA degradation is the combined reaction of Mn(III) and Mn(IV) with BPA. Synthetic MnO_2 comprised approximately 13% (mol/mol) surface-associated Mn(III) and exhibited approximately 2-fold higher BPA degradation rates than surface-Mn(III)-free synthetic MnO_2. BPA degradation by Mn(III) yielded 14

transformation products, nine of which had not been observed during BPA degradation mediated by surface-Mn(III)-free synthetic MnO_2, suggesting mechanistic differences. The results indicate that both Mn(III) and Mn(IV) can effectively degrade BPA and surface-associated Mn(III) increases the reactivity of MnO_2.

BPA is found associated with sediments and soils due to its hydrophobicity (log K_{OW} of 3.42). In chapter 3, superfine powdered activated carbon (SPAC) was used as a BPA sorbent to assess the degradation of BPA by oxidized Mn species. SPAC strongly sorbed BPA and desorption required organic solvents. No degradation of adsorbed BPA was observed with synthetic, solid α-MnO_2; however, the degradation of adsorbed BPA occurred following the addition of soluble Mn(III). Small-angle neutron scattering data suggested that both adsorption and degradation of BPA occurred in SPAC pores. The observations demonstrate that Mn(III) mediates the oxidative transformation of dissolved and adsorbed BPA.

BPS and BPAF are two major BPA substitutes with potential estrogenic effects; however, information on their transformation are limiting. Chapter 4 demonstrates that *Erythrobacter* sp. strain SD21, a manganese (Mn) oxidizing bacterium, effectively transforms BPA, BPS, and BPAF in the absence of Mn. The complete transformation of BPA and BPS was observed by strain SD21, but BPAF was transformed at a lower rate. BPA has no inhibitory effect on the growth of strain SD21; however, the growth of strain SD21 was sensitive to BPS and BPAF. Strain SD21 harbors genes encoding monooxygenases, which are likely involved in the transformation of three bisphenols through hydroxylation. The results indicate that the Mn-oxidizing bacterium, strain SD21 is capable of BPA, BPS, and BPAF transformation. Overall, the findings highlight that environments with active Mn-cycling are hotspot areas for the degradation of bisphenols and emphasize their role in controlling human exposure to bisphenols.

This doctoral study reveals that Mn-cycling-related biogeochemical processes play a vital role in the attenuation of organic contaminants and have implications for improving the remedial treatment of contaminants. Surface-associated Mn(III) increases the reactivity of MnO_2, which offers opportunities for engineering more reactive MnO_2 (nano)particles for the removal of BPA, other bisphenols, and a broader range of contaminants. The natural oxidant, soluble Mn(III), mediated the degradation of adsorbed BPA, a finding with implications for managing the fate and longevity of BPA in soils and sediments. The discovery that an Mn(II)-oxidizing bacterium transforms BPA, BPS, and BPAF even in the absence of Mn advances understanding of the fate of bisphenols in environments and contribute to our understanding of processes that attenuate bisphenols in the environment.

Vita

Yanchen Sun was born in Zaozhuang City, Shandong Province, China. He completed his undergraduate study in Environmental Engineering at the University of Jinan in 2014. He then obtained two master's degrees in Environmental Science, one from the Institute of Applied Ecology, Chinese Academy of Sciences and another from the Water and Environment program at the University of Copenhagen, both awarded in 2017. After that, Yanchen came to the U.S. and pursued his doctoral study in Environmental Engineering at the University of Tennessee under the guidance of Dr. Frank E. Löffler. His doctoral study mainly focuses on the abiotic and biotic degradation of emerging contaminants using an integrated approach that combined physical characterization, analytical chemistry, and microbiology. He also conducted research investigating nitrous oxide reduction in tropical forest soils and permafrost soils using cultivation and bioinformatics approaches. Upon graduation from the University of Tennessee, Yanchen expects to continue research in the area of environmental sciences making new discoveries and developing transformative solutions to address pressing environmental challenges.